REPORT DOCUMENTATION PAGE

Form Approved
OMB No. 0704-0188

PLEASE DO NOT RETURN YOUR FORM TO THE ABOVE ADDRESS.

1. REPORT DATE *(DD-MM-YYYY)*	2. REPORT TYPE	3. DATES COVERED *(From - To)*
01-12-2005	Interim Report	August 2003-December 2005

4. TITLE AND SUBTITLE

Disturbances from shock/boundary-layer interactions affecting upstream hypersonic flow

5a. CONTRACT NUMBER

5b. GRANT NUMBER

F49620-03-1-0030

5c. PROGRAM ELEMENT NUMBER

6. AUTHOR(S)

Craig Ryan Skoch

5d. PROJECT NUMBER

5e. TASK NUMBER

5f. WORK UNIT NUMBER

7. PERFORMING ORGANIZATION NAME(S) AND ADDRESS(ES)

Purdue University, School of Aeronautics and Astronautics

8. PERFORMING ORGANIZATION REPORT NUMBER

none

9. SPONSORING/MONITORING AGENCY NAME(S) AND ADDRESS(ES)

Air Force Office of Scientific Research, Dr. John Schmisseur
875 North Randolph Street
Suite 325, Room 3112
Arlington, VA 22203

10. SPONSOR/MONITOR'S ACRONYM(S)

AFOSR

11. SPONSOR/MONITOR'S REPORT NUMBER(S)

12. DISTRIBUTION/AVAILABILITY STATEMENT

Approved for public release. Distribution unlimited.

13. SUPPLEMENTARY NOTES

Ph.D. Thesis documenting performance of unique national research facility.

14. ABSTRACT

Large disturbances and decreased Mach number in the core flow were sometimes found in the downstream end of the nozzle of the Boeing/AFOSR Mach-6 Ludwieg Tube at Purdue University. The cause of the disturbances has been identified using Kulite pressure transducer, hot wire, and hot film measurements. These disturbances were found to be separations caused by shock/boundary-layer interactions in the diffuser, often originating from shocks generated at the sting support. Some disturbances were found to propagate upstream about 100 boundary layer thicknesses. The large upstream effect is due to the laminar boundary layers being very susceptible to separation. Attempts to prevent the separations from propagating upstream included an improved sting mount, compression rings to thin the boundary layer, and trip rings to trip the boundary layer. These attempts were not successful. A diffuser section with an increased area is proposed to prevent the separations from propagating upstream.

15. SUBJECT TERMS

hypersonic laminar-turbulent transition, quiet wind tunnels, shock/boundary-layer interaction

16. SECURITY CLASSIFICATION OF:			17. LIMITATION OF ABSTRACT	18. NUMBER OF PAGES	19a. NAME OF RESPONSIBLE PERSON
a. REPORT	b. ABSTRACT	c. THIS PAGE			Steven P. Schneider, Professor
U	U	U	Unlimited	132	19b. TELEPHONE NUMBER *(Include area code)* 765-494-3343

DISTURBANCES FROM SHOCK/BOUNDARY-LAYER INTERACTIONS AFFECTING UPSTREAM HYPERSONIC FLOW

A Thesis

Submitted to the Faculty

of

Purdue University

by

Craig Ryan Skoch

In Partial Fulfillment of the

Requirements for the Degree

of

Doctor of Philosophy

December 2005

ACKNOWLEDGEMENTS

This work and my studies were funded by the Air Force Office of Scientific Research under Grant F49620-03-1-0030, monitored by John D. Schmisseur.

I would like to thank my major professor, Dr. Steven P. Schneider, for beginning the work with the Boeing/Air Force Mach-6 Ludwieg Tube, and allowing me to contribute to its development. I would also like to thank the rest of my examination committee, President Martin C. Jischke, Dr. Steven H. Collicott, and Dr. Stephen D. Heister, for their suggestions and input.

I would like to thank Madeline Chadwell, Robin Snodgrass, Jerry Hahn, and Jim Younts, for their excellent craftsmanship and assistance when things went wrong and Joan Jackson for giving me a hard time when I needed to order items.

My friends/officemates were helpful for bouncing ideas off of and at times distracting me from my research. I would like to thank Shann Rufer, Ben Kuperman Matthew Borg, Tom Juliano, Tyler Robarge, Shin Matsumura, and Justin Smith.

I would like to thank my family for their love and support over these many, many years of school, and my girlfriend and proofreader, Madison Natt, for her assistance and understanding when I was extremely busy finishing.

I would also like to thank God and all of my friends at Purdue Lutheran Ministry. Their support and friendship continue to help me grow spiritually.

TABLE OF CONTENTS

Page

Page

Page

LIST OF FIGURES

Figure Page

Figure Page

Figure Page

Figure Page

Figure Page

Figure Page

Figure Page

ABSTRACT

Skoch, Craig R., Ph.D., Purdue University, December 2005. Disturbances from Shock/Boundary-Layer Interactions Affecting Upstream Hypersonic Flow. Major Professor: Steven P. Schneider.

Large disturbances and decreased Mach number in the core flow were sometimes found in the downstream end of the nozzle of the Boeing/AFOSR Mach-6 Ludwieg Tube at Purdue University. The cause of the disturbances has been identified using Kulite pressure transducer, hot wire, and hot film measurements of the flow in the tunnel. These disturbances were found to be separations caused by shock/boundary-layer interactions in the diffuser, often originating from shocks generated at the sting support. Some disturbances were found to propagate upstream about 100 boundary layer thicknesses. The large upstream effect is due to the laminar boundary layers being very susceptible to separation. Attempts to prevent the separations from propagating upstream included an improved sting mount, compression rings in the diffuser to thin the boundary layer, and trip rings, in the nozzle and diffuser, to trip the boundary layer. These attempts were not successful in eliminating the separation in the nozzle. A diffuser section with an increased area is proposed to prevent the separations from propagating upstream.

CHAPTER 1 – INTRODUCTION

In supersonic flow, disturbances can only travel downstream. However, near the wall, in the boundary layer, part of the flow is subsonic. In this region, it is possible for disturbances to be transmitted upstream, causing surprising effects. This thesis examines this effect in Purdue's Mach-6 Ludwieg tube because it has been found that shock/boundary layer interactions in the diffuser can separate the flow far upstream in the nozzle. This effect is also important for hypersonic vehicles when shock/boundary layer interactions are present.

1.1 Importance of Quiet Tunnels

Laminar to turbulent transition is important to hypersonic cruise vehicles, hypersonic reentry vehicles, and high-speed missiles, though its causes are not well understood. On the National Aerospace Plane (NASP), estimates of the transition location varied anywhere from 20 to 80 percent of the length of the body[1]. Predicting the transition location is important because turbulent boundary layers can have heating levels that are 2-8 times that of laminar boundary layers. In places where laminar boundary layers exist, it may be possible to use a metallic Thermal Protection System (TPS) instead

of a heavier and more expensive ceramic or composite TPS, which is often required when turbulent boundary layers are present[2]. There are some instances where a turbulent boundary layer is desired, as in the case of the Hyper-X program, where a turbulent boundary layer entering the inlet assists with operation of the scramjet engine.[3] Whether a laminar or turbulent boundary layer is desired, more information about the causes of transition is needed in order to predict and control where it occurs.

Information about transition from most high-speed wind tunnels is often inaccurate and misleading, because of higher levels of free-stream noise in wind tunnels, as compared to flight. Fisher and Dougherty tested the transition location for a 10-degree cone in flight, and in wind tunnels of various noise levels, for Mach numbers ranging from 0.5 to 2.0. The tunnels with noise levels only about twice that of flight had good agreement with the flight data up to about Mach 1.2, but agreement diminished at higher Mach numbers. The tunnels with noise levels an order of magnitude higher than flight showed poor agreement at any Mach number.[4] Pate and Schueler were able to find a correlation for the transition Reynolds number based on wind-tunnel free-stream noise and tunnel size for sharp plates and cones.[5] Stainback correlated transition location to tunnel noise for sharp cones.[6] These findings show that tunnel noise can have a dominant effect on transition location.

The problem with noisy tunnels is that the mechanisms that lead to transition can be completely different than at flight noise levels. The causes of transition found in conventional tunnels may not be relevant to the causes of transition in flight. Tunnel noise can affect not only transition location, but also the trends in location. According to the e^N method for determining transition, transition should occur at a lower Reynolds

number on a cone than a flat plate. Quiet tunnel measurements support this. In noisy conditions, the cone transitions 2.2 to 2.5 times later than the flat plate at Mach 3.5.[7] Some important factors that affect transition are bluntness, angle of attack, and roughness. Studies of all of these effects have been influenced by wind tunnel noise. Varying the noise levels affects both the values and the trends discovered in these studies.[8] In order to obtain wind tunnel data on transition that can be used to learn about flight conditions, the research needs to be performed in quiet-flow wind tunnels, which are tunnels with free-stream noise levels comparable to flight.

There are three causes of free-stream disturbances in a wind tunnel. One source is vorticity fluctuations that originate in the settling chamber. These have been found to be insignificant above Mach 2.5.[5] Another source is entropy fluctuations. Elimination of these requires good mixing of heated air to achieve a uniform temperature. The third source is acoustic waves. Laufer showed that the free-stream fluctuations in noisy tunnels are caused by acoustic disturbances.[9] These acoustic disturbances occur when the boundary layer on the walls of the wind tunnel transitions from laminar to turbulent. The source of the acoustic disturbances can be found by following Mach lines upstream from spatial increases in free-stream disturbances.[10]

1.2 Shock/Boundary-Layer Interactions

Shock/boundary-layer interactions are an important problem for hypersonic vehicles. These occur whenever a shock comes in contact with another surface. Some

examples of shock/boundary layer interactions are an impinging shock, a bow shock intersecting a deflected flap, and a glancing shock, where the wing meets the body of the vehicle. For scramjets, the shock structure and the boundary layer interactions can become quite complex, as shown in Figure 1.

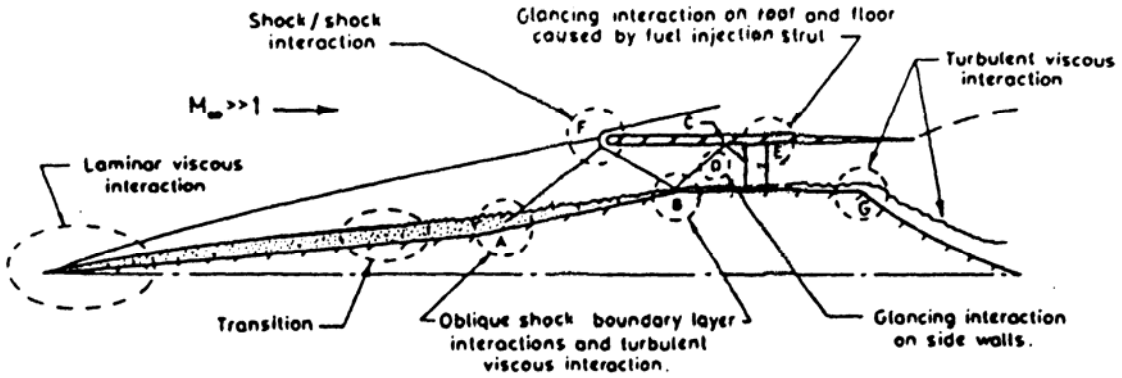

Figure 1: Shock/boundary-layer interactions in a scramjet inlet.[11]

One of the simplest types of shock/boundary-layer interaction is when an oblique shock impinges on a wall. In inviscid flow, there would be a straightforward shock reflection. With a boundary layer, this becomes more complicated, as shown in Figure 2 and in the enlarged view in Figure 3. In the boundary layer, the velocity drops so that it reaches the no-slip condition at the wall. In supersonic flow, a portion of the boundary layer near the wall is subsonic. Since the Mach number also drops when moving closer to the wall, the oblique shock bends and becomes weaker until it reaches the sonic line in the boundary layer, where it disappears.[12] In the subsonic portion of the boundary layer, information from the pressure rise due to the shock is sent upstream, allowing a more gradual pressure increase near the wall. The increase in pressure ahead of the place where the shock impinges on the boundary layer causes the boundary layer to thicken, or if the shock is strong enough, to separate. The thicker or separated boundary layer causes

a shock to emanate from the boundary layer upstream. The upstream shock will interact with the initial oblique shock.

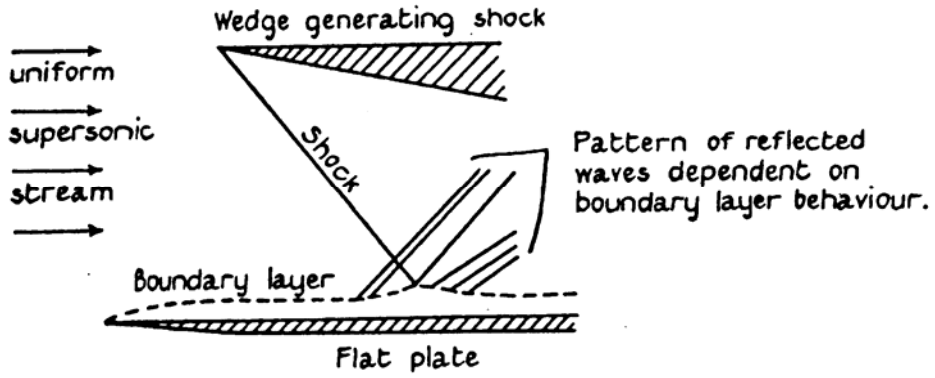

Figure 2: Oblique shock impinging on a boundary layer.[13]

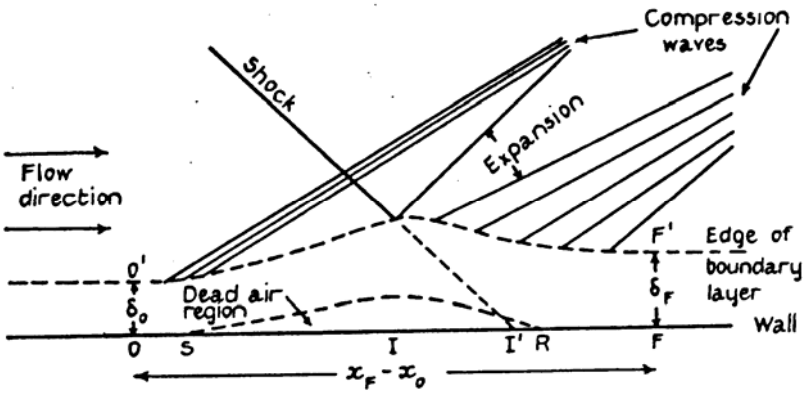

Figure 3: Detail of boundary layer where oblique shock impinges.

A turbulent boundary layer has a subsonic region that is much smaller than a laminar boundary layer, which allows a shock to separate a laminar boundary layer much more easily. To generate comparable separation regions, a shock must be 5-10 times stronger with a turbulent boundary layer than with a laminar boundary layer. It has been shown experimentally that shocks impinging on a laminar boundary layer can cause separation at least 100 boundary layer thicknesses upstream of the impingement location.[14] The impinging shock can also have an effect on transition. At very low

Reynolds numbers, the boundary layer will be laminar before and after the shock. At a higher Reynolds number, where the flow is near transitional, the flow will be laminar before the shock and separation, but reattach as a turbulent boundary layer.[15] Since the subsonic portion of the boundary layer is thicker for laminar boundary layers, it is also possible that unsteady fluctuations might feed upstream, and cause transition to occur sooner, as observed at Langley Research Center.[16] As this earlier transition would then generate a turbulent boundary layer with reduced upstream influence, this could be a very unsteady situation.

Other shock/boundary layer interactions are shown in Figure 4 and Figure 5. The flow over the compression wedge is very similar to the impinging oblique shock. The main difference is that the pressure increase is caused by the geometry of the wall instead of by a shock. The wedge flow shown in Figure 4 shows a compression corner, as is common in scramjet inlets. With the two compression ramps, there will also be a shock/shock interaction where the shocks from the first and second inclines intersect. The glancing interaction is depicted in Figure 5. The interaction occurs when a shock intersects a side wall and is complicated and three-dimensional.

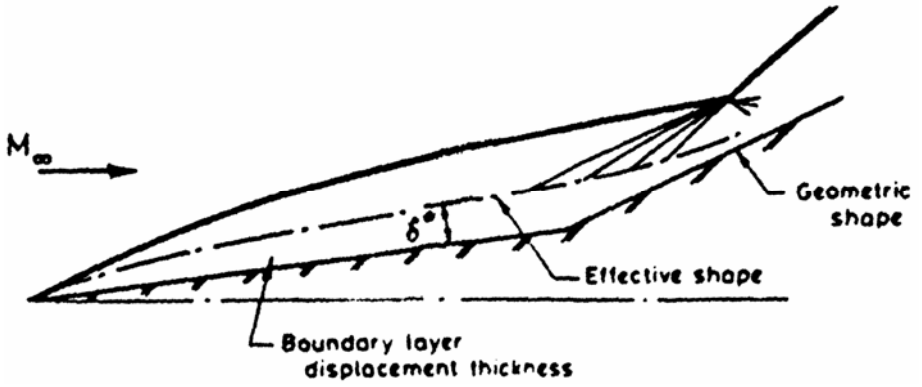

Figure 4: Shock/boundary layer interaction on a wedge.

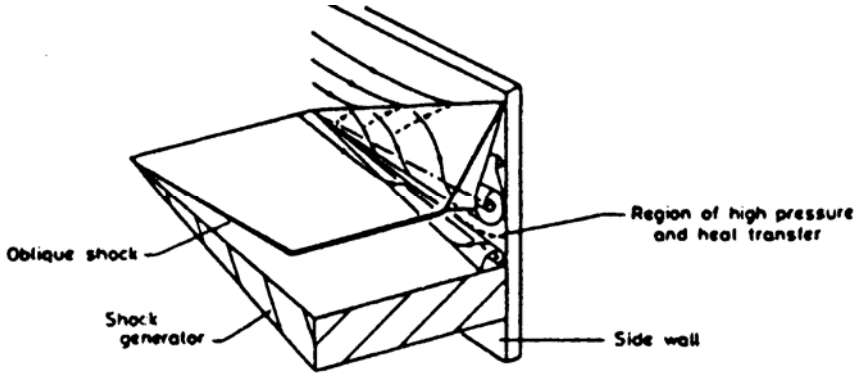

Figure 5: Shock/boundary layer interaction with a glancing shock.

In the Mach-6 tunnel, shock/boundary-layer interactions are found primarily when shocks impinge on the sidewall of the tunnel, though there are likely glancing shock interactions as well. The shocks originate from the sting support or from models placed in the tunnel, and separate the boundary layer quite severely when laminar boundary layers are present.

1.3 Jets in Transverse Flow

Jets in transverse supersonic flows are used for many applications, such as reaction control systems, thrust vector control, and injection systems for scramjets. All of these cases can have large effects on the general flow. In control systems, the change in the flow can result in forces that add to the control forces, or completely counter the intended jet force.[17] In hypersonic flow, these large flow changes could also create large heating effects that must be considered. The use in scramjets is primarily for fuel injection and mixing,[18] but jets in transverse flow have also been demonstrated to be

useful as controllable trip mechanisms[19] that could help ensure that turbulent flow enters the engine.

Figure 6 shows a diagram of an underexpanded jet in a supersonic transverse flow. In the underexpanded case, the static pressure of the jet is lower than the static pressure of the main flow. The lower static pressure of the main flow compared to the jet causes the jet to expand until a normal shock matches the static pressure to the main flow. Upstream of the jet, there is a boundary layer separation and a shock from the front of the separation. Downstream of the jet, there is also separated flow and a possible reattachment. In a three-dimensional case, such as a circular jet instead of an infinite span slot, the flow field is much more complicated, involving a curved shock.

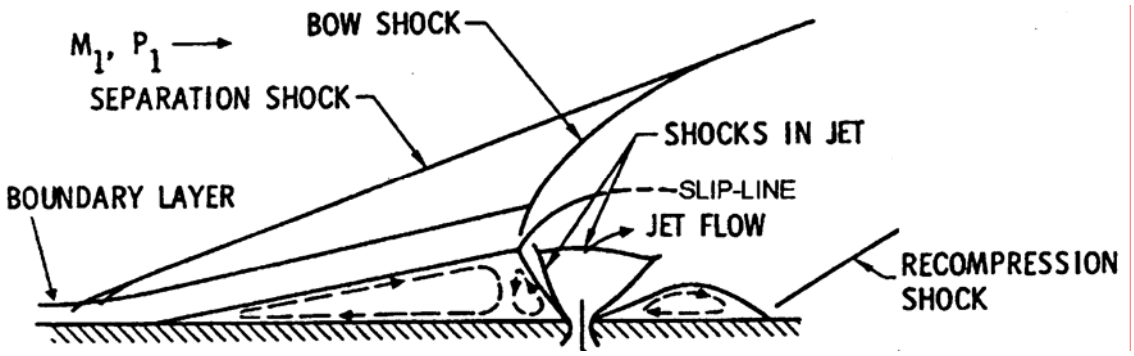

Figure 6: Diagram of jet interaction in supersonic transverse flow.

The transitional state of the boundary layer can also have a large impact on how the jet affects the flow. If the boundary layer approaching the jet is laminar, there will be a much larger interaction than if it was turbulent.[20] If the boundary layer is near transition, the jet can move the transition location forward. There has been significant research on this for the two-dimensional case, but the effect of the jet on transition is not well known for a three-dimensional jet.

Jets are present in the diffuser of the Mach-6 Tunnel when the passive bleed system is used and were present when the double-wedge sting support was used. The passive bleed system takes the bleed air and reintroduces the air to the diffuser with two large jets angled downstream, as will be described in more detail in Chapter 3. When the double wedge was used with nothing placed in the sting mount, the air would enter the hole in the center and jet out to the side in the center of the double wedge, as will be described in more detail in Chapter 3. The double wedge was replaced because it was found to cause large disturbances upstream.[21,22]

1.4 Research Objectives

In the Purdue Mach-6 Ludwieg tube, shock/boundary-layer interactions often cause large separations at the end of the nozzle. These shock/boundary-layer interactions disrupt the flow and reduce the Mach number. In some cases the separations result in large unsteady fluctuations. This tunnel is much more susceptible to this problem than other tunnels, because the boundary layers must be kept laminar in order to have quiet flow. Laminar boundary layers are much easier to separate than the turbulent boundary layers most other tunnels have. NASA Langley has operated quiet tunnels without this problem by using an open jet test section. It is not feasible to run an open jet with a Ludwieg tube because of the time required to evacuate the air from a large open test section.

Little research has been done examining large upstream influences of shock/boundary-layer interactions due to the difficulty of maintaining laminar boundary layers. The present research is also unique in the size of the laminar boundary layers being examined. The nozzle of the Purdue tunnel is over 8 feet long, allowing very thick laminar boundary layers to develop. The primary objectives of this research were to find and understand the source of the disturbances seen in the nozzle, and to reduce the upstream influence in the nozzle. Due to the scale of the problem and the limited previous work in this area, the second objective was not completed, though this research has led to ideas that promise to resolve this issue. Results from this research can also be used in other applications, such as scramjet inlets, where flows are often laminar, and shock/boundary-layer interactions are abundant.

CHAPTER 2 – APPARATUS AND EQUIPMENT

2.1 Purdue Mach-6 Facility

The Mach-6 quiet-flow wind tunnel at Purdue University is a Ludwieg Tube. A Ludwieg Tube consists of a long cylindrical tube (the driver tube) holding compressed air, a Laval nozzle, a testing area, a diffuser, and a fast-acting valve open to the atmosphere or the vacuum system[23] (Figure 7). Once the valve is opened, an expansion wave travels upstream through the testing area and up the driver tube, accelerating the flow. The expansion wave reflects between the upstream end of the driver tube and the contraction, reducing the stagnation pressure quasi-statically with each reflection from the contraction. Supersonic flow stops when the pressure differential drops too low. The Purdue tunnel uses a double-diaphragm system for the fast-acting valve, and a vacuum tank to get the pressure ratio required to obtain Mach-6 flow. A gate valve has also been added between the diaphragms and the vacuum tank, which allows the tunnel to be opened without pumping the entire vacuum tank up to atmospheric pressure.

Initial designs for the Mach-6 Ludwieg Tube can be found in References 24 and 25. Fabrication details and measurements of constructed hardware can be found in References 26, 27, 28, 29, and 30. The main advantage of the Ludwieg Tube is that it is very economical to run. The requirements for compressors and vacuum pumps are much

less demanding than for a blow-down tunnel. The drawback is that the run-time is only on the order of several seconds. The short run-time is not a major problem as it is possible with computers and digital oscilloscopes to take a large quantity of data in a short period of time.

A schematic of the Purdue facility is shown in Figure 7. The construction is primarily stainless steel from the driver tube to the end of the nozzle. The beginning of the nozzle is highly polished electroformed nickel. Downstream of the nozzle the tunnel is carbon steel. The diaphragms used are acetate or aluminum depending on the initial driver tube pressure, which can range from 5 to 300 psia. The driver tube is heated to 160°C to prevent liquefaction by using direct current through the stainless steel. The air put into the driver tube is dried and filtered to remove particulates and oil. The dew point, when measured, was always found to be -20 to -35 °C. The boundary layer is removed before the throat and routed to one of two locations. The first location is upstream of the diaphragms. This is called the passive bleed system, because when the diaphragms burst, the low pressure in the diffuser pulls the air through the bleed system. The second option is to route the air directly to the vacuum tank. This is called the active bleed system, because a quick-opening valve must be triggered to open after the start of the run. Once the diaphragm bursts, the startup period is approximately 0.25 seconds, though if the active bleed system is used, the tunnel can take up to 2 seconds to become operational. The total runtime is about 5 to 10 seconds.

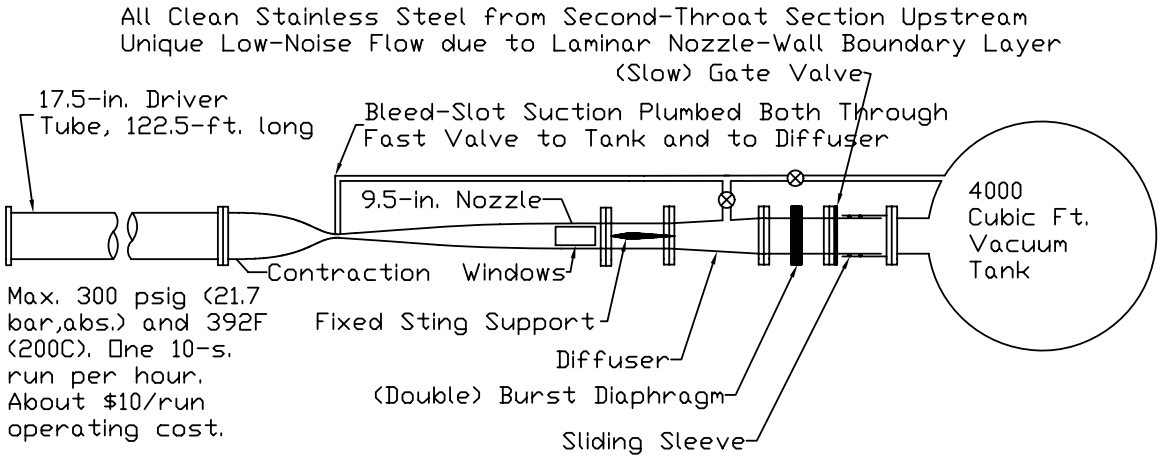

Figure 7: Schematic of the Mach 6 Purdue Quiet Flow Ludwieg Tube.

2.2 Kulite Pressure Transducers

The mean flow and fluctuations are measured in the nozzle using Kulite XCQ-062-15A fast pressure transducers. A picture of this Kulite mounted in a Pitot probe is shown in Figure 8. These semiconductor diaphragm-type transducers have a diameter of about 0.062 inches. The full-scale pressure range is 0-15 psia; the transducers are mechanically stopped above about 18 psia so that the calibration remains stable even though the transducers see full stagnation pressures of up to 300 psia before the run starts. These mechanically-stopped transducers are essential to obtaining sufficient signal-to-noise ratio on the small Pitot pressures obtained at Mach 6 (about 3% of the stagnation pressure). These transducers are compensated for temperatures to 400 °F. The same type of Kulite is also used for measuring static pressure on the tunnel walls, though the static pressure is so low that the accuracy is very limited, so the measurements are useful for qualitative purposes only.

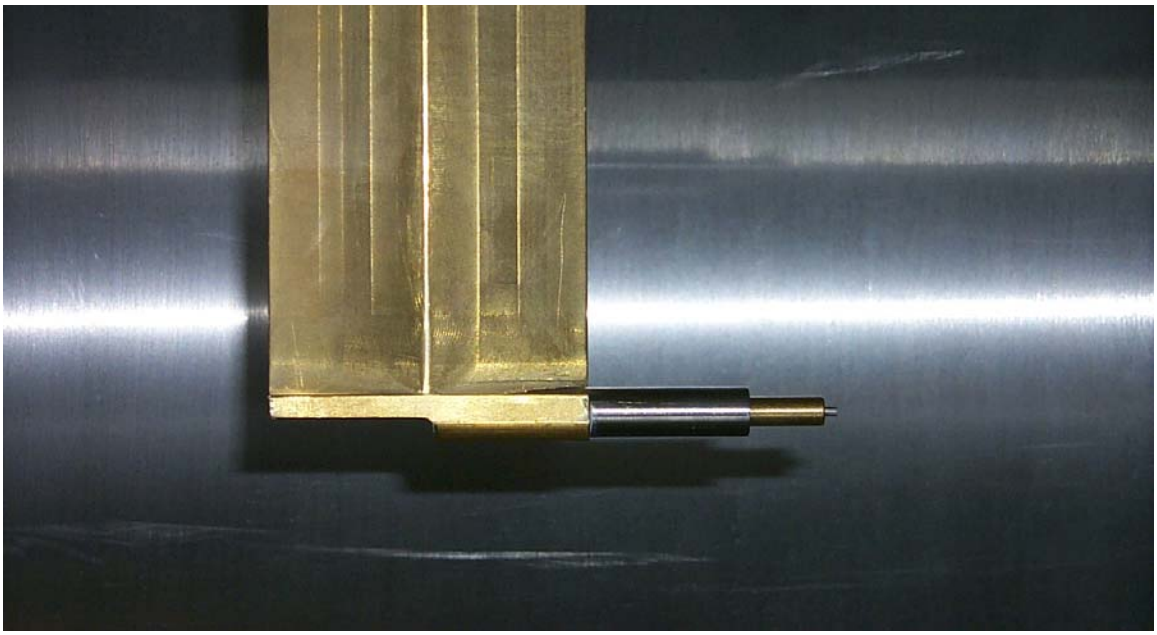

Figure 8: Picture of Kulite mounted in Pitot probe.

A second type of Kulite pressure transducer, model number XTEL-190-200A, is installed flush with the contraction wall, near the entrance to the contraction, at z=-34.5 inches, where z is the distance downstream of the nozzle throat. This Kulite has a diameter of 0.190 inches, a full-scale pressure range of 200 psia, and is compensated for temperatures up to 400 °F. This Kulite measures the static pressure in the driver tube. Because the Mach number is very low, the pressure at the beginning of the contraction can be assumed to be the tunnel stagnation pressure.

A third type of Kulite is installed to monitor the pressure in the plenum for the bleed suction. This XT-123CE-190-300SG Kulite is 0.190 inches in diameter, has a full-scale pressure range of 300 psia, and is compensated for temperatures up to 350 °F.

The signals from all three Kulites are obtained using custom electronics. Voltage-reference chips are used to supply 10.00 V to the transducers. The output signals are amplified by an INA103 instrumentation amplifier chip, supplying a gain of 100. The

output is then high-pass filtered using an RC filter at about 840 Hz, and then amplified by a further factor of 100, to obtain high-resolution measurements of small fluctuations. These Kulite electronics were previously used with the Mach-4 Ludwieg Tube for several years.[31]

2.3 Hot Films

The Pitot probe that is used on the tunnel centerline only indirectly measures what is occurring in the boundary layer of the nozzle. Boundary-layer profiles made with the Pitot probe give some idea of what is happening near the walls, but sometimes cause interference with the boundary layer. To gain additional understanding of the flow near the tunnel wall, a custom Senflex hot-film array was procured from Tao of Systems Integration, Inc. This array, shown in Figure 9 and Figure 10, is attached to a window blank in the last section of the nozzle. The flow direction in Figure 9 is from top to bottom, and in Figure 10 the flow direction is into the picture. The sensors are spaced at 1/4-inch intervals axially along the center of the array. Additionally, there are off-center sensors next to the first, last, and center axial locations. The off-center sensors are located 1/2-inch from the centerline of the array.

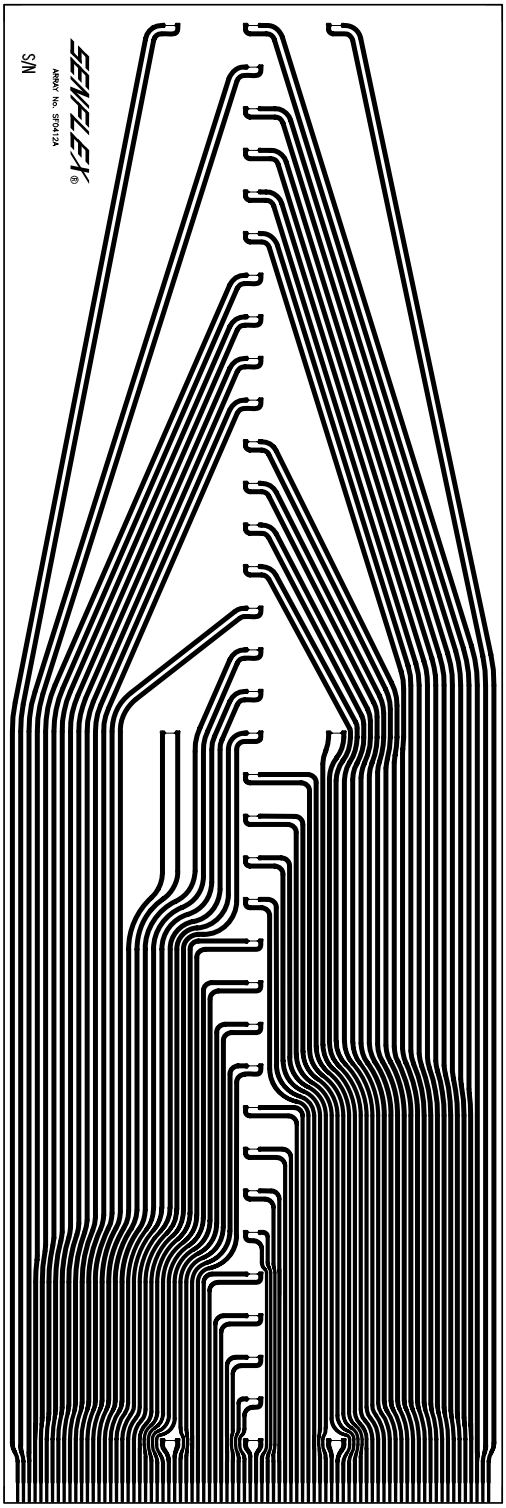

Figure 9: Small hot-film array (9x3 inches).

Figure 10: Picture of hot-film array mounted in the tunnel. Flow is from lower left to upper right.

There are ten Bruhn-6 Constant Temperature Anemometers[32,33] (CTAs) that can be used to take data from ten hot films, simultaneously. Only eight CTAs are shown in Figure 11, due to the limited number of oscilloscope channels. On the front of each CTA is a dial that sets the balance resistance, though the number shown is half of the actual balance resistance. The current through the hot films should be limited to about 100 mA, which corresponds to an overheat ratio of about 1.3, which was used for all of the hot film measurements. The outputs from the CTA are DC (DC-coupled) and DCF (DC Fluctuations). The DCF output can be offset using a trimpot in each CTA. The trimpot was adjusted to keep the initial DC output ±100 mV to allow good resolution on the oscilloscopes. Since the hot films are not calibrated, the actual DC output is not critical,

and the hot film traces that are not AC coupled at the oscilloscope are shown with the pre-run voltage offset to zero.

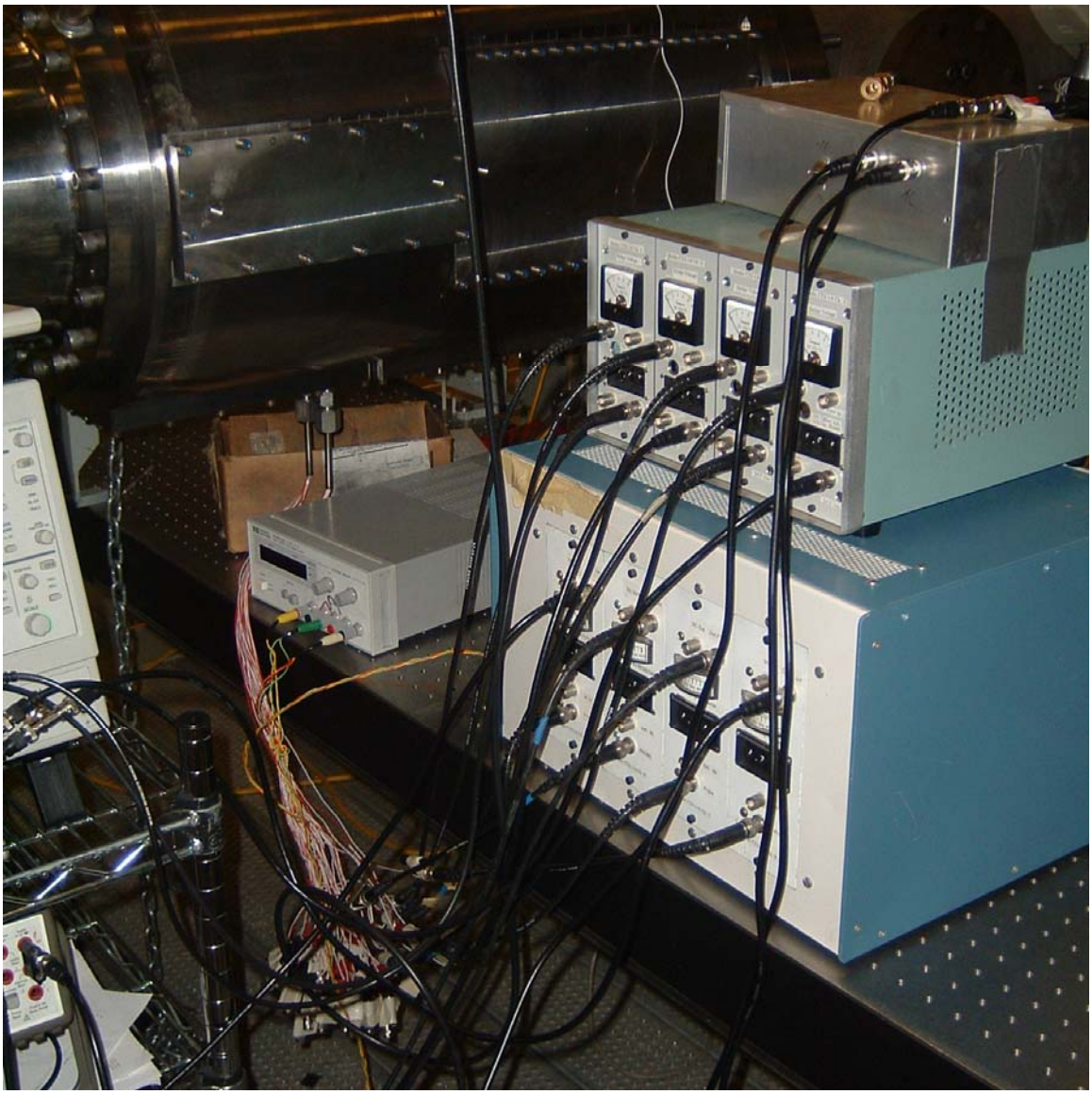

Figure 11: Picture of hot films connected to the constant temperature anemometers.

Using simultaneous data from multiple hot films, it could be possible to see the movement of transition, and also to find separation points by looking for differences in voltage or a phase reversal in the signals from the hot films.[34] The hot films allow direct

information about what is happening at the tunnel wall and a clearer understanding of the conditions of the boundary layer.

2.4 Hot Wires

Since the Kulite Pitot probe can disturb the boundary layer, and hot-film measurements are limited to the surface, hot wires were also used to make measurements in the boundary layer. These should disturb the flow less, because they have a much smaller sensor and probe penetrating the boundary layer. However, the hot wires were also found to disturb the boundary layer when near the wall. The hot wires are made of Platinum 10%/Rhodium, and have a diameter of 0.00015 inches. All of the measurements made with the hot wires were uncalibrated and used a TSI IFA 100 constant temperature anemometer with the 1:1 bridge. A picture of a hot wire in its mount is shown in Figure 12 and a drawing with dimensions is shown in Figure 13. The strut length of 19.9 mm is less than the boundary layer thickness, so interference is expected when the probe is near the wall.

Figure 12: Picture of hot wire in mount.

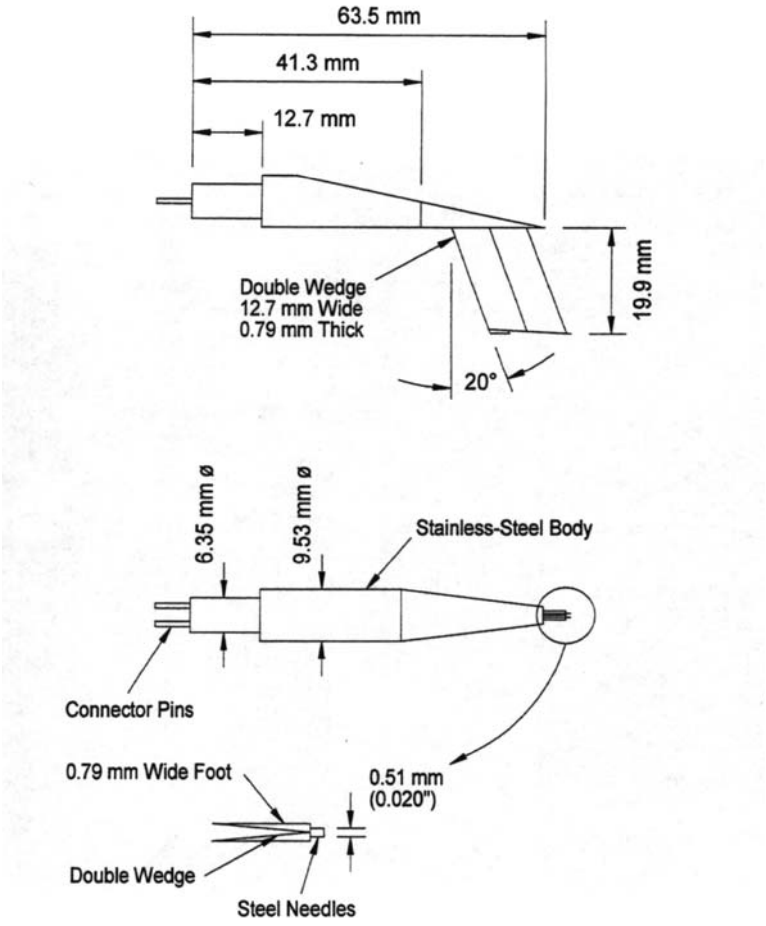

Figure 13: Drawing of hot wire.

2.5 Oscilloscope Data

The data collection was performed using LeCroy and Tektronix oscilloscopes. The LeCroy oscilloscopes used were model numbers 9304AM and 9314AL. The Tektronix oscilloscopes used were model numbers 5034B and 7104. The LeCroy oscilloscopes collected data at 10 or 25 kHz and was used for the data taken with the double wedge, and the hot film traces that were AC coupled. The Tektronix oscilloscopes were used to take the Pitot and hot wire data at 200 kHz, and the hot film data that was DC coupled at 100 kHz. The Tektronix oscilloscopes have a feature called Hi-Res mode that allows data to be taken at about 14 bits at the listed sampling frequencies, while the LeCroy oscilloscopes collect 8-bit data. The Hi-Res mode collects 8-bit data at a much higher rate, averages the data on the fly, then stores the data with more bits.

2.6 Effect of Bleed Lip on Quiet Flow

As mentioned previously, the boundary layer is removed before the throat. This is done at the bleed slot, shown in Figure 14. The bleed lip is very critical in whether the flow is laminar or turbulent in the nozzle, which determines if the tunnel is quiet or noisy. The original nozzle is a nickel-electroform with an extremely fine polish. This nozzle ran quiet with stagnation pressures below 8 psia, though it had been expected to run quiet to pressures as high as 150 psia.

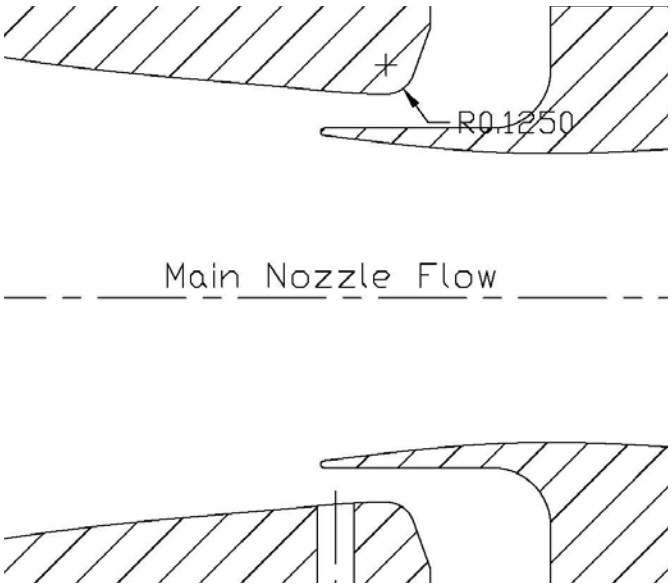

Figure 14: Schematic of bleed slot and bleed lip.

In order to determine what was happening close to the throat, a new aluminum surrogate nozzle was built, shown in Figure 15. This did not have the fine polish of the original nozzle and was not as expensive, so it could have instrumentation put in, without worry of damage. This surrogate nozzle ran quiet to 20 psia initially, about two and a half times higher than the original highly polished nozzle. The end of the surrogate nozzle did not exactly match the contour of the rest of the nozzle as originally built. Initially, there was a backward facing step at z=19.02 inches of about 0.002 inches. The end of the surrogate nozzle was machined to better match the rest of the nozzle, resulting in quiet flow up to 37 psia. The RMS Pitot fluctuations for each of the nozzle configurations, as discussed, are shown in Figure 16. Several runs were each used to get many points for this figure. As the run progresses, the driver tube pressure drops by about 30%. This allows data from a range of pressures in a single run. Each point is calculated using 0.1 seconds of data. The initial driver tube pressures for the runs in this

figure, and in all similar figures in this thesis, can be found in the Appendix. For these and all other runs shown in this dissertation, the initial driver-tube temperature was 160 °C.

Figure 15: Picture of aluminum surrogate nozzle.

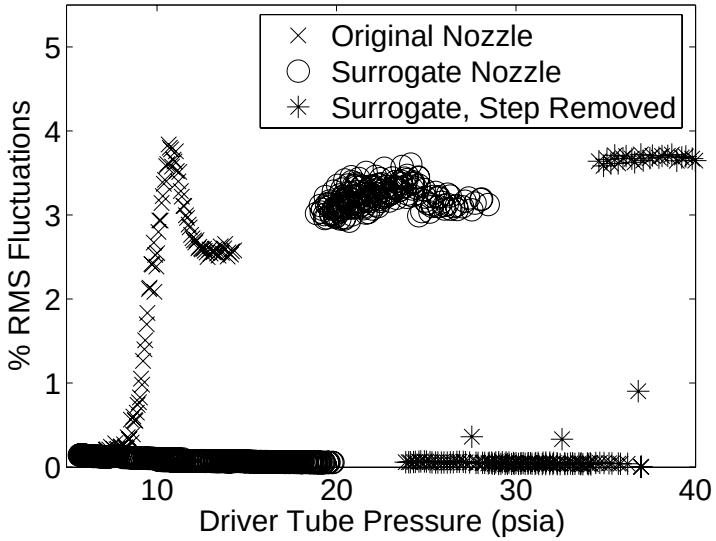

Figure 16: RMS Pitot fluctuations on centerline, at z=75.3 inches, for original and surrogate nozzles.

When the original nozzle throat was built, it was not measured, for fear of damaging the fine polish. Since the less carefully built nozzle was quiet to such higher pressures, the original nozzle was measured to try to figure out why this occurred. The measurements at four different angles are shown in Figure 17. The 90-degree measurement shows a discontinuity in the contour at the edge of the bleed lip. This is also present, to a lesser degree, on the 270-degree measurement. The surrogate nozzle was also measured for comparison, as shown in Figure 18. These measurements show much smoother contours, which is clearly the reason for the improved performance. It is believed that when the electroform was removed from the original mandrel, the original nozzle was distorted slightly out of round. The bleed lip was then machined assuming an axisymmetric nozzle. This created a slight slope discontinuity, resulting in a severe reduction in quiet flow.

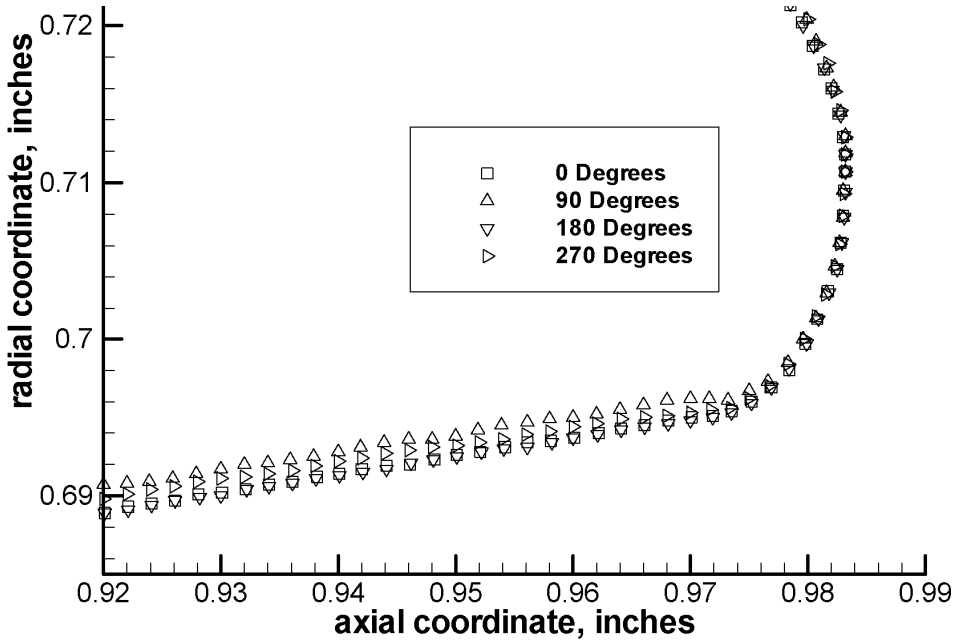

Figure 17: Measurements of original nozzle.

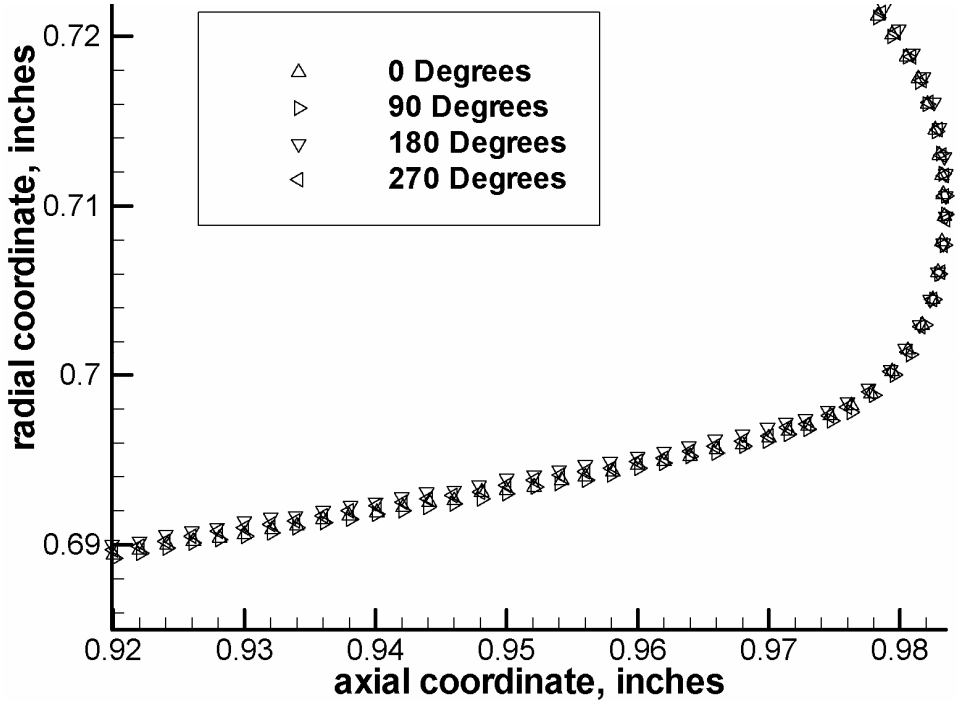

Figure 18: Measurements of surrogate nozzle.

2.7 Active and Passive Bleed Systems

The bleed system that was used for all of the runs previous to this section was a passive system. This system, described in detail in Reference 27, could possibly be responsible for large noise levels in the diffuser that feed forward. It was passive because the bleed flow was reintroduced to the tunnel upstream of the diaphragm section, so the bleed flow started automatically when the tunnel was started. The passive system was replaced with an active system that directed the bleed flow directly to the vacuum tank. The active system uses a fast-acting valve that is triggered when the run starts, to activate the bleed slot flow. The tunnel schematic in Figure 7 shows the routing of these systems.

Figure 19 shows pressure traces from the Pitot on the centerline at z=75.3 inches, the contraction Kulite, and the plenum Kulite for a run with an initial driver tube pressure of 14.571 psia. The AC Pitot trace shows Pitot data that has been high-pass filtered to allow examination of the Pitot fluctuations. The plenum Kulite trace shows that about 1.5 seconds after the flow started, the air had been sucked out of the bleed lines, which is significantly longer than the 0.25 seconds required with the passive system.[35] The contraction trace shows a slight increase in slope when the bleeds begin working, indicating that the massflow out of the driver tube increases at this time, as expected. At this pressure, there appears to be little change in the DC or AC Pitot traces, as the flow is noisy, whether the bleeds are open or closed.

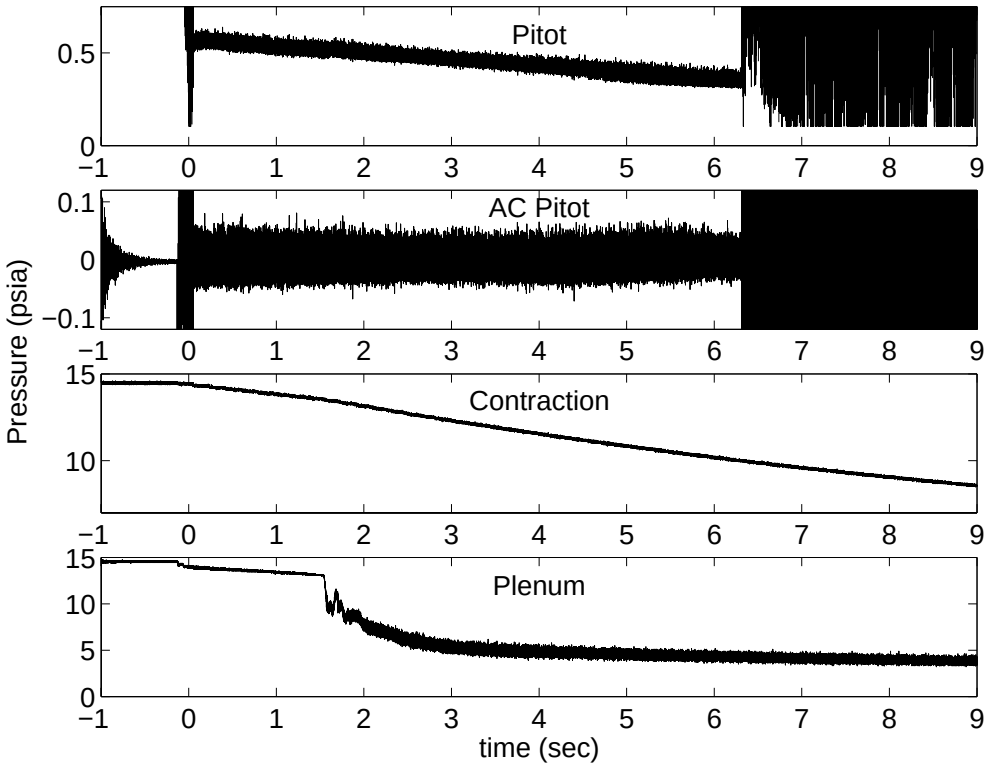

Figure 19: Traces showing timing with an initial driver-tube pressure of 14.5 psia.

Figure 20 shows similar data for a run with an initial driver-tube pressure of 7.98 psia. The plenum pressure seems to drop at about the same time in the run, but there is an oscillation present after this, because the bleed-system valve requires a pressure difference across it to hold it open. At the low pressures used here, there is barely enough pressure difference, and the valve flaps. The Pitot traces show noisy flow at the beginning of the run, when the bleed system is inoperable, and this drops to quiet flow after the pressure in the suction plenum has dropped low enough to allow choked flow through the bleed slot. The Pitot trace seems to have intermittent quiet flow near the beginning of the active bleed-slot flow, due to the plenum pressure oscillating above and below the pressure ratio necessary for choked flow. Once there is choked flow in the

bleed slot, the fluctuations in the suction plenum do not appear to feed forward and affect the main flow, indicating successful isolation of the contraction from the suction piping.

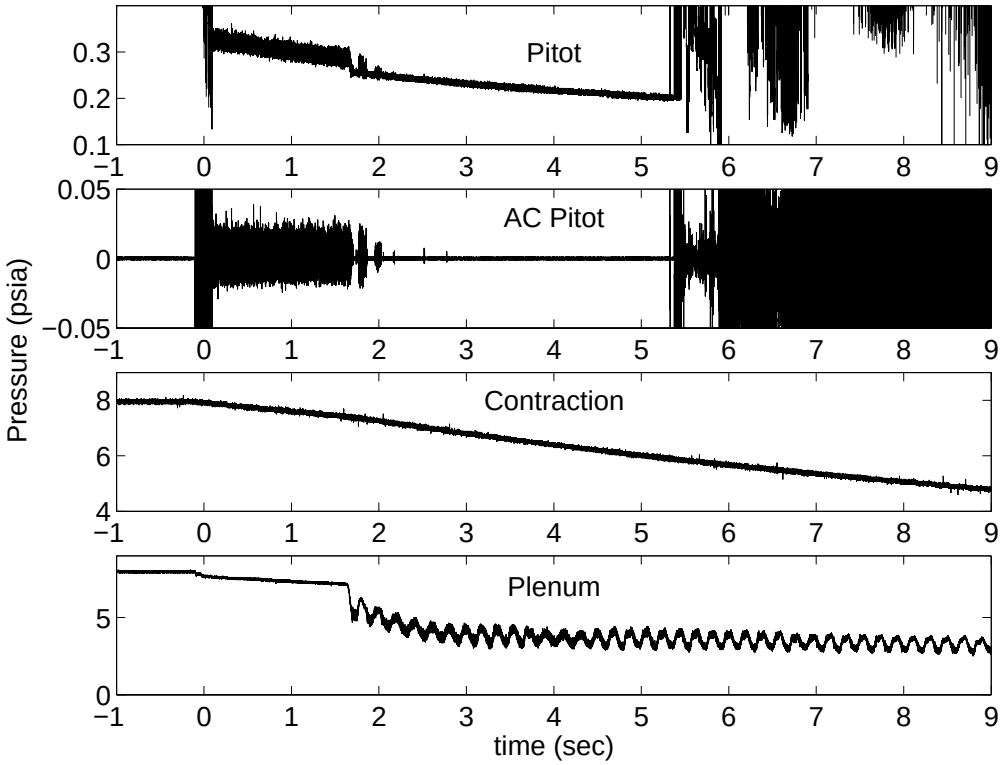

Figure 20: Traces showing timing with an initial driver tube pressure of 8 psia.

In general, the passive system is preferred because it increases the amount of time that the tunnel operates with laminar boundary layers. If it is found that the jets from the bleed system entering the diffuser cause problems that cannot be avoided, it would be advisable to try to replace the "quick" opening valve on the active bleed system with one that is not dependent on the pressure differential to open.

CHAPTER 3 – DIFFUSER EFFECTS ON UPSTREAM FLOWFIELD

This chapter describes measurements showing that disturbances generated in the diffuser can influence the flow upstream in the nozzle. The result of these disturbances is very little useful Mach-6 flow when the tunnel is operating with laminar boundary layers. The separations examined in this chapter show the problems that the shock/boundary-layer interactions in the diffuser cause and the sources of these interactions. Attempts to reduce the distance upstream that the separation extends are detailed in the following chapters.

3.1 Effects of Diffuser Configuration with Double Wedge

Tests were performed examining the effect that the configuration of the tunnel diffuser has on the nozzle flow. Immediately downstream of the nozzle was a double wedge that acted as a second throat for the tunnel, shown in Figure 21. At the center of it was a sting mount, which allowed a 2-inch diameter sting to be screwed into the double wedge, enabling the use of models. A schematic of the double-wedge sting mount in the tunnel is shown in Figure 22 and a complete description can be found in Reference 27.

Three configurations were examined by changing the models supported from the sting mount. The first configuration used a 2-inch base diameter blunt cone, with a nose radius of about 1/4 inch and about a 30-degree half angle, mounted in the sting mount. This is shown in Figure 23. The second configuration used nothing in the sting mount, which left an open hole down the center, and likely produced jets shooting out of holes in the center of the double wedge, about a third of the way down its length, shown in Figure 24. The third configuration used a 2-inch diameter, flat-faced cylinder in the sting mount.

Figure 21: Picture of the front of the double wedge.

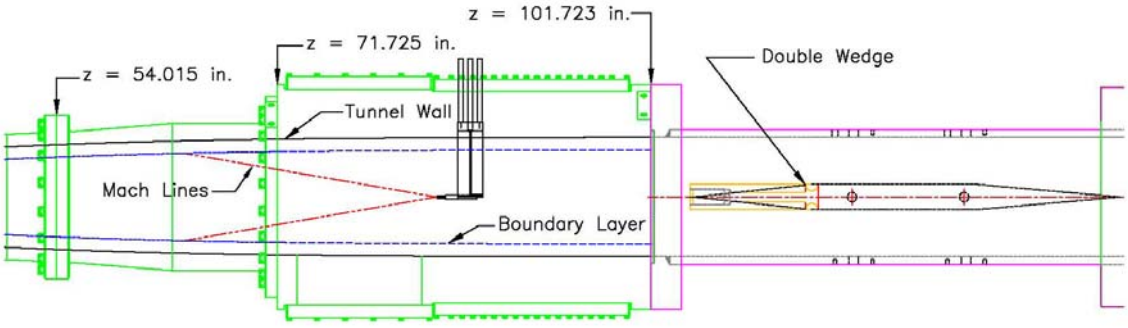

Figure 22: Schematic of double wedge sting mount in diffuser.

Figure 23: Picture of 2-inch diameter blunt cone.

Figure 24: Picture of the side of the double wedge viewed through a porthole.

3.1.1 Pitot Data with Double Wedge

Figure 25 shows Pitot pressure traces for the three different configurations. The data in Section 3.1 was taken with the original nozzle, so driver-tube pressures above 8 psia have a turbulent boundary layer, and below 8 psia the boundary layer is laminar. These traces all had an initial driver tube pressure of 14.2 psia (±1%) and had the Pitot probe placed on the centerline at z=84.3 inches. A schematic of this is shown in Figure 22. The cases with the empty sting mount and the cylinder in the sting mount show much higher fluctuations early in the run than in the case with the blunt cone. The early fluctuations are followed by even higher fluctuations before dropping down to a noise level similar to the noise seen with the cone. The effect is similar when the initial driver-tube pressure is 45 or 80 psia. However, at lower pressures of 8 and 10 psia, or at a higher pressure of 130 psia, there is little difference between the three cases. Figure 26 shows the cases with an initial driver tube pressure of 7.85 psia (± 2%). It is interesting that the downstream flow can affect the upstream flow so significantly since information does not travel upstream in a supersonic flow. This appears to be a shock/boundary layer interaction causing upstream separation, as discussed in Chapter 1. This data shows that disturbances in the diffuser can have a very large impact on the flow in the nozzle.

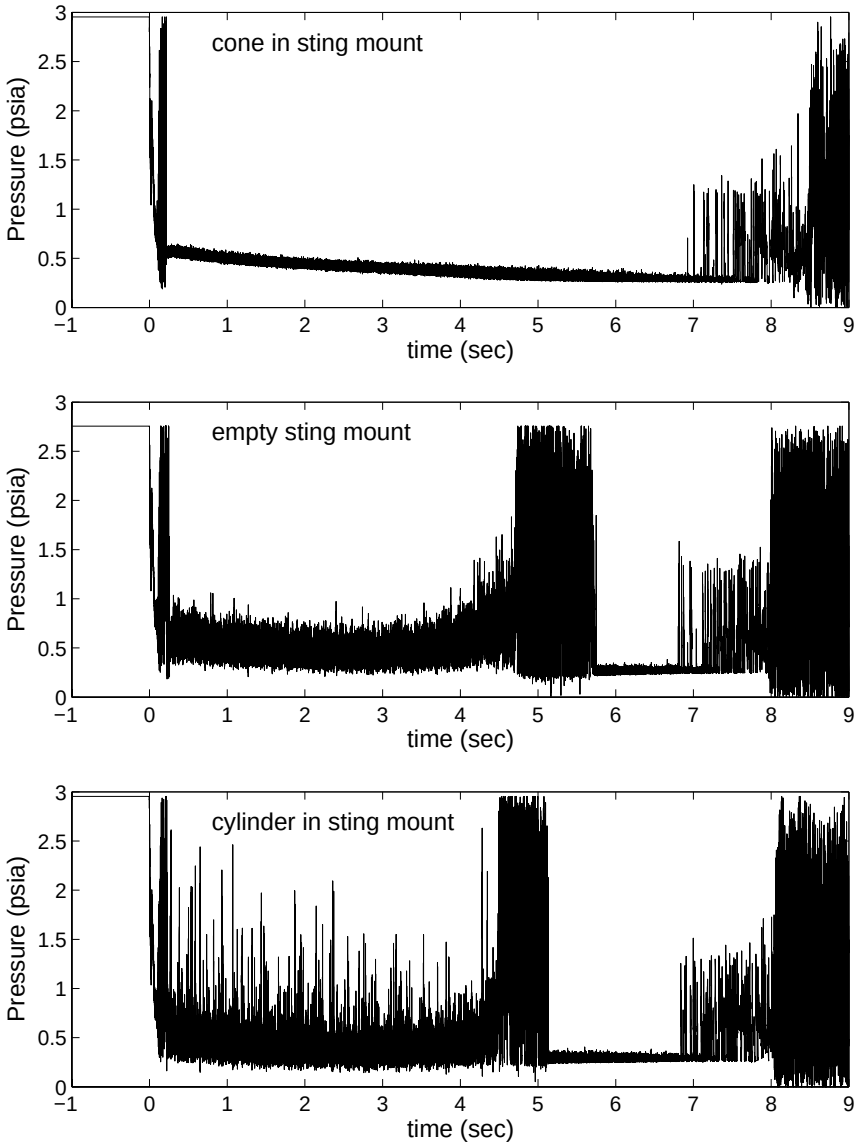

Figure 25: Pitot traces at 14.2 psia with different double-wedge sting mount configurations.

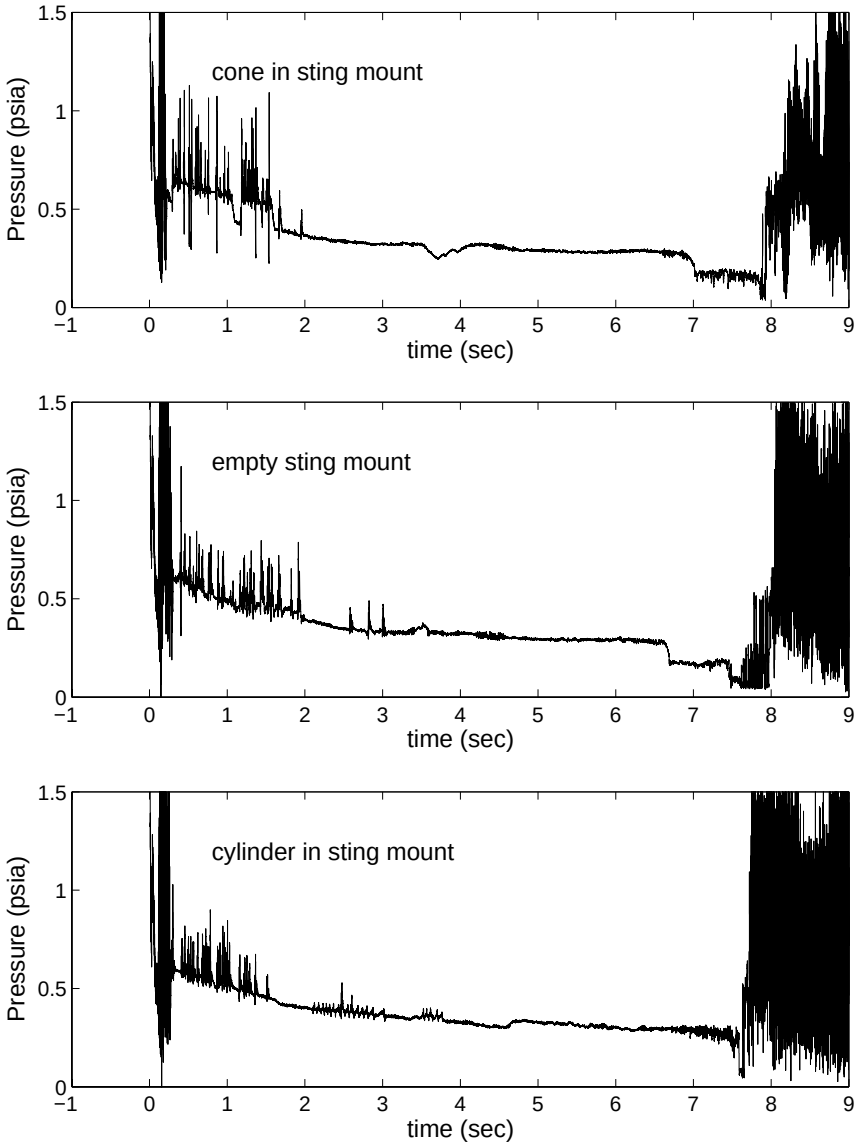

Figure 26: Pitot traces at 7.85 psia with different double-wedge sting mount configurations.

3.1.2 Sidewall Kulite Measurements with Double Wedge

Twenty ¼”-20 holes were drilled and tapped in the double wedge section at five different axial locations. At each axial location there are four holes located at 45, 135, 225, and 315 degrees azimuthal angle, measured clockwise from the top when looking downstream. These holes allow Kulites to be placed flush with the wall and measure the static pressure in the diffuser. Two Kulites were used to get static pressure at two different locations at the same time. Since the static pressure at Mach 6 is less than 0.01 psia when the stagnation pressure is less than 1 atmosphere, it is not expected that the XCQ-062-15A Kulite is very accurate. The accuracy is quoted to be 0.1% of full scale, or 15 psia, which results in an accuracy of 0.015 psia.

Figure 27 shows sample traces of the Pitot pressure on the centerline at z=84.3 inches, along with static traces at two different axial locations. The diffuser Kulites were at 135 degrees clockwise from the top azimuthally when looking downstream, and were at z-locations of 104.85 inches (before the double wedge) and 132.75 inches (after the double wedge). The initial driver tube pressure was 14.3 psia for these runs. The configurations tested were with the 2 inch blunt cone in the sting mount and with the sting mount empty.

In parts (a) and (b) it can be seen that the flow quality is markedly worse with the empty sting support. This is probably because the shock from the blunt face of the empty sting mount is more severe, and there are jets out of the side of the double wedge, further disrupting the flow. Parts (c) and (d) and parts (e) and (f) show a much different static profile between the two cases as well. It is interesting that the noise is larger in front of

the double wedge with the empty sting (comparing d and f) and larger behind the double wedge with the blunt cone (comparing c and e).

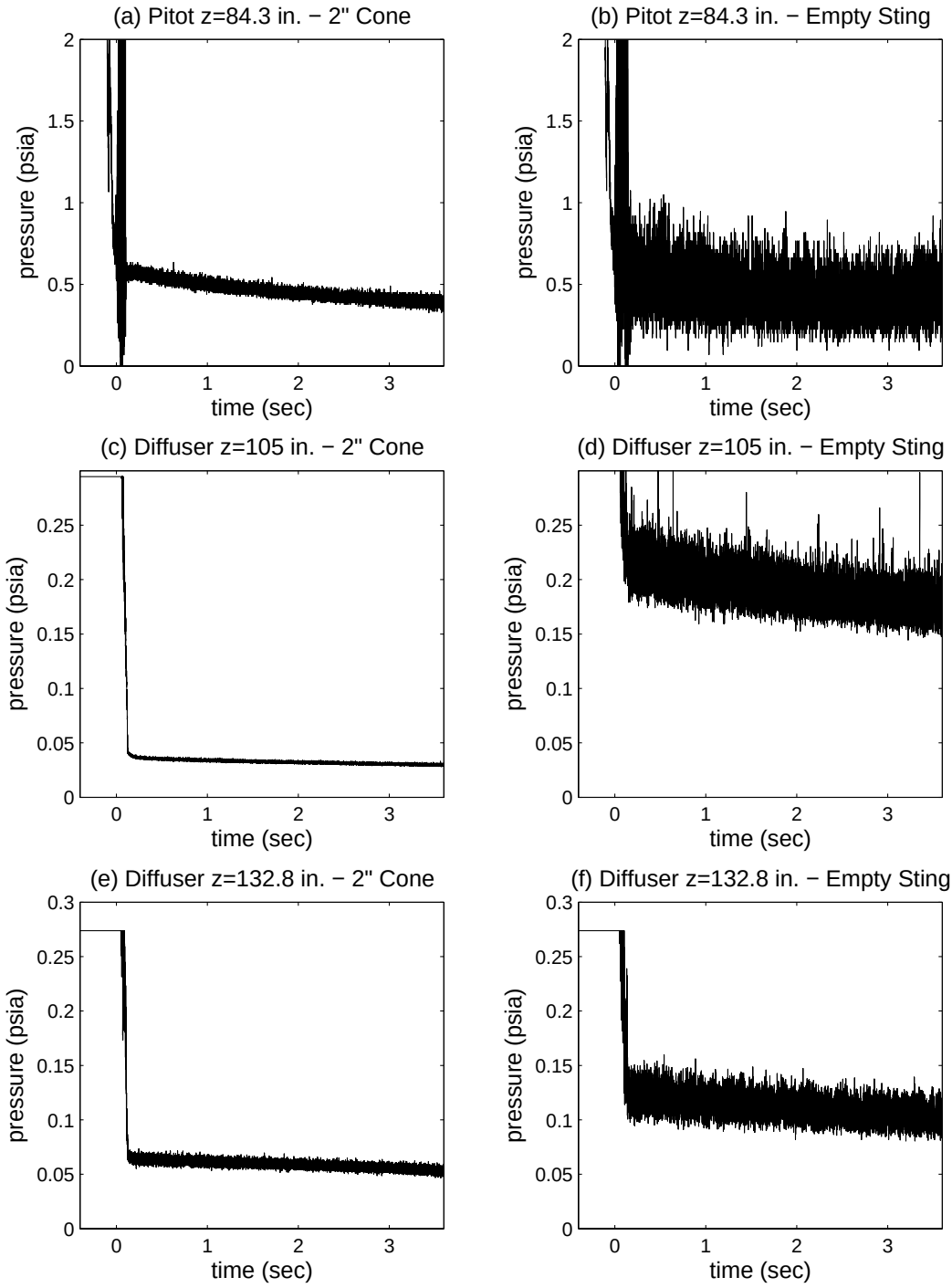

Figure 27: Pitot and static diffuser traces for 14.3 psia driver tube pressure.

Figure 28 shows a similar set of traces for an initial driver tube pressure of 10 psia. In comparing the blunt cone and empty sting cases, there does not seem to be much difference at this pressure for the Pitot or diffuser traces. It should be noted that when the pressure rises in the Pitot traces in parts (a) and (b), there doesn't seem to be any noticeable change in the diffuser traces. The pressure rise in the Pitot trace corresponds to the pressure that the boundary layer in the nozzle changes from turbulent to laminar, as discussed in Section 2.5. It is possible the flow is separated in the diffuser whether the incoming boundary layer is laminar or turbulent. When it is laminar, however, the separation can extend further upstream so that the effects can be seen with the Pitot probe. While using a blunt cone improves the flow quality over the empty sting mount, this is still far short of the quiet flow that is desired.

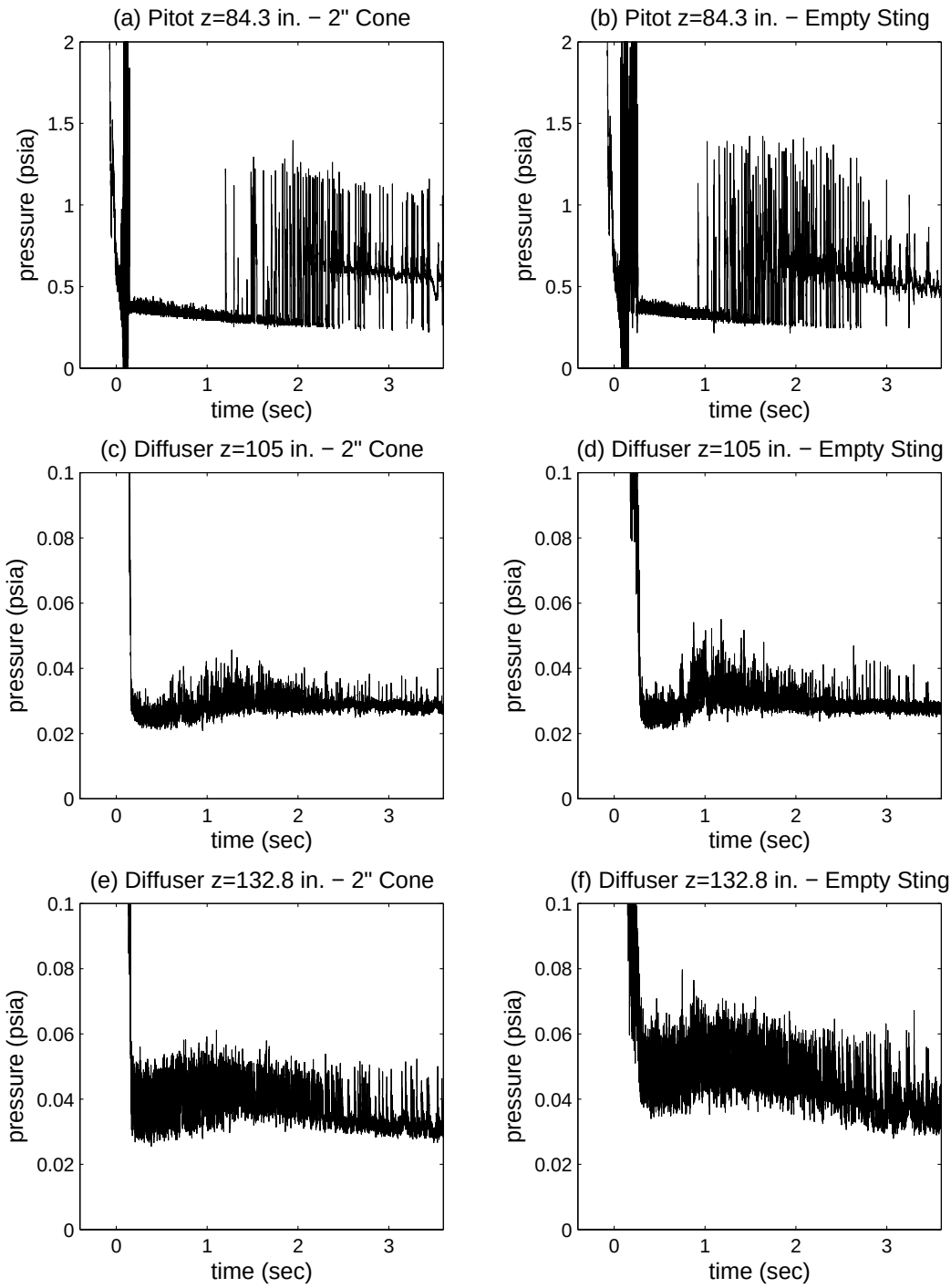

Figure 28: Pitot and diffuser traces for 10 psia driver tube pressure.

A 3-inch diameter sharp cone with a 14-degree half angle, shown in Figure 29, was also placed in the sting mount, as this was believed to generate a weaker shock than the blunt cone. The traces using the sharp cone did not differ significantly from those using the blunt cone. Figure 30 through Figure 32 show data for two runs with initial driver tube pressures of 14.417 psia for the 2" blunt cone run, and 14.486 psia for the 3" sharp cone run. Figure 30 shows Pitot measurements at z = 75.3 inches, Figure 31 shows static pressure in the diffuser at z = 105.0 inches, and Figure 32 shows static pressure in the diffuser at z = 132.75 inches. All of these plots show nearly identical traces for the run using the 2" blunt cone and the one using the 3" sharp cone. This indicates that the strength of the shock impinging on the wall is not much different than the blunt cone, or that this shock from these models is not the primary disturbance source.

Figure 29: Picture of 3-inch diameter sharp cone.

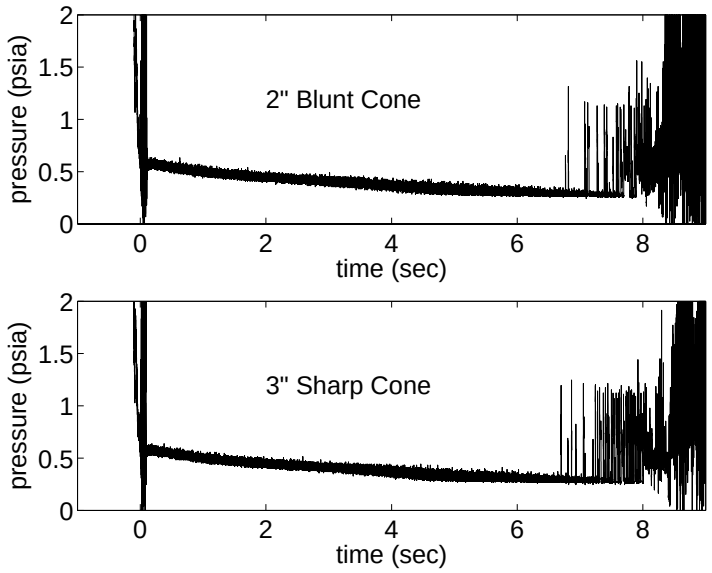

Figure 30: Pitot pressure at z=75.3 inches.

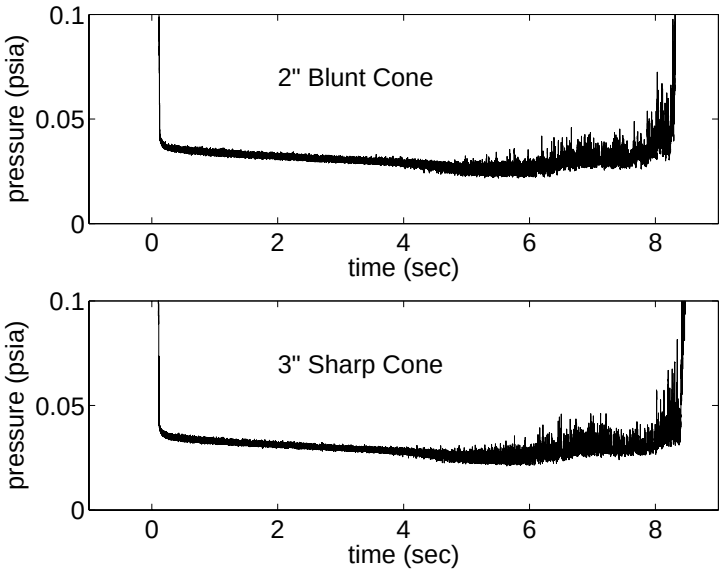

Figure 31: Diffuser static pressure at z=105.0 inches.

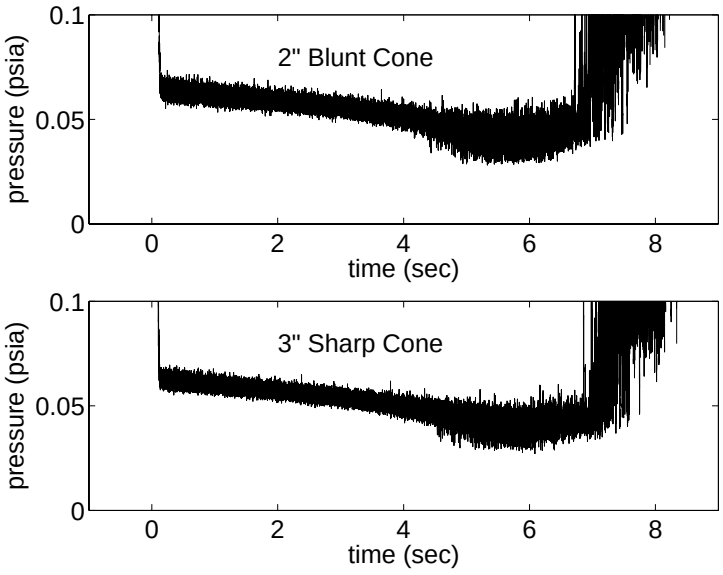

Figure 32: Diffuser static pressure at z = 132.75 inches.

3.1.3 Double Wedge with Blunt Cone

The best case with the double-wedge sting support is with either the 2-inch blunt cone or the 3-inch sharp cone, as these have the lowest levels of disturbances. With the blunt cone, there is a large decrease in Mach number when the pressure drops below about 9 psia, as shown in Figure 33. The figure shows data from five different runs. Each point uses 0.1 seconds of data, allowing data points to be calculated at a range of driver tube pressures in a single run. The Mach number is calculated with the Rayleigh Pitot formula using stagnation pressure after the shock from the Pitot probe and the freestream stagnation pressure as measured in the beginning of the contraction. Further information about the runs used to make this plot and all similar plots can be found in

Table 1 in the Appendix. The decrease in Mach number corresponds to the pressure at which the nozzle begins to have laminar boundary layers as discussed in the Section 2.5.

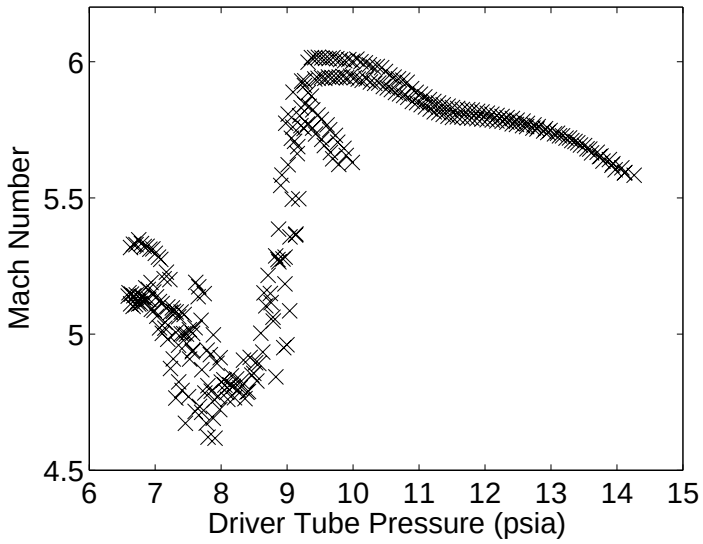

Figure 33: Mach number with double wedge using Pitot probe on centerline at z=84.5 inches.

Figure 34 shows the RMS Pitot fluctuations for the same data. The decrease in Mach number corresponds to a huge increase in fluctuations. Quiet flow would be considered anything below about 0.1 percent, though quiet flow is shown in this figure with levels slightly higher, due to electronic noise. At driver tube pressures above 12 psia, the fluctuations are 3.5 to 4 percent, which is caused by turbulent boundary layers. As the driver tube pressure decreases below 12 psia, there is a slight increase in noise caused by turbulent spots as the flow begins to become laminar. Around 9 psia the large fluctuations occur, though there is some data that shows quiet levels that are intermittent with the huge fluctuations. The large fluctuations are caused by an unsteady separation resulting from a shock from the double wedge impinging on the tunnel wall. This

separation does not propagate as far forward when the boundary layers are turbulent since turbulent boundary layers are much more difficult to separate. [36]

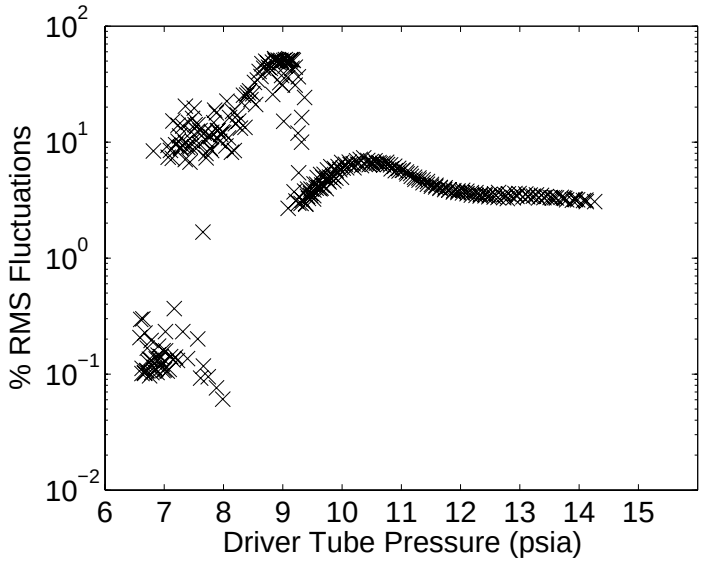

Figure 34: Percent RMS fluctuations with double wedge (with blunt cone) using Pitot probe on centerline at z=84.5 inches.

It is possible to trip a turbulent boundary layer at the beginning of the nozzle by closing the bleed valves to prevent air from being sucked through the bleed system. Figure 35 shows the comparison between the bleeds open and bleeds closed cases. The initial driver-tube pressures for these runs were 10.02 and 10.01 psia, respectively. When the bleeds are closed, the boundary layer is turbulent and there is no separation. This verifies that the fluctuations below 9 psia are due to the boundary layer becoming laminar and not to some other change occurring as the driver-tube pressure drops.

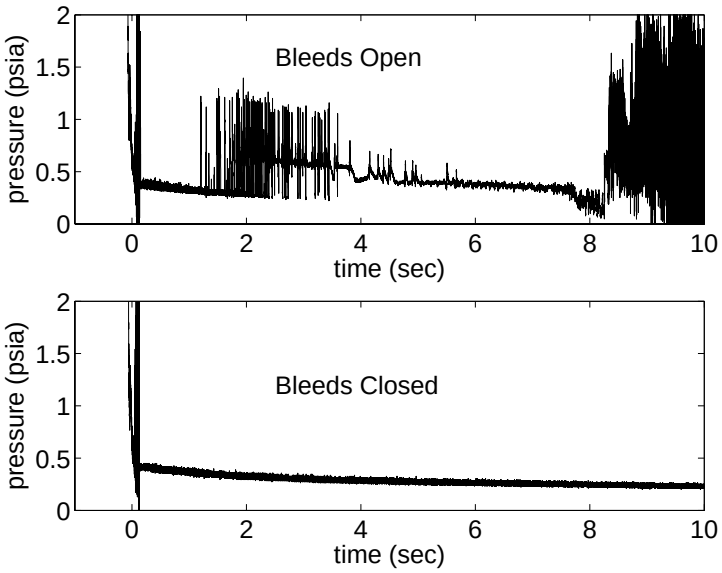

Figure 35: Comparing bleeds-open to bleeds-closed cases.

3.2 Measurements with No Sting Mount

Since there was such a large effect from placing different objects in the sting mount of the double wedge, it was decided to examine the effect of removing the double wedge completely. If this was the cause of the separation, then the separation would disappear with the double wedge removed.

3.2.1 Pitot Data with No Sting Mount

Figure 36 compares the flow quality with and without the double wedge. All of the data shown in this and all following sections had an incoming laminar boundary layer on the tunnel wall, unless otherwise noted. This required that the surrogate nozzle throat

be used for all runs with driver-tube pressures above 8 psia. The Pitot probe was located at z=84.3 inches for both cases, as shown in Figure 22. The data shown here is from two runs, both with an initial driver tube pressure of 7.98 psia. Figure 36 shows that with the double wedge removed, the flow is attached for most of the run, except for a few isolated spots late in the run in which a separation becomes evident. Removing the double wedge reduced, but did not fully eliminate, the separation problem.

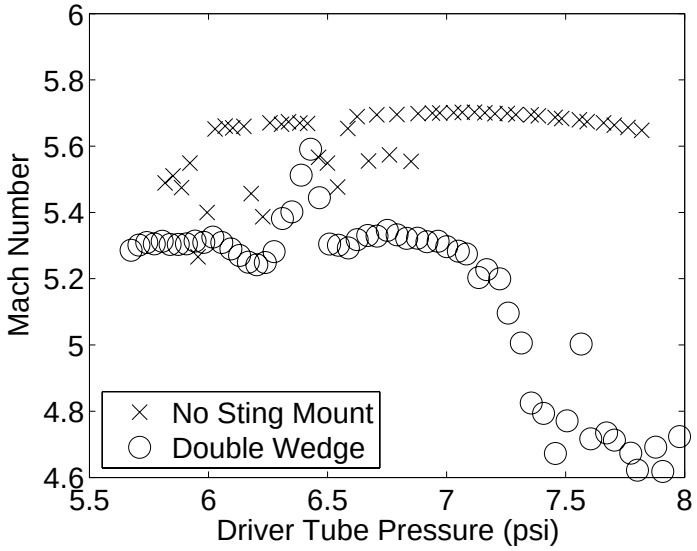

Figure 36: Comparison of Mach number on centerline at z=84.3 inches, with and without the double wedge.

Figure 37 and Figure 38 show the effect of axial location on the separation observed with the sting mount removed. The Pitot probe was placed at z-locations of 75.3, 84.5, and 93.5 inches. Figure 39 shows a schematic of the longer Pitot probe at z= 75.3 inches and the short probe at z=93.5 inches. Only one probe can be placed in the tunnel at a time, and either probe can be moved to measure at z=84.5 inches. The initial driver tube pressure was 8.03 psia for all three runs. The Pitot probe shows flow that is rarely separated at z=75.3 inches, a little more separated at z=84.5 inches, and always

separated at z=93.5 inches. It is unknown why the Mach number is lower at z=84.5 inches than it is at z=75.3 inches when no separation is apparent. Figure 38 shows again that the noise levels are extremely high when the unsteady separation occurs. This large noise level ranges from about 20 to 50 percent.

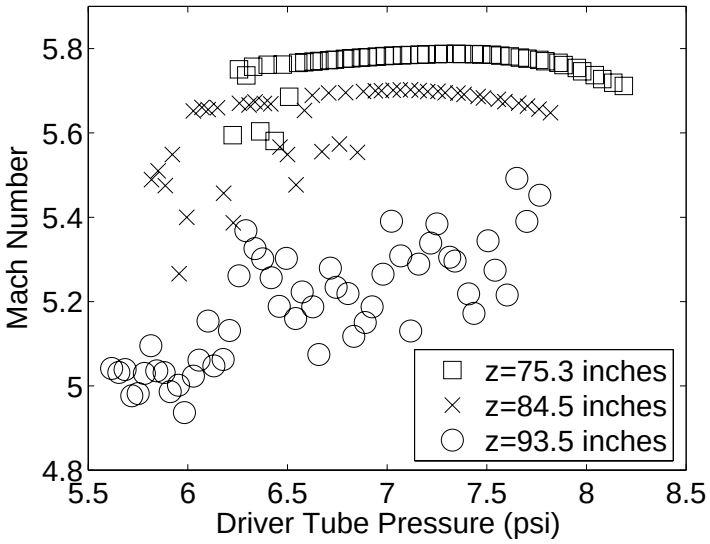

Figure 37: Effect of axial location on Mach number with pressure below 8 psia.

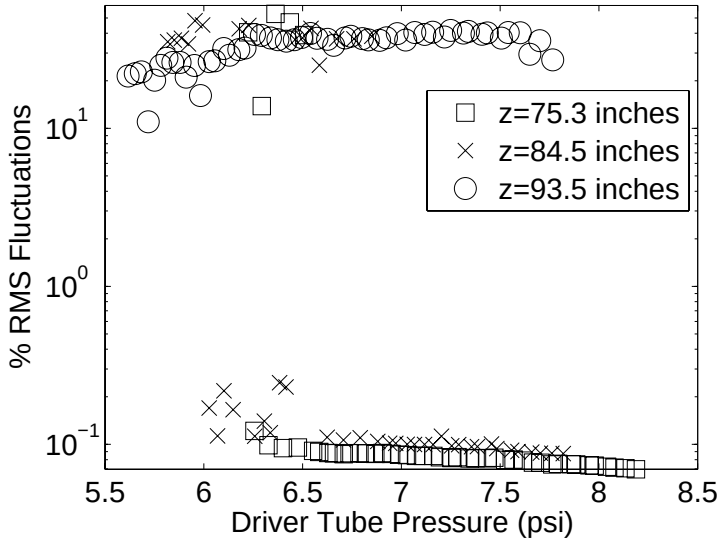

Figure 38: Effect of axial location on noise with pressure below 8 psia.

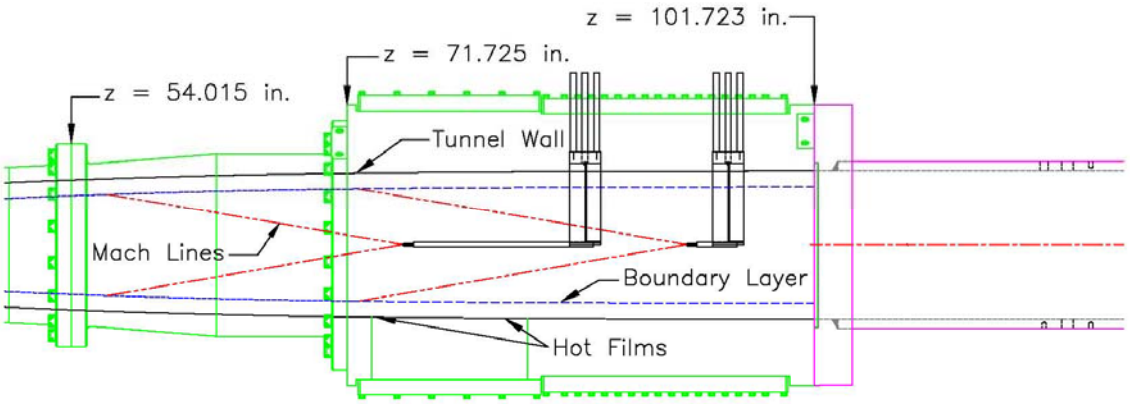

Figure 39: Schematic showing a Pitot probe at z=75.3 inches and one at 93.5 inches.

Figure 40 and Figure 41 show the effect of axial location on the separation observed with the sting mount removed at higher pressures. These runs were performed with the surrogate nozzle, so the beginning of the nozzle had laminar boundary layers over a larger pressure range, as discussed in the Section 2.5. The figures show that the higher-pressure flow remains attached as far back as can currently be measured with a Pitot probe on the centerline. The noise levels indicate quiet flow at all of these axial locations.

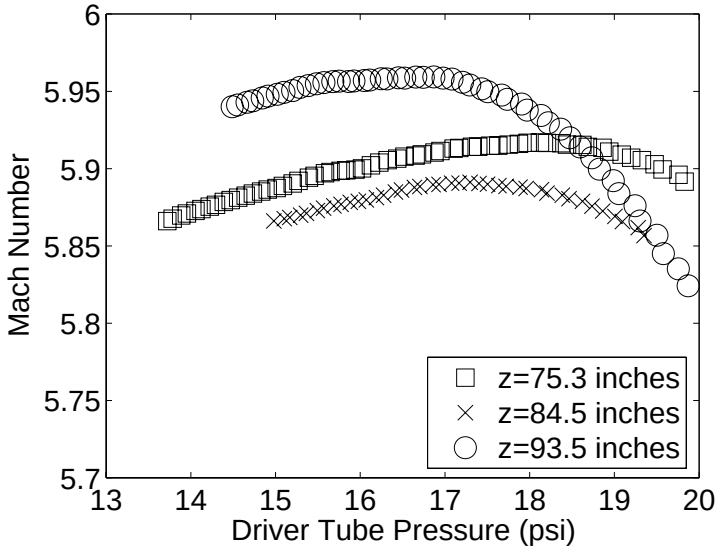

Figure 40: Effect of axial location on Mach number with Pitot at z=84.5 inches and pressure below 20 psia.

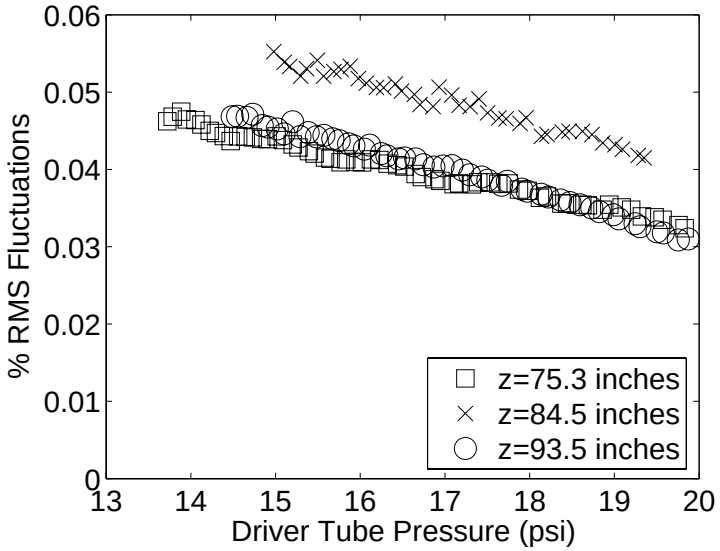

Figure 41: Effect of axial location on noise with Pitot at z=84.5 inches and pressure below 20 psia.

3.2.2 Hot-Film Measurements with No Sting Mount

Measurements with laminar boundary layers do not cause any evident fluctuations above the electronic noise of the hot films. Figure 42 contains a section of a run with an initial driver tube pressure of 8.03 psia, showing disturbances with the sting mount removed. The top trace shows the Pitot probe at z=93.5 inches and the bottom three traces are from hot films at various axial locations. The acoustic origin of the Pitot probe is approximately 73 inches, which is very close to the front hot film sensor. There are corresponding fluctuations on all sensors at approximately the same times, although the Pitot is on the centerline with an acoustic origin well upstream. The hot films show that the fluctuations are largest near the aft sensor and decrease further forward. Some of the smaller fluctuations in the z=80.70-inches trace do not propagate forward to the other hot film locations. This indicates that the disturbances are diminishing as they travel forward.

When a single fluctuation is examined more closely, the movement of the separation can be seen in time, as shown in Figure 43. The disturbance appears on the hot film at z=80.70 inches at approximately 0.435 seconds into the run. This disturbance does not show up on the hot film at z=73.45 inches until about 0.438 seconds, which gives a convection speed of the disturbance of about 60 m/sec.

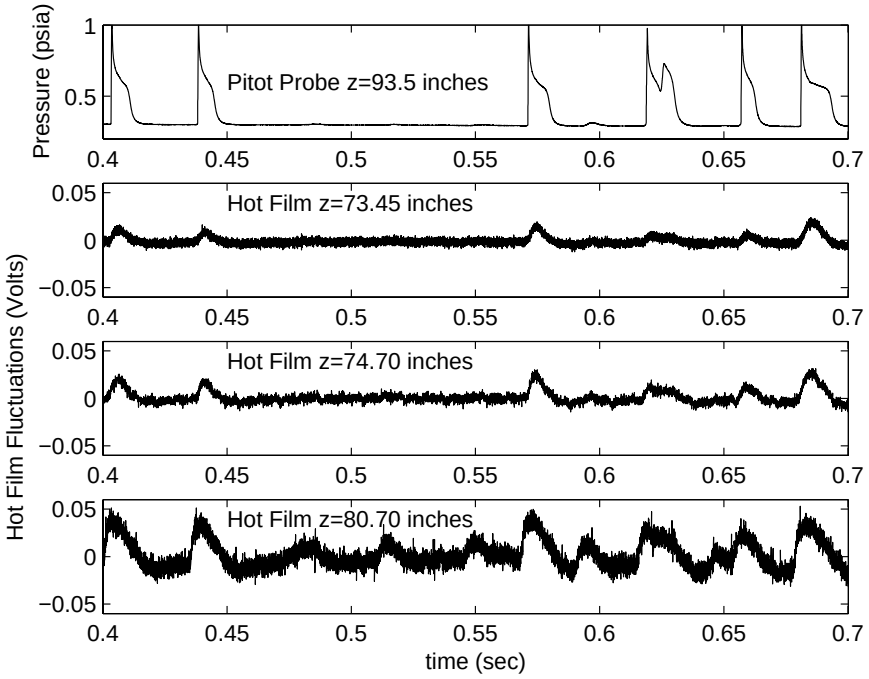

Figure 42: Pitot and hot film data showing unsteady disturbances with no sting mount.

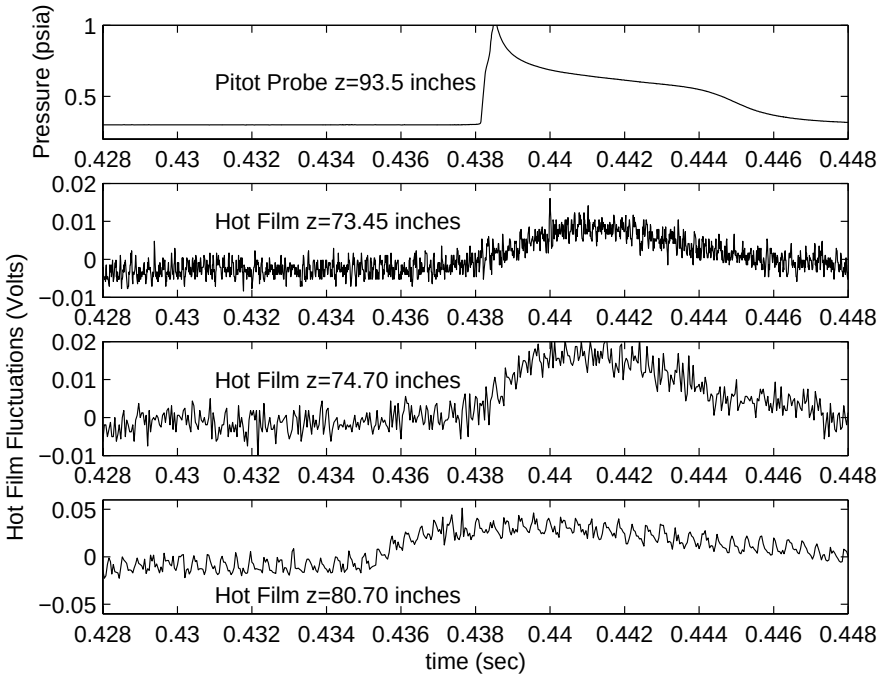

Figure 43: Close-up of unsteady disturbances traveling forward.

3.2.3 Boundary-Layer Measurements with No Sting Mount

Boundary-layer profiles were obtained to get direct information about the boundary layer. The Pitot probe gives indirect information about the boundary layer very far forward, and the hot films give information about what is happening at the wall. The purpose of the profiles was to verify that there are indeed unseparated laminar boundary layers when the sting mount is removed, though difficulties with probe interference caused the measurements to not be as clean as desired. The profiles also give an idea of the thickness of the undisturbed boundary layer.

With the double-wedge sting mount, there was never an unseparated laminar boundary layer that extended to z=75.3 inches, near the end of the nozzle where it could have been measured. With the sting mount removed, it was possible to obtain laminar boundary layer profiles. A schematic of the Pitot probe in the boundary layer is shown in Figure 44. Pitot boundary-layer profiles were measured using two methods. The Pitot probe was held by a traverse that could be programmed to move throughout the run. Because the probe moved during the run, each point was taken at a different time in the run, and a different driver-tube pressure, since the driver-tube pressure falls during runs. The other method was to move the probe only between runs, which allowed points to be compared at the same time after the run started and at the same driver tube pressure.

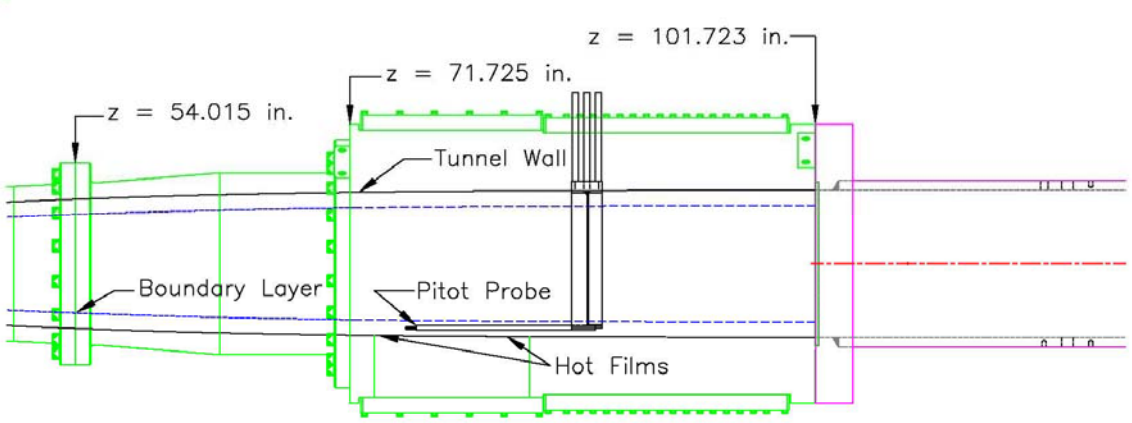

Figure 44: Schematic of the end of the nozzle with the Pitot probe in the boundary layer at z=75.3 inches.

Figure 45 shows boundary layer profiles where the data at each height is taken from a different run. The initial driver tube pressures were 20.00 psia (± 0.40%) for the ten runs used in the profile. Profiles are shown with data averaged for 0.1 seconds starting at 0.5, 1.3, 2.4, and 3.4 seconds after the start of the run. The average driver tube pressures during these times were, 19.57, 18.61, 17.31, 16.23 psia (± 0.35%), respectively. The freestream pressure is different for each time period because of the stagnation-pressure drop throughout the run. The experimental data is compared to the results from a finite-difference boundary layer method. The mean flow was computed using the method of characteristics for the nozzle, assuming a 1/4-inch displacement thickness, which is expected at the design stagnation pressure of 150 psia. The boundary-layer computations were then performed using the stagnation pressures and stagnation temperatures calculated at each time using isentropic relations, assuming an initial stagnation temperature of 160 °C. The core flow pressure is slightly low for each of the times shown. This is because at a lower stagnation pressure, the boundary layer thickness

is larger, resulting in a smaller area ratio, which gives a lower core Mach number and a higher Pitot pressure. Other than this slight difference, the agreement is very good.

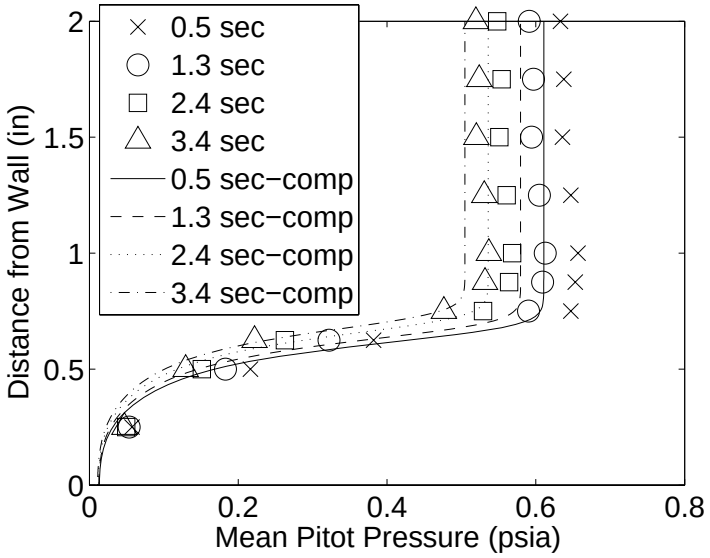

Figure 45: Boundary-layer profiles at z=75.3 inches and initial pressure of 20 psia.

In order to counter the effect of the pressure drop, the pressures are nondimensionalized by the stagnation pressure as measured at the beginning of the contraction, throughout the run. The nondimensionalized profiles are shown in Figure 46. The nondimensionalization collapses the data in the freestream, but not as well inside the boundary layer, which is also seen with the computations. Figure 46 shows a laminar boundary layer thickness of about 3/4 inches at z=75.3 inches. It looks like the boundary layer is slightly thicker later in the run than it is at the beginning, though more points near the edge of the boundary layer would help make this clearer. The change in boundary-layer thickness can also be seen in the computational data.

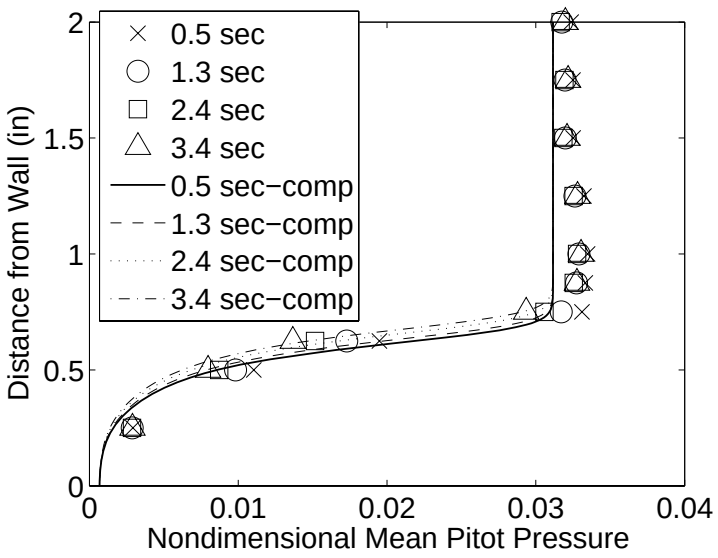

Figure 46: Boundary-layer profiles at z=75.3 inches and initial pressure of 20 psia with Pitot pressure nondimensionalized by tunnel stagnation pressure.

Figure 47 shows profiles at three axial locations. Two runs were performed for each profile; one with the probe starting 0.25 inches from the wall, and one with the probe starting 0.375 inches from the wall. The probe then traversed in 0.25 inch increments away from the wall five times, and then back toward the wall four times. At each location, the probe stopped for 0.1 seconds. There is a split in the profile because of the pressure drop during the run and each point being taken at a different time during the run. By nondimensionalizing the mean Pitot pressure by the stagnation pressure the data collapses pretty well as shown in Figure 48. The figure shows boundary layer thicknesses of slightly less than 1 inch for the front two locations and about 1 inch for the z=84.5 inches profile. The data is again compared to computations, showing good agreement. The boundary layer thicknesses and profiles look very similar to the ones shown in Figure 46. This shows that profiles can be obtained by automatically traversing during the run, allowing far fewer runs per profile.

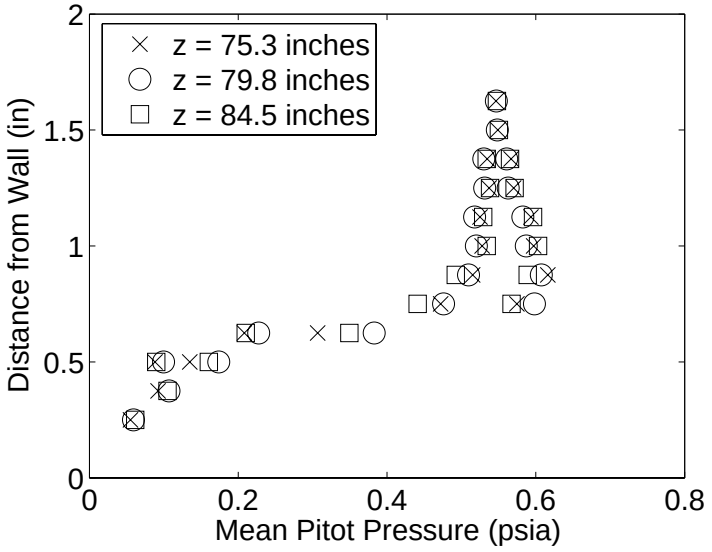

Figure 47: Boundary-layer profile at z=75.3 inches and initial pressure of 20 psia using moving traverse.

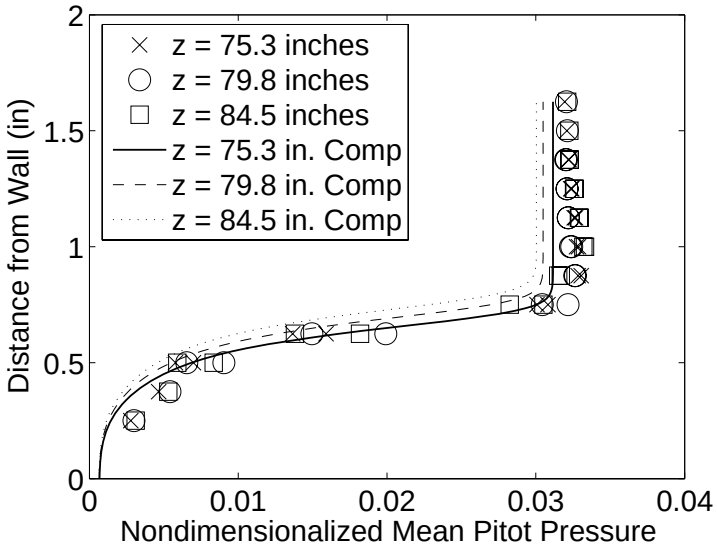

Figure 48: Boundary-layer profile at z=75.3 inches and initial pressure of 20 psia, using moving traverse and nondimensionalized Pitot pressure.

The profiles shown in the previous plots compared well with the computations. However, it was noticed that when the probe is within about 1.5 inches of the wall, the hot films stop showing the unsteady disturbance, as shown in Figure 49. These runs were

done with the Pitot probe stationary. The hot film traces taken with the probe 1.25 inches or closer to the wall did not have the large spikes present until near the end of the run. In the hot film traces 1.75 inches and farther from the wall, the spikes are always present. The Pitot sensor has a diameter of 0.060 inches, but is held by a tube that expands quickly to 0.3125-inches, and extends back 10 inches. It appears that the Pitot probe disrupts the boundary layer, though this does not have a large impact on the measured profiles.

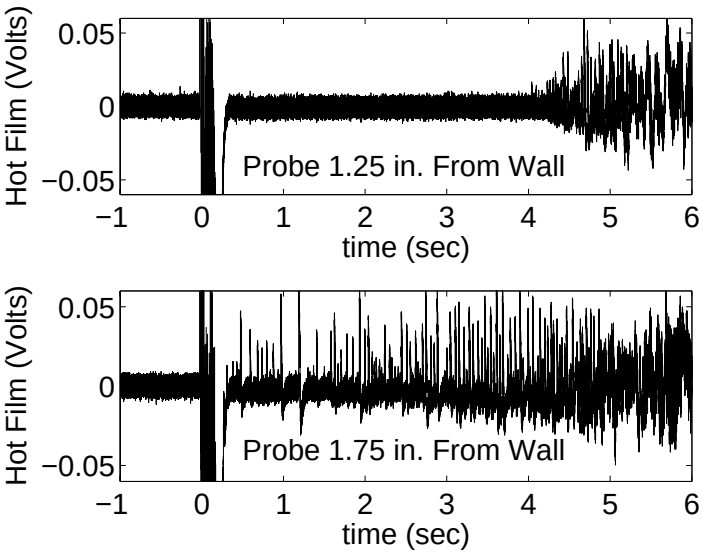

Figure 49: Traces from hot films at z=73.45 inches with the Pitot probe at different heights above the wall.

Hot wire profiles were also obtained, to examine the boundary layer using data taken by a different method. The profiles with the hot wire were measured using the traverse moving throughout the run. The resistance of the hot wire in the runs in this section was 10.47 ohms. A balance resistor of 18.72 ohms was used, giving an overheat ratio by resistance of 1.8. The hot wire was tuned with a frequency response of 200 kHz.

Figure 50 shows boundary layer profiles with initial pressures of 20 and 37 psia at an axial location of z=84.5 inches. Each profile consists of four runs. The hot-wire voltages are nondimensionalized using voltages from separate runs at 20 and 37 psia with the hot wire 4.5 inches from the wall, or just slightly below the centerline. This should counter the effect of the voltage drop through the run due to drop in stagnation pressure. The resulting data was nondimensionalized to between 0 and 1 to allow comparison to computational data. The experimental data is compared to mass flux data nondimensionalized to between 0 and 1. The hot wire data should be proportional to mass flux, but since the hot wire is uncalibrated, no actual mass flux data can be calculated. The profiles give good agreement with the computation on shape and boundary layer thickness, though there seems to be more scatter than in the Kulite data.

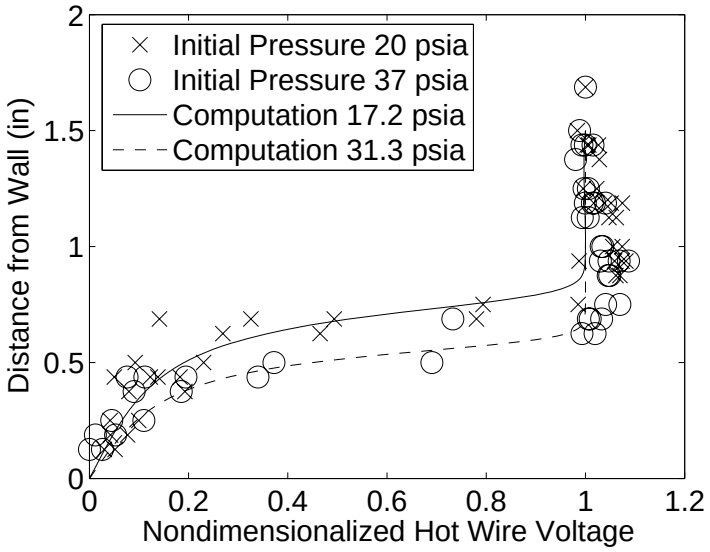

Figure 50: Hot Wire profiles at z=84.5 inches using a moving traverse and nondimensionalized hot wire voltage.

A boundary-layer profile was also performed with the bleeds closed, which trips a turbulent boundary layer at the bleed lip. Figure 51 shows the turbulent boundary layer

profile. This profile consists of six runs with the traverse moving automatically through the run. The boundary layer profile is compared to a computation assuming a fully turbulent boundary layer from the throat with a simple two-layer eddy viscosity model. This again shows good agreement between the computation and experiment.

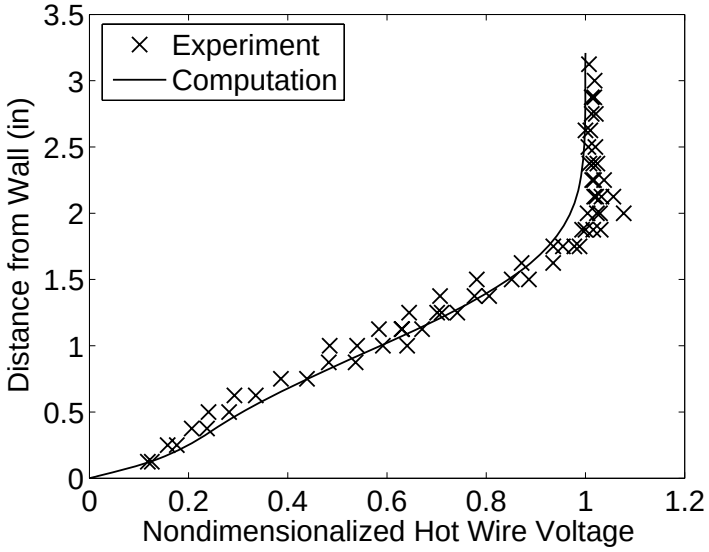

Figure 51: Hot Wire profile at z=84.5 inches, initial pressure of 37 psia, and bleeds closed, using moving traverse and nondimensionalized hot wire voltage.

With the Pitot probe, boundary layer interference was seen by observing hot-film disturbances disappear when the probe was near the wall. These disturbances were seen on the hot films only at very low pressure. To see if this was also the case with the hot wire, a run was performed at 8 psia, with the automatic traverse, while observing the hot films. Traces from the hot wire at z=84.5 inches and the hot film at z=73.45 inches are shown in Figure 52. The horizontal axis is time during the run. The black vertical lines show the movement of the hot wire. Between the thin bands, the probe is stationary for 0.1 seconds. The probe moves 1/4" with each movement, and moves away from the wall 5 times, then back toward the wall 5 times to end in the starting location. The bands

where the probe is 1/8” from the wall and 1.375” from the wall are marked with arrows. The noise levels are low in the hot film trace except when the probe is more than 7/8” from the wall. When the probe is farther than 7/8” from the wall, then the disturbances can be seen both on the hot film and the hot wire trace.

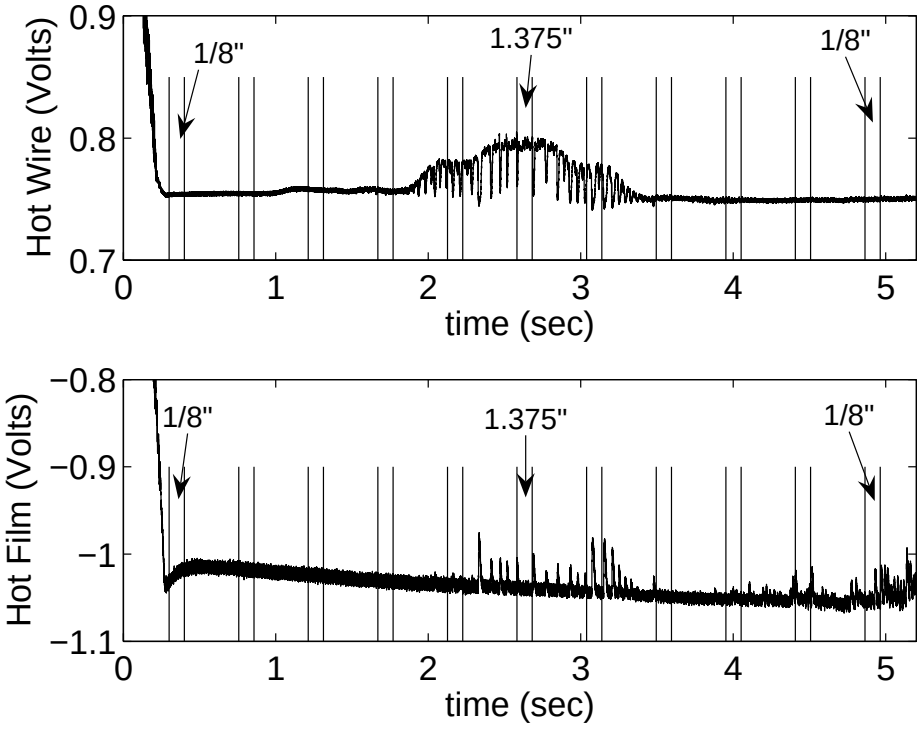

Figure 52: Hot wire and hot film traces with moving traverse at 8 psia.

The boundary-layer profile data that was measured was very close to that found in computations. This allows measurement of the boundary-layer thickness, and demonstrates that the computations are accurate. There was some probe interference, though this did not have a large impact on the profiles measured. It is possible to build a hot wire with a longer strut to reduce probe interference.

3.3 Jets from Bleed System

It was shown in Section 3.2.1 that when the double-wedge sting mount is removed, the separation at the end of the nozzle is not as large. This indicates that another, lesser, disturbance is causing the separation with an empty diffuser. Figure 53 shows a diagram of where the bleed air is reintroduced into the diffuser when the passive bleeds are used.

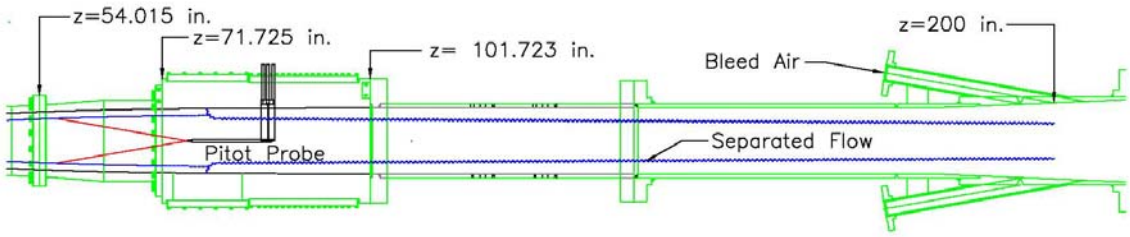

Figure 53: Diagram of end of nozzle and diffuser.

The active system was used to see if the jets from the passive bleeds might be causing the unsteady disturbances. Figure 54 shows the Mach number for the two configurations with the Pitot probe placed at z=93.5 inches. The initial driver-tube pressures were 8.03 psia for the passive bleeds, and 8.00 psia for the active bleeds. This figure shows that the large unsteady separation is not present with the active bleeds. Figure 55 shows the noise levels for the same data. The noise levels are extremely high with the passive bleeds, and quiet when the active bleeds are used.

As shown previously in Section 3.2.2, the unsteady separation shows up on the hot film sensors. A hot film at z=73.45 inches is shown in Figure 56. The fluctuations that are present with the passive bleeds and no sting mount do not show up with the separation that occurs with the sting mount. The trace of the hot film with the active bleeds shows a larger noise level in the first two seconds of the run, before the bleed

system is operating. The noise level in the first two seconds is typical of turbulent boundary layers present when the bleeds are closed. After the bleed system starts, the noise falls away and there is no large unsteady separation. All of this indicates that the separation with no sting mount is caused by the disturbances generated by these jets propagating forward over 120 inches.

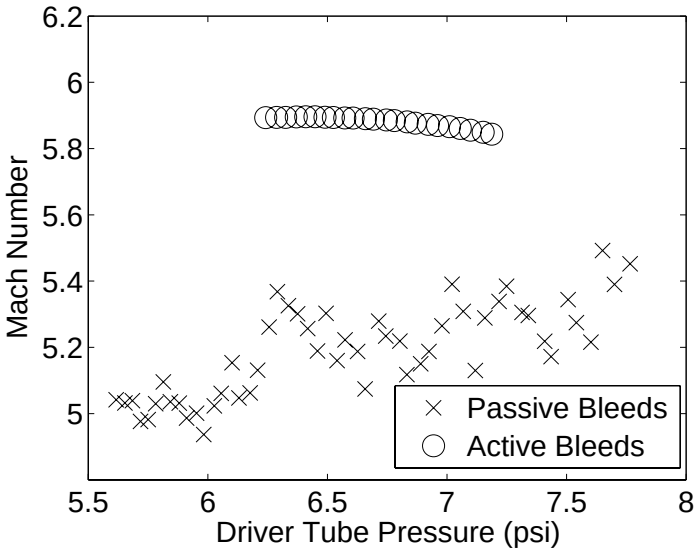

Figure 54: Effect of jets from bleeds on Mach number with Pitot at z=93.5 inches and pressure below 8 psia, with the sting mount removed.

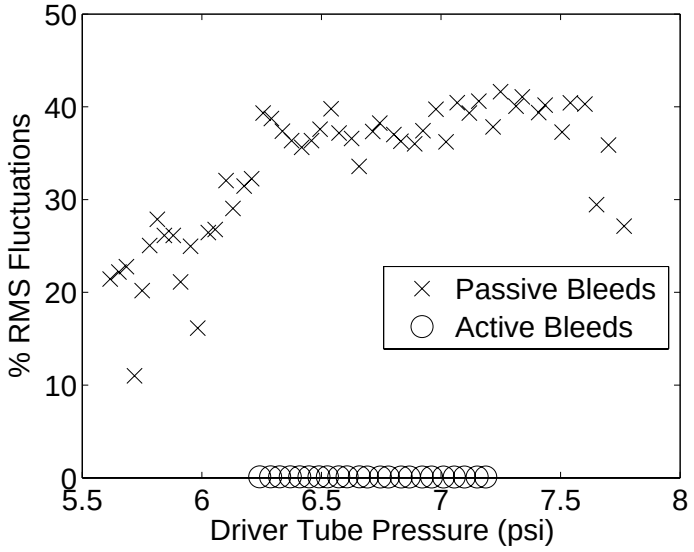

Figure 55: Effect of jets from bleeds on noise with Pitot at z=93.5 inches and pressure below 8 psia.

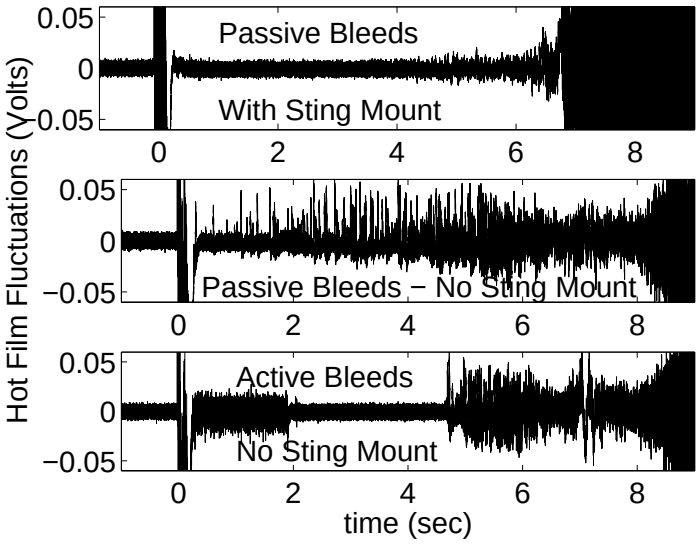

Figure 56: Effect of jets from bleeds shown with hot film at z=73.45 inches.

3.4 Separation with New Sting Mount

Since the results from the last section indicated that the double wedge was causing a separation problem that decreased when the double wedge was removed, a new streamlined sting mount was built, as shown in Figure 57 and Figure 58. It is necessary to have some sort of sting support in order to place a model in the tunnel. The new sting mount was designed to have less blockage than the double wedge. A sting can be placed in the hole in the center of the sting mount, and this sting can protrude forward into the end of the nozzle to hold a model. The tests of the sting mount in this section were performed with the hole in the center of the sting mount empty and laminar incoming boundary layers. Details on the streamlined sting mount can be found in Reference 37.

Figure 57: New sting mount, looking downstream.

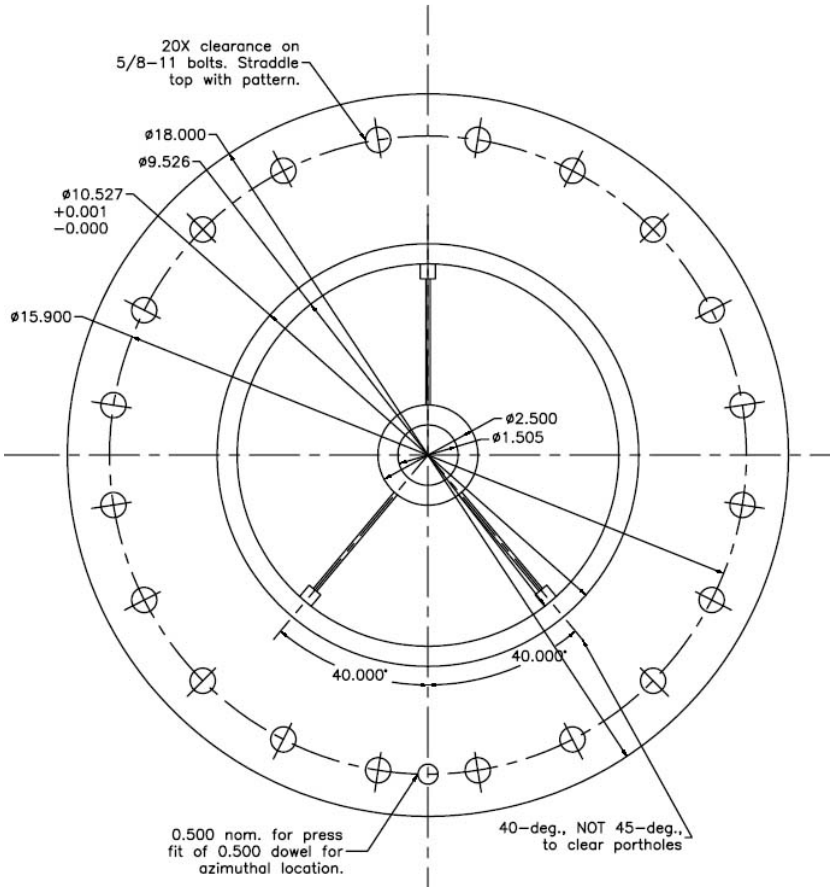

Figure 58: Schematic of new sting mount, looking downstream (From Prof. Steven Schneider).

3.4.1 Pitot Measurements with the Streamlined Sting Mount

Figure 59 shows a schematic of the end of the nozzle and beginning of the diffuser. The streamlined sting mount is installed and the Pitot probe is at z=84.5 inches. Figure 60 compares the Mach number for runs with and without the sting mount with the Pitot probe at z=84.5 inches. The initial driver tube pressures were 8.03 psia for the run with no sting mount and 8.01 psia for the run with the sting mount. Lower Mach numbers indicate a higher Pitot pressure, probably caused by a separation. The case with

the sting mount has some attached flow early in the run at the higher pressures, then a separation that increases towards the end of the run. This effect is likely more of a function of the downstream pressure rise during the run, than of the upstream pressure drop. Figure 61 shows the noise levels for the same data. The noise levels are low except when the separation occurs. The separations result in huge noise levels of 30 to 50 percent.

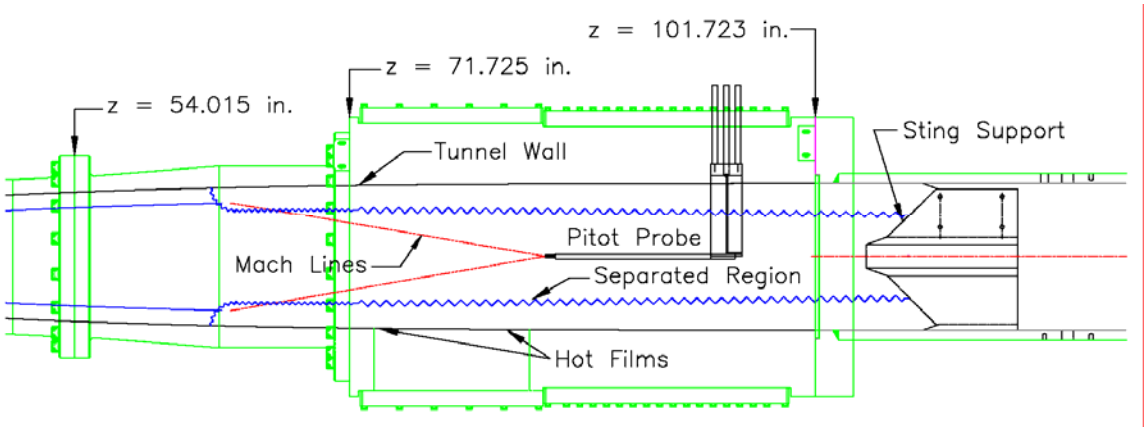

Figure 59: Schematic with streamlined sting mount and Pitot probe at z=84.5 inches.

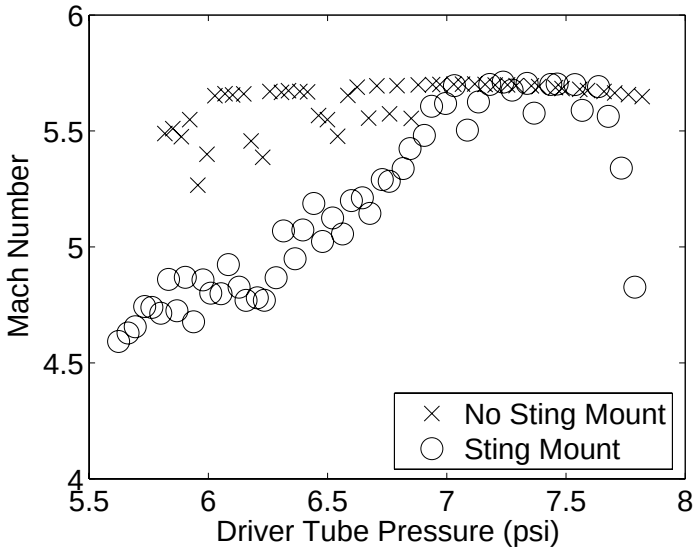

Figure 60: Effect of sting mount on Mach number with Pitot on centerline at z=84.5 inches and pressure below 8 psia.

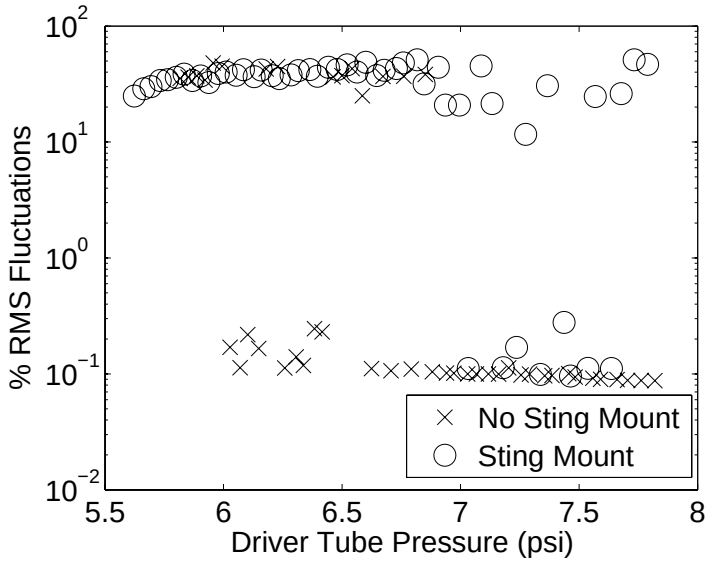

Figure 61: Effect of sting mount on noise with Pitot on centerline at z=84.5 inches and pressure below 8 psia.

The effect of the sting mount was also compared at higher driver tube pressures, as shown in Figure 62 and Figure 63. The initial driver tube pressures were 19.96 psia for the run with no sting mount and 20.01 psia for the three runs with the sting mount. With the sting mount, the separation is still present, but it is less consistent than at lower pressures. The amount of separated flow was not very consistent between the three runs with the sting mount, though separation is present at some point during all three runs. This inconsistency indicates that the acoustic origin, for the probe at z=84.5 inches, is near the furthest forward location that the separation reaches under these conditions. Figure 63 shows the noise levels are again very large when the separation is present.

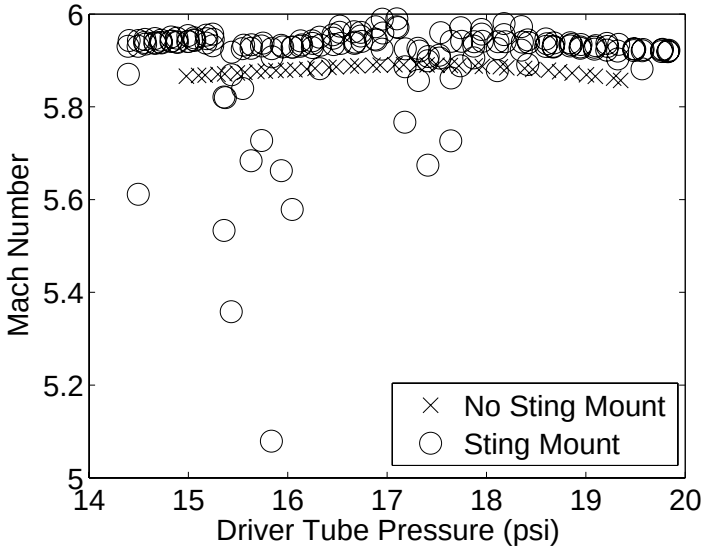

Figure 62: Effect of sting mount on Mach number with Pitot on centerline at z=84.5 inches and pressure below 20 psia.

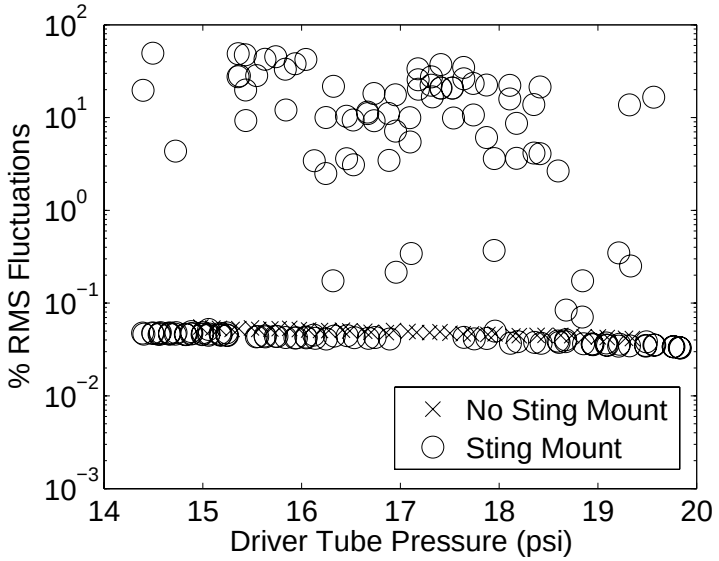

Figure 63: Effect of sting mount on noise with Pitot on centerline at z=84.5 inches and pressure below 20 psia.

At higher pressures, the separation takes on an odd dependence on time during the run. Figure 64 shows Pitot pressure traces at z=93.5 inches for initial driver tube pressures ranging from 20 to 37 psia. For the runs with an initial driver tube pressure of

30 to 37 psia the Pitot probe shows attached flow after startup. About 0.5 seconds into the run, the flow separates and remains separated until about 4 to 4.5 seconds after the start of the run. With an initial driver tube pressure of 25 psia, the flow is attached at the beginning of the run but does not reattach after it separates. The run with an initial driver tube pressure of 20 psia is separated through the whole run. Figure 65 shows Mach number as a function of run time for the same data. The Mach numbers around 5 in this plot indicate separated flow.

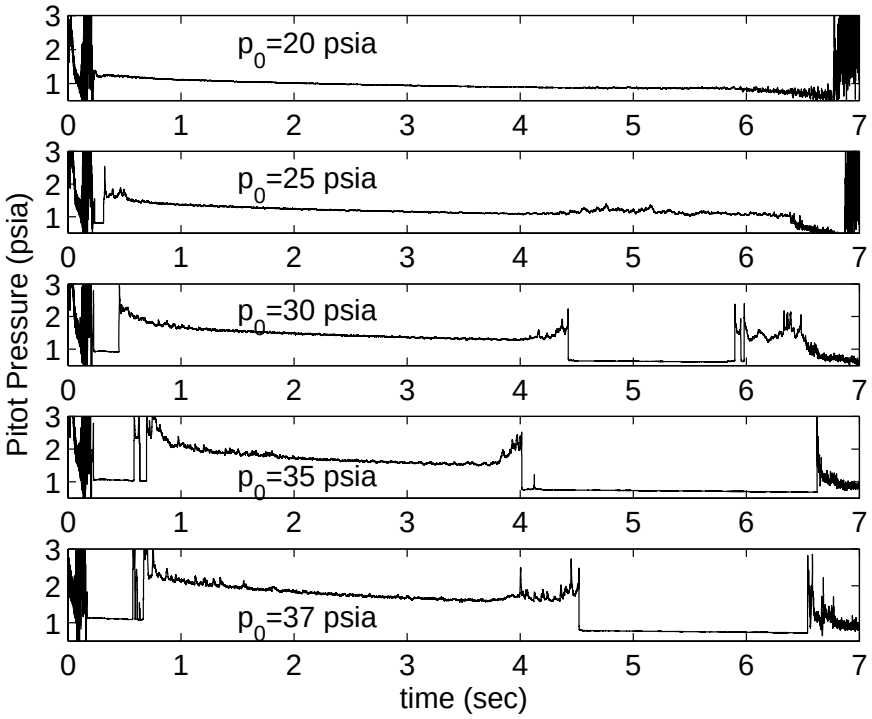

Figure 64: Pitot pressure traces at z=93.5 inches for several initial driver tube pressures.

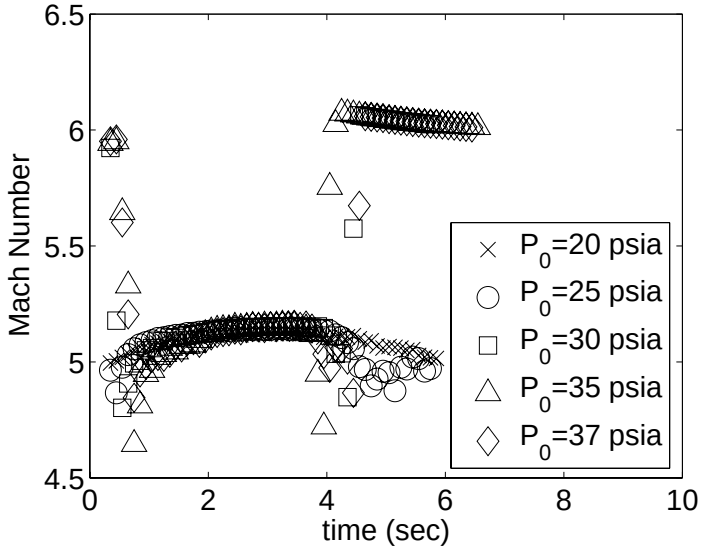

Figure 65: Mach numbers for data shown in Figure 64.

The separation can also be observed with the hot films, as shown in Figure 66. This figure shows the 37 psia Pitot pressure trace from Figure 64 with three hot film traces for the same run. The separation moves across all of the hot films very quickly. Examining the data very closely, it appears the separation crosses all hot films in less than 1 msec. Figure 67 shows the effect of axial location on the separation, with an initial driver tube pressure of 37 psia. Only the aft location shows any separation, and only in the middle of the run. The two forward locations do not show any separation at all, indicating the separation does not extend forward far enough to be measured by the Pitot probe at those locations, which means the disturbances are traveling forward about 60 boundary layer thicknesses to be observed with the probe at z=93.5 inches, but less than about 70 boundary layer thicknesses, where the disturbances could be observed with the Pitot probe at z=84.5 inches.

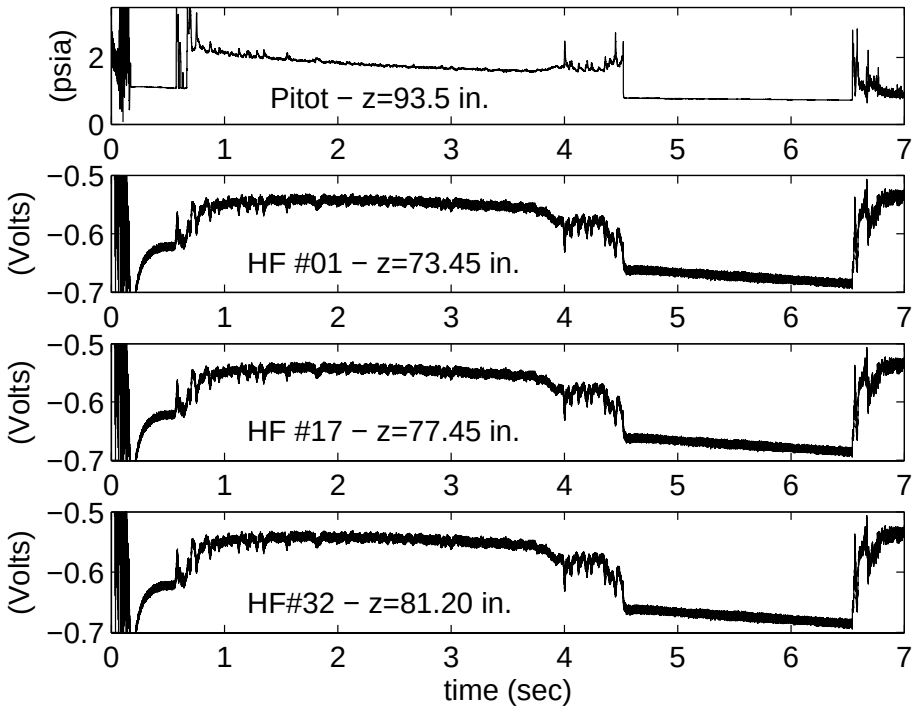

Figure 66: Traces of Pitot pressure and hot film voltages, with an initial driver tube pressure of 37 psia.

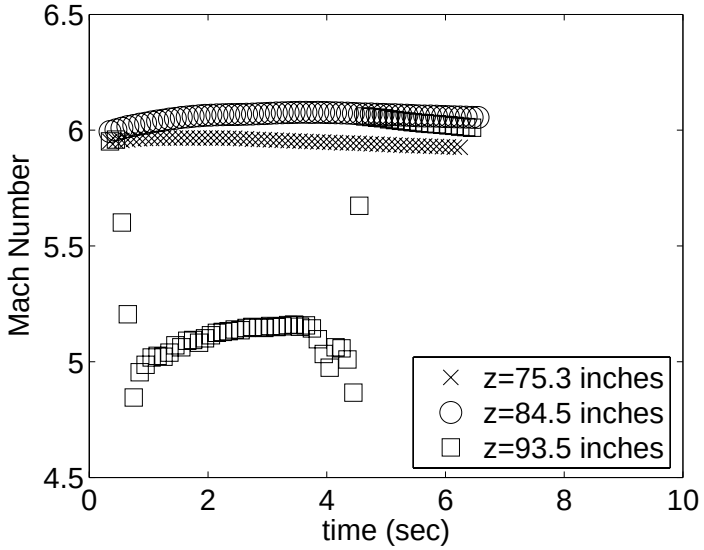

Figure 67: Effect of axial location on separation, with an initial driver tube pressure of 37 psia.

There are several things that change during a run that could possibly be related to this odd separation behavior. During the run, the stagnation pressure drops, the stagnation temperature drops, the boundary layer in the driver tube grows, the boundary layer in the nozzle grows, and the back pressure in the vacuum pressure rises. The effect of the last of these was examined by varying the initial vacuum-tank pressure. For all previous runs, the initial vacuum-tank pressure was 2.0 torr. Figure 68 shows Pitot pressure traces for four different initial vacuum pressures. The largest effect of increasing the vacuum pressure is that the length of the run is shortened. For all cases, the flow starts attached and separates about 0.5 seconds into the run. The reattachment at about 4.2 seconds is only seen in the top two traces in the figure. The two cases with the higher initial vacuum pressure do not show reattachment, but this is due to the run ending before this would normally occur. One or more of the other changes during the run must be responsible for this, but no likely theory has been discerned at this point.

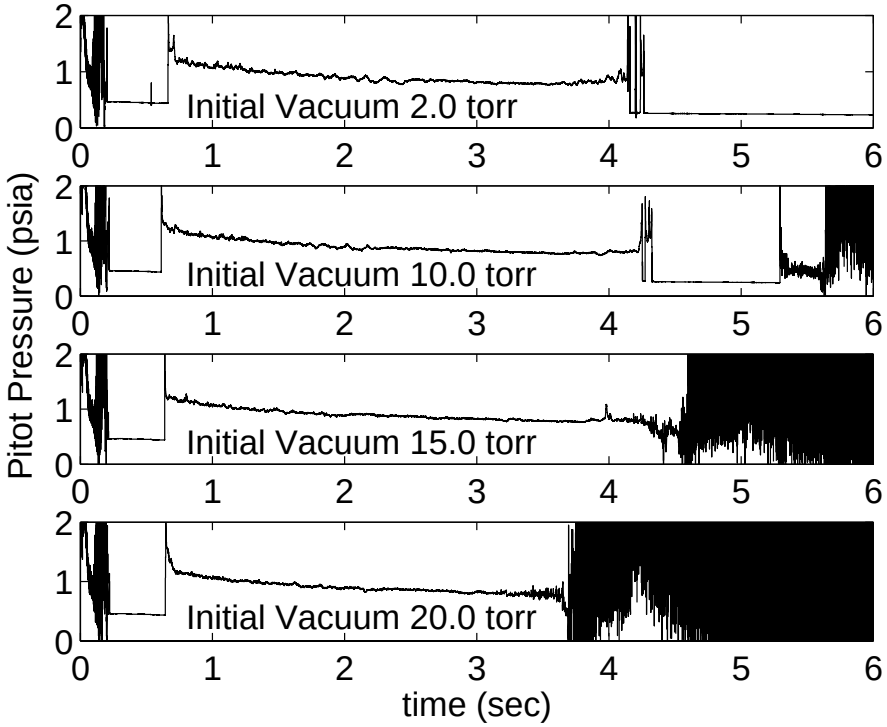

Figure 68: Pitot pressure traces on the centerline at z=93.5 inches, with 37 psia initial driver-tube pressure, and varying initial vacuum pressure.

3.4.2 Hot Film Measurements with the Sting Mount

With the sting mount in place, there is a separation that extends in front of the hot films, which can be observed using the Pitot probe. Figure 69 shows hot film traces at z=73.45 inches with and without the sting mount. The voltages shown are the difference in the voltage from the pre-run voltage. There is a noticeable difference in the voltage when the flow is separated using the sting mount. There is no difference in the fluctuations, which means that if this data is high-pass filtered, as in Figure 56, information on the separation is lost. In future work, when a model is placed in the

tunnel, the hot films could be used to get an idea if shocks from the model are separating the flow far upstream, as long as an unseparated-boundary-layer baseline can be obtained at the same pressure.

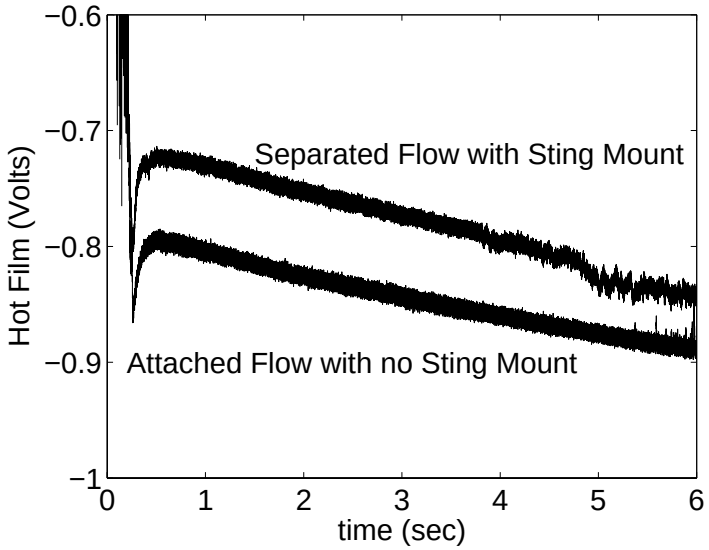

Figure 69: Hot film traces at z=73.45 inches with and without the sting mount, with an initial driver-tube pressure of 20 psia.

3.4.3 Boundary-Layer Measurements with the Sting Mount

Boundary layer measurements were made with the sting mount in place to get a direct measurement of the separated boundary layer. Figure 70 shows boundary layer profiles using a Kulite Pitot probe at two different axial locations, with an initial driver tube pressure of 8 psia. The Kulite data is compared to computations of an undisturbed laminar boundary layer. The profile at z=75.3 inches does not show a boundary-layer thickness larger than the computation, but the core flow has a higher Pitot pressure,

indicative of a separation. The profile at z=84.5 inches seems to have a little more scatter in the edge of the separated region, but shows a separation of about 1.25 to 1.5 inches. The profiles show a separation that is larger further back, as expected, since the separation originates in the diffuser, and gets smaller as it propagates forward.

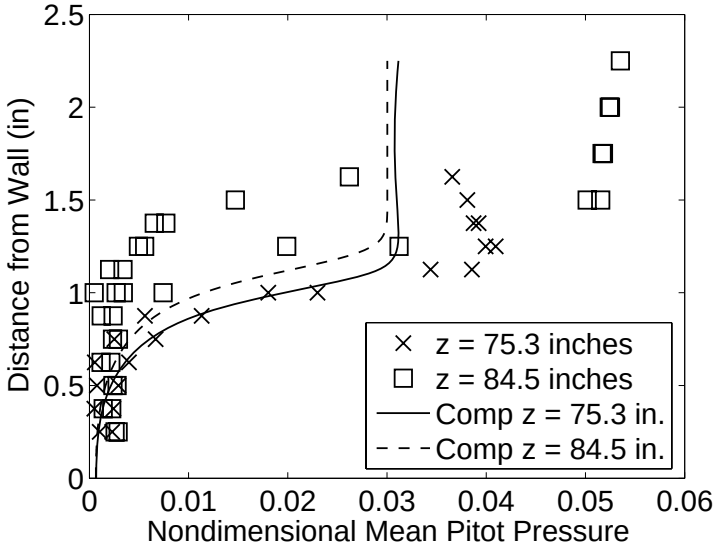

Figure 70: Profiles of separation, with an initial driver tube pressure of 8 psia, nondimensionalized by tunnel stagnation pressure.

Profiles were also obtained with a hot wire, as shown in Figure 71. The hot wire probe could not reach as far forward as the Kulite Pitot probe, so profiles were measured at z=84.5 inches and z=93.5 inches. The voltages for the hot wire were scaled to between 0 and 1. The figure shows a separation of approximately 1.5 inches at the forward location and about 2 inches at the aft location. Figure 72 shows a comparison between the hot wire and Kulite profiles at z=84.5 inches. The voltage for the hot wire and the nondimensional Pitot pressure was scaled to go between 0 and 1 so that the profiles could be compared directly. These profiles show fairly good agreement.

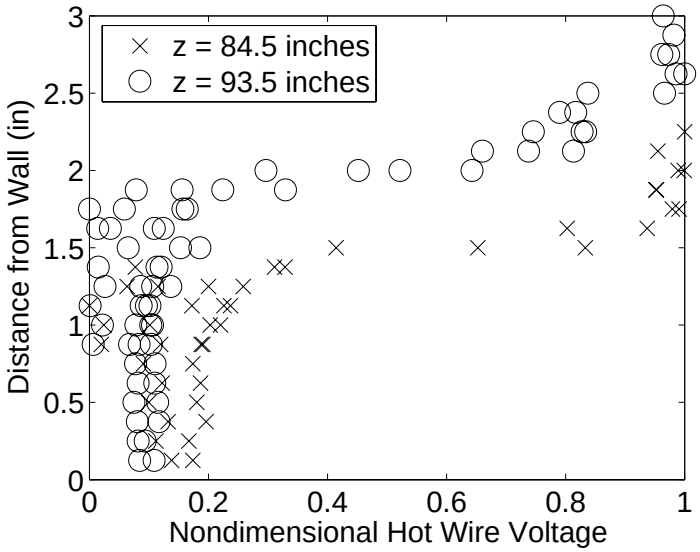

Figure 71: Profiles of separation with hot wire, with an initial driver tube pressure of 8 psia.

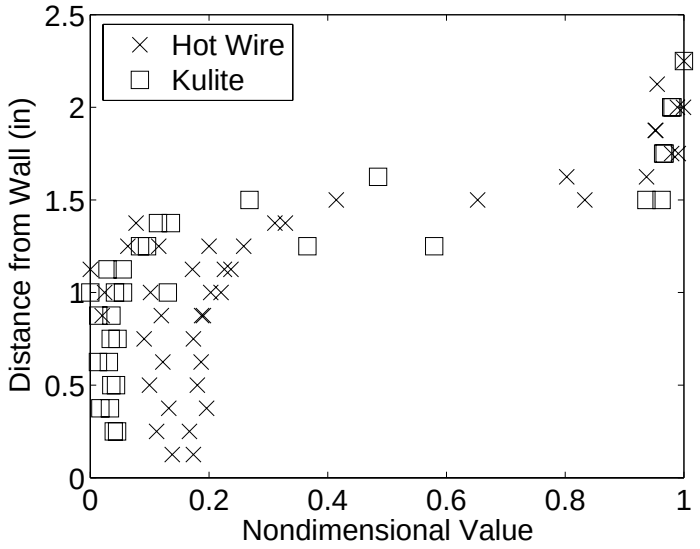

Figure 72: Comparison of profiles at z=84.5 inches, using hot wire and Kulite, with an initial driver tube pressure of 8 psia.

Figure 73 shows profiles of the separation with an initial driver tube pressure of 20 psia at three different axial locations. The separation is not as large at this higher

pressure. At z= 75.3 inches, there appears to be little separation at all. The separation is about 1 inch at the middle location and about 1.25 inches at the aft location. Figure 74 shows a comparison between the profile at 84.5 inches with the Pitot probe and one taken with a hot wire. The hot wire shows a separation of about 0.75 inches, while the Pitot probe shows a separation of about 1.25 inches. The cause of this disagreement is not known. The Kulite did not show interference large enough to drastically change the profile when the sting mount was removed.

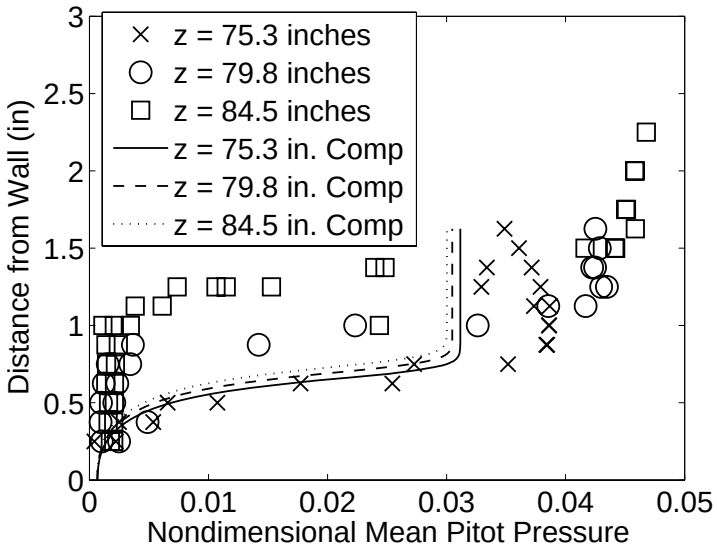

Figure 73: Profiles of separation, with an initial driver tube pressure of 20 psia.

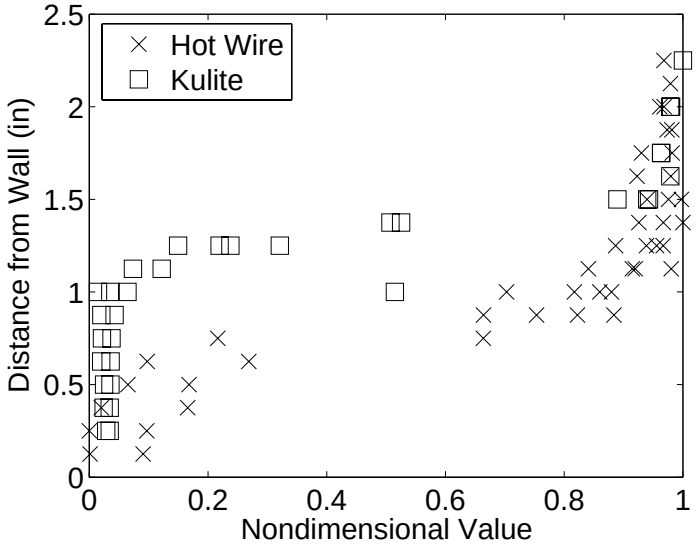

Figure 74: Comparison of profiles at z=84.5 inches, using hot wire and Kulite, with an initial driver tube pressure of 20 psia.

3.5 Chapter Summary

The empty double wedge sting mount was found to cause extremely large fluctuations far forward into the nozzle that probably indicate a tunnel unstart. This was present whether the incoming boundary layer was laminar or turbulent. When a blunt cone was placed in the double-wedge sting mount, the disturbances became much smaller, but still caused a large separation when the incoming boundary layer was laminar. With the double wedge sting mount removed, the separation with a laminar boundary layer disappeared except at very low pressures, below about 8 psia, where a large unsteady separation was still present. This was found to be caused by disturbances from the bleed system jets in the diffuser propagating very far upstream into the nozzle. Measurements

of the unseparated laminar and turbulent boundary layers were found to agree well with computations. A new streamlined sting mount was built to try to reduce the upstream influence of the sting mount, but separation was still present with an incoming laminar boundary layer. At pressures above 25 psia, the flow is attached at the beginning and the end of the run, but separated in the middle. This appears to have something to do with time during the run, more than driver tube pressure, since it occurs as a function of run time over a wide range of pressures. This has yet to be explained.

The shock/boundary-layer interactions observed in this tunnel could also cause problems with a hypersonic flight vehicle. The large laminar boundary layer in this tunnel is unusual for a wind tunnel, but for a large vehicle cruising in the upper atmosphere, thick laminar boundary layers are very likely. Shocks will interact with the boundary layers in inlets, where wings attach, and where control surfaces are used. If shock/boundary-layer interactions cause large separations as they have in this Purdue tunnel, there could be large unexpected effects in the overall aerodynamics of the vehicle.

CHAPTER 4 - EFFORTS TO REDUCE UPSTREAM EFFECTS

Since the sting mount is required to place a model in the tunnel, it is necessary to prevent the separation caused by the sting mount in order to test a model under quiet conditions. Compression rings and a trip ring were tested to try to prevent the disturbances generated by the sting support from propagating upstream when the boundary layer is laminar. The idea of the compression ring is to thin the boundary layer, which should reduce the ability of disturbances to travel upstream. The trip ring is intended to trip the boundary layer from laminar to turbulent. Since turbulent boundary layers are much less likely to separate than laminar boundary layers, tripping the boundary layer before any shock/boundary-layer interactions should reduce the separation. Since boundary-layer separation extending into the nozzle is only a problem with laminar boundary layers, all data shown in this chapter were taken with an incoming laminar boundary layer.

4.1 Description of Compression and Trip Rings

The compression rings consist of an axisymmetric wedge that can be placed along the inner wall of the tunnel, as shown in Figure 75. The trip ring consists of a 1/4-inch

thick ring that has 18 set screws measuring 1/4"-20. These set screws protrude into the flow at 20 degree intervals around the trip ring. The set screws used varied from 1 inch to 2.5 inches long. The picture of the trip ring in Figure 76 has set screws that are 1.5 inches long. The compression rings and trip rings were machined out of a 10-inch diameter polypropylene rod.

Figure 75: Picture of 0.75-inch maximum thickness compression ring in front of sting mount.

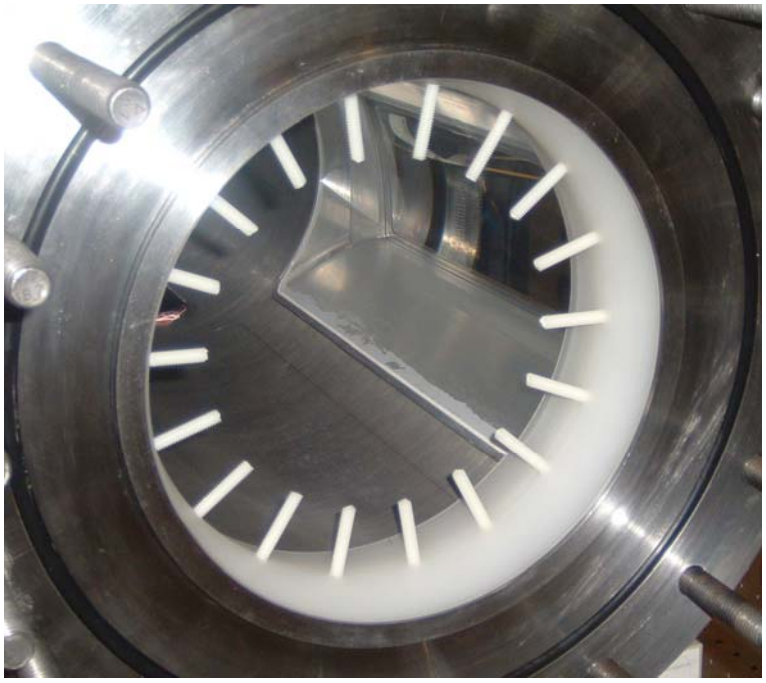

Figure 76: Picture of trip ring with 1.5-inch set screws at end of nozzle.

Figure 77 shows the end of the nozzle with the Pitot probe placed at z=75.3 inches. With an empty sting mount, the Pitot probe at this location shows unseparated laminar flow at the acoustic origin on the wall, somewhere near z=54 inches. The schematic shows a 1 inch maximum-height wedge with a 10-degree symmetric wedge angle that is placed just in front of the sting support.

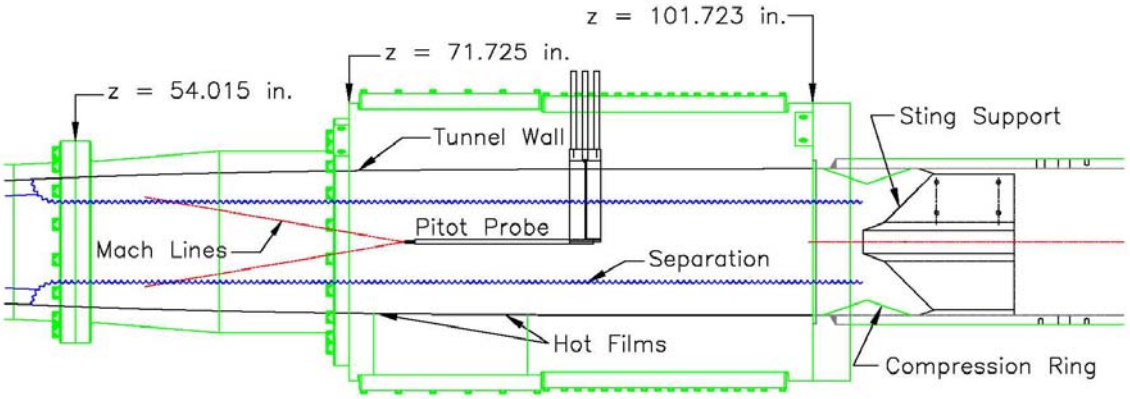

Figure 77: Schematic of the end of the nozzle with a 1-inch compression ring.

Figure 78 shows a schematic with the trip ring. In this schematic, the trip ring is drawn with 2.5-inch setscrews. The Pitot probe is shown at z=84.3 inches. At this location, with an empty sting mount, the probe data indicates separated flow, as in Figure 60, indicating that the separation occurs somewhere before a z-location of above 64 inches when traced to the acoustic origin. The location of the acoustic origin is highly speculative as it greatly depends upon the boundary layer thickness.

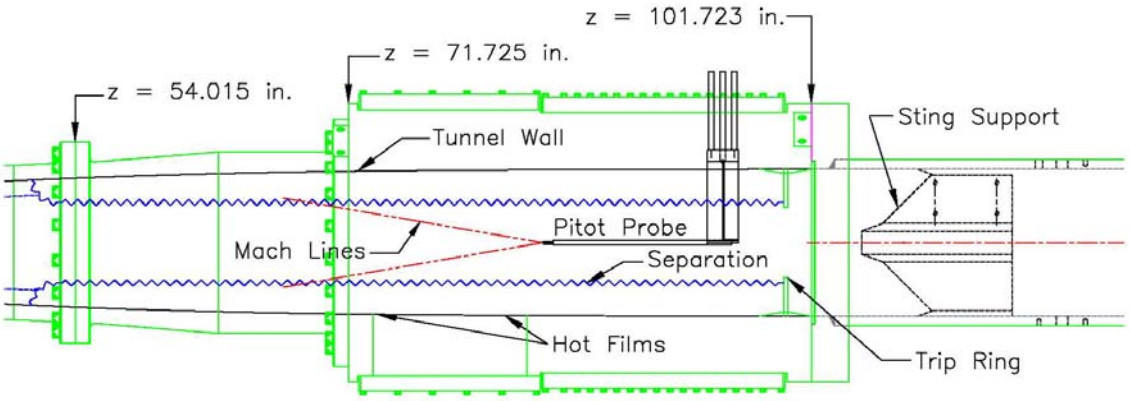

Figure 78: Schematic of the end of the nozzle with 2.5 inch trips.

4.2 Effect of Compression Rings

The first compression ring used had a 1-inch maximum thickness, and a symmetric wedge angle of 19 degrees. The compression ring was placed after the nozzle and in front of the sting mount, as shown in Figure 77. The effect of using this compression ring can be seen in Figure 79. The data without the compression ring does not show separation at the forward location of z=75.3 inches, but the separation can be

seen when the Pitot probe is moved back to z=84.5 inches. The data with the compression ring shows separated flow at both locations. With the compression ring in place, the separated region is larger than with the sting mount alone. Figure 80 shows the RMS fluctations for the same data. It is interesting that the only run showing high noise levels is without the compression ring at z=75.3 inches. There are two possible reasons for the data with the compression ring showing low noise levels, even though the Mach number indicates separated flow. It is possible that the front of the separated region is far enough in front of where the Pitot probe is measuring that any unsteadiness is not seen, and there is a laminar shear layer. It is also possible that the front of the separation caused by the compression ring is very steady. The separation at z=84.5 inches seems to have some time dependence, as it increases throughout the run. The separations with the compression ring are much steadier than with only the sting mount.

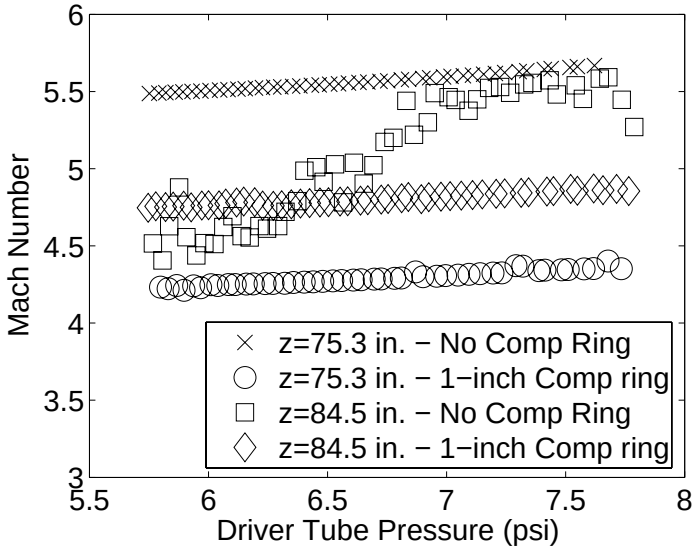

Figure 79: Mach numbers using 1-inch compression ring, with initial driver tube pressure of 8 psia.

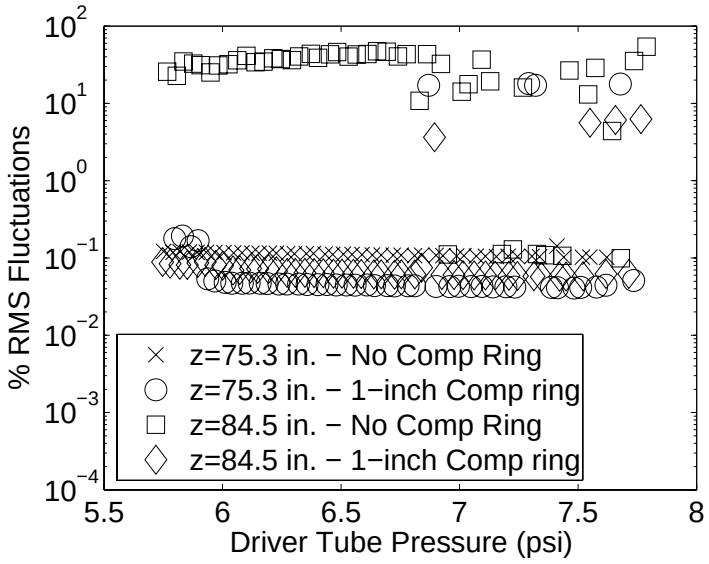

Figure 80: RMS fluctuations using 1-inch compression ring, with initial driver tube pressure of 8 psia.

The larger separation with the 1-inch, 19-degree compression ring could be caused by a wedge angle that is too large, or by too much blockage in the tunnel. To see if the wedge angle was the problem, a new 1-inch compression ring with a symmetric 10 degree angle was built. To see if the blockage was an issue, a 0.75-inch compression ring was built with a symmetric 15.5-inch wedge angle. These cases were compared to an empty tunnel, which means no compression ring was placed in front of the sting mount. Figure 81 shows the Mach numbers from the Pitot probe at z= 75.3 inches. The lower Mach numbers with the compression rings indicate a separated boundary layer at the acoustic origin at around 54 inches. The Pitot probe does not show separated flow at this location with an empty tunnel. Figure 82 shows noise levels that are lower for part of the run using the compression rings. This is because the separated flow results in a Pitot pressure three times higher than the unseparated flow, and this Pitot pressure is used to nondimensionalize the RMS fluctuations. It is very interesting that it is possible to get

quiet noise levels with separated flow. This indicates that it is possible to have a very steady separation that does not radiate noise.

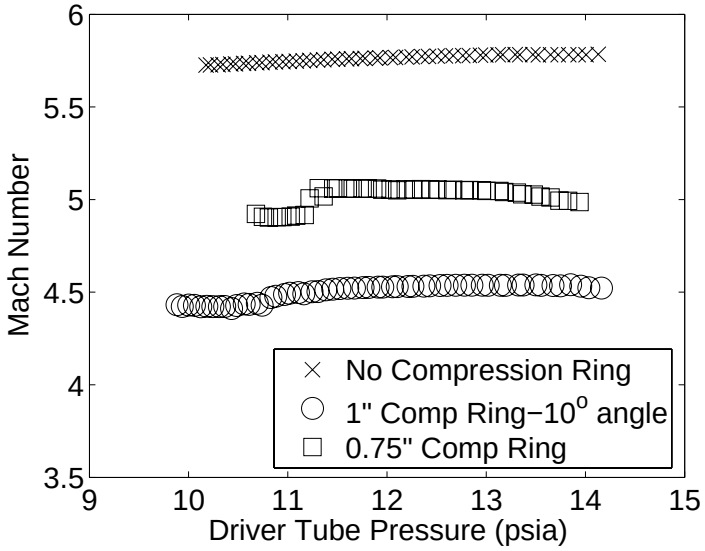

Figure 81: Mach numbers with compression rings, with Pitot at z=75.3 inches, and initial driver tube pressure of 14.5 psia.

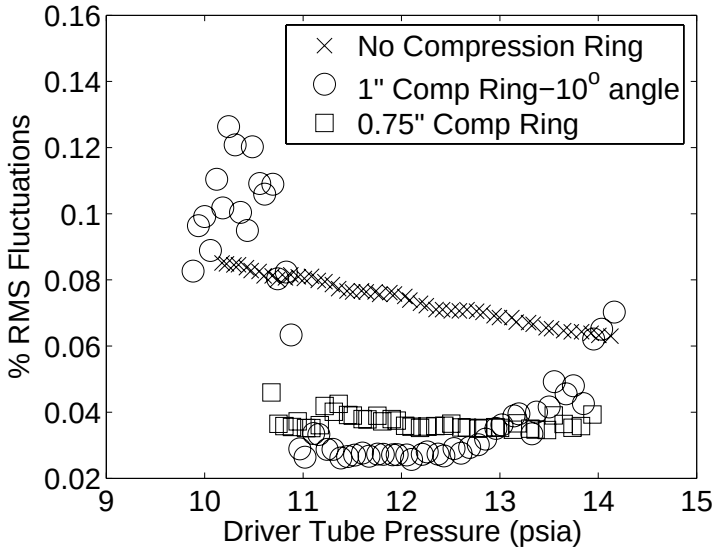

Figure 82: RMS fluctuations with compression rings, with Pitot at z=75.3 inches, and initial driver tube pressure of 14.5 psia.

4.3 Effect of Trip Ring

The trip ring is designed to try to trip the flow to turbulent before it gets to the sting mount. Since turbulent boundary layers are much less susceptible to separation, tripping the boundary layer should reduce the upstream influence of the shock/boundary layer interaction. The trip ring was tested with various trip heights. Figure 83 and Figure 84 show the Mach number and RMS fluctuations with the Pitot probe at z= 75.3 inches. Figure 83 shows that the 1.5-inch and 2.5-inch set screws in the trip ring increase the separation at the end of the nozzle. The 1-inch set screws do not have an effect on the Pitot probe data at this location. Figure 84 shows that the 2.5 inch set screws greatly increase the noise level, while the 1.5 inch set screws do not have this effect until very near the end of the run, even though both increase the separation. It is possible that the 2.5-inch trips, which stick farther out of the boundary layer, cause a more unsteady separation.

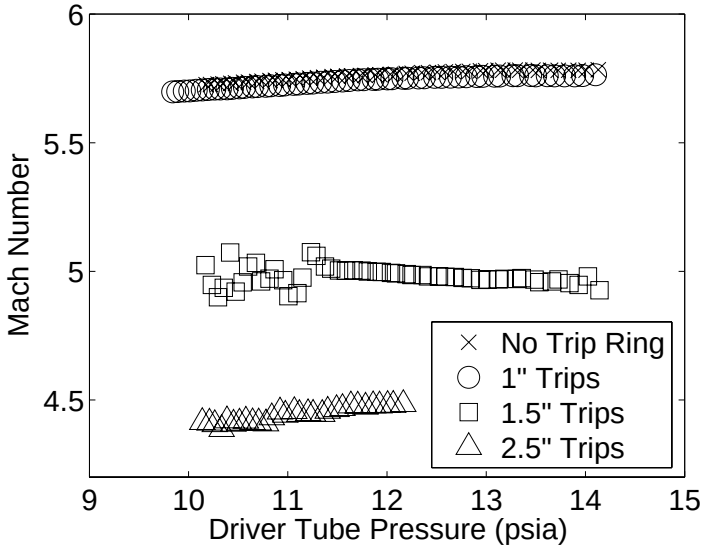

Figure 83: Mach numbers using trip ring, with Pitot probe at z=75.3 inches, and initial driver tube pressure of 14.5 psia.

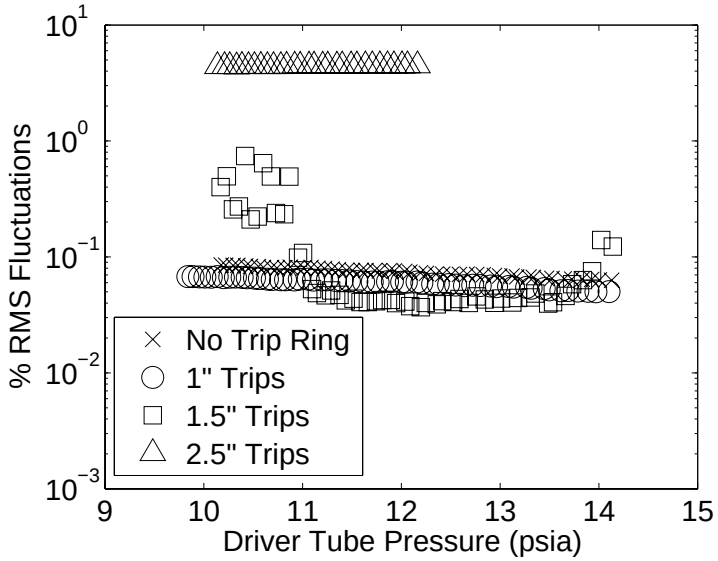

Figure 84: RMS fluctuations using trip ring, with Pitot probe at z=75.3 inches, and initial driver tube pressure of 14.5 psia.

Figure 85 and Figure 86 show the data with the trips, with the Pitot probe moved back to z= 84.3 inches. In Figure 85, the Pitot probe shows similarly separated flow with or without the trip rings. Figure 86 shows that the noise levels are about twice as large

with the 2.5 inch trips as with the 1 inch trips or no trips. Since the larger noise becomes present when the 2.5-inch trips are used, disturbances must be propagating forward. It is interesting that the noise levels with the 2.5-inch trips are much higher with the probe at z=75.3 inches than at z=84.5 inches. It likely that with the probe at z=84.5 inches, the acoustic origin is near the front of the separation, which is unsteady and causing larger fluctuations.

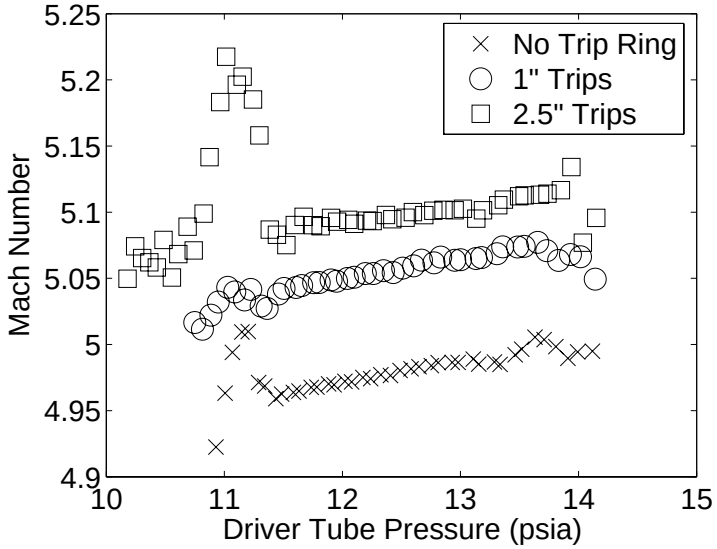

Figure 85: Mach numbers using trip ring, with Pitot probe at z=84.5 inches, and initial driver tube pressure of 14.5 psia.

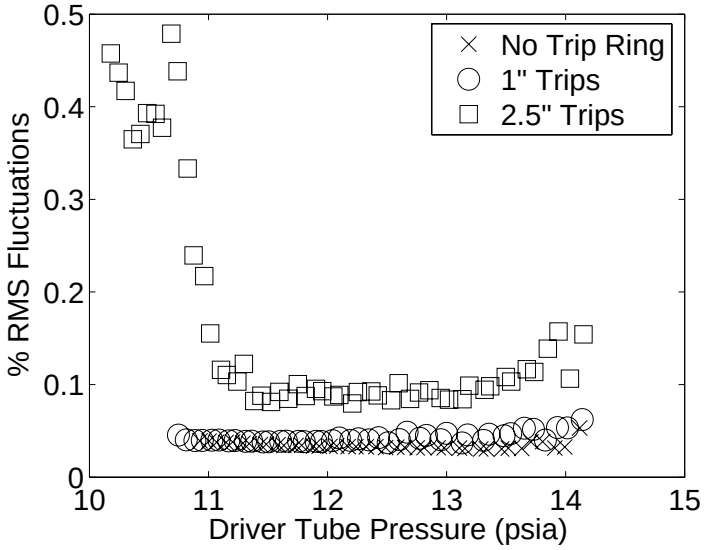

Figure 86: RMS fluctuations using trip ring, with Pitot probe at z=84.5 inches, and initial driver tube pressure of 14.5 psia.

For many flows, boundary layer transition occurs some distance downstream of the trip location. It is possible that placing the trips right in front of the sting mount does not allow enough distance for transition to take place. A new trip ring was built that could be placed further upstream at z=70.05 inches, as shown in Figure 87. Figure 88 shows the Mach number as calculated using data from a Pitot probe on the centerline of the tunnel at two axial locations, with an initial driver tube pressure of 8 psia. At the forward location, the trips do not show a significant effect. At the aft location, the trips appear to set up a more stable and smaller separation than in the case with only the sting mount. Figure 89 shows the RMS fluctuations for the same data. Only the run with the Pitot probe at the aft location and no trip ring shows high noise levels, which supports the idea that the trip ring causes a more stable separation to occur. The low noise levels are slightly above 0.1% due to electronic noise.

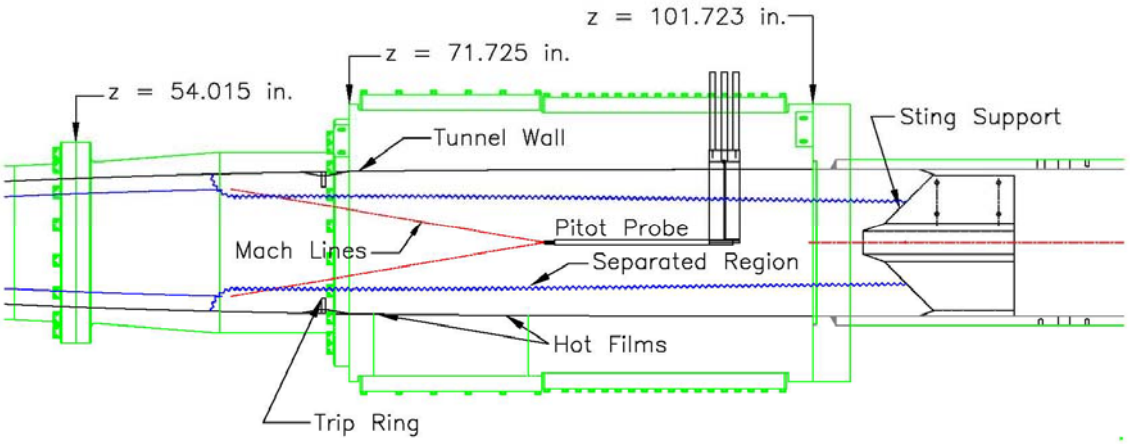

Figure 87: Schematic of end of nozzle with trip ring placed at z=70.05 inches.

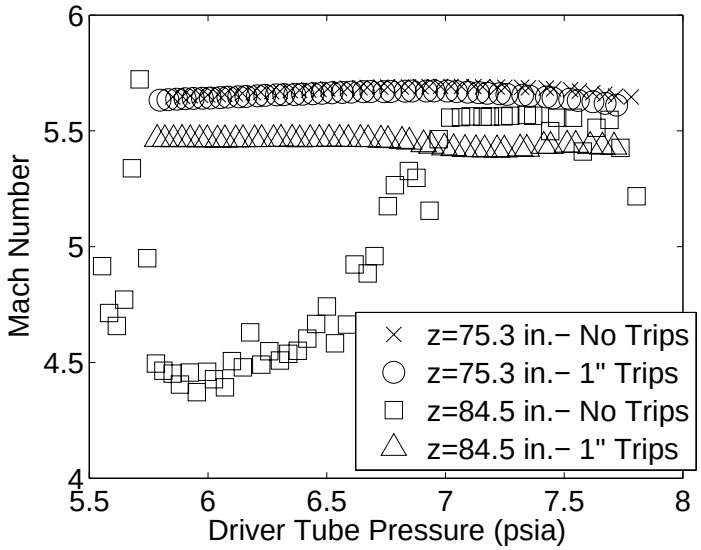

Figure 88: Mach number with trips placed at z=70.05 inches, and initial driver tube pressure of 8 psia.

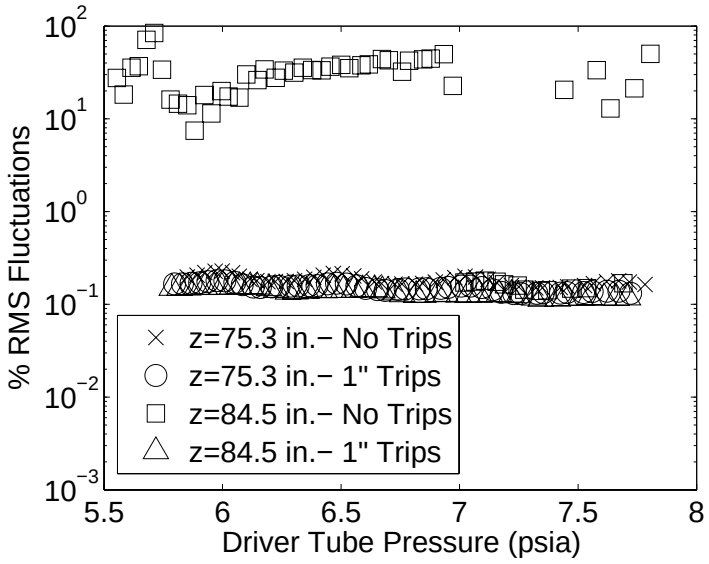

Figure 89: RMS fluctuations number with trips placed at z=70.05 inches, and initial driver tube pressure of 8 psia.

Figure 90 shows Mach numbers for the same forward trips at a higher initial driver tube pressure of 20 psia. The separation with no trip ring is smaller than at lower pressures, according to the data taken by the Pitot probe at z=84.5 inches. The effect of the trip ring here is similar to the effect at lower pressure. The trip ring creates a smaller separation, and as shown by the RMS fluctuations in Figure 91, this separation appears more stable than is present with the sting mount alone.

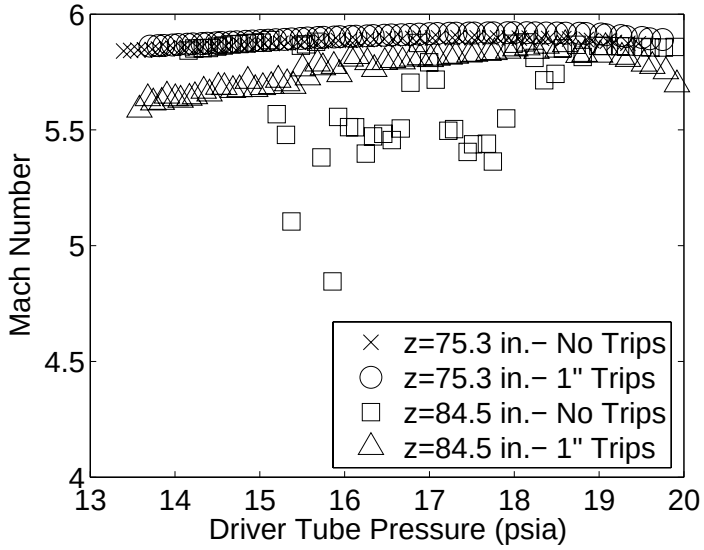

Figure 90: Mach number with trips placed at z=70.05 inches, with an initial driver tube pressure of 20 psia.

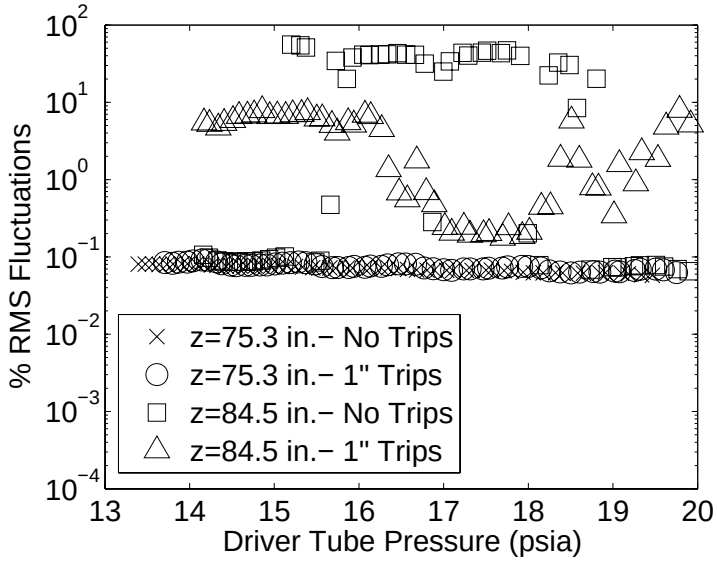

Figure 91: RMS fluctuations with trips placed at z=70.05 inches, with an initial driver tube pressure of 20 psia.

At even higher pressures, with an initial driver tube pressure of 37 psia, the trip ring has no effect or increases the separation at the locations measured. Figure 92 shows the Mach number for the same trip rings at this higher pressure. The Pitot probe at

z=84.5 inches does not show a separation at this pressure. When the trip ring is added, a separation is present, as indicated by the reduced Mach number. There is no effect seen by the Pitot probe measurements farther forward at z=75.3 inches. Figure 93 shows the RMS fluctuations for these runs. Unlike the previous data at lower pressures, the trip ring shows increased fluctuations with the probe at z=84.5 inches. It is possible that since the separation doesn't propagate as far forward at the higher pressures, the acoustic origin of the Pitot probe is closer to the front of the separation. If this is unsteady, it could account for some of the fluctuations measured.

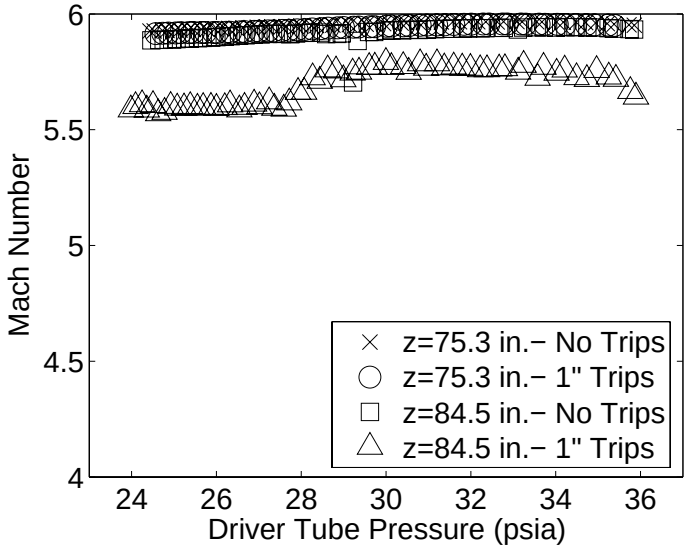

Figure 92: Mach number with trips placed at z=70.05 inches, with an initial driver tube pressure of 37 psia.

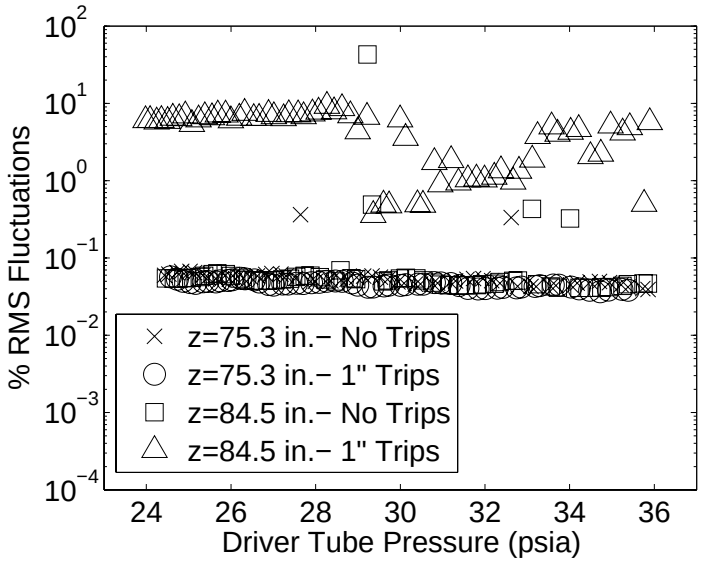

Figure 93: RMS Fluctuations with trips placed at z=70.05 inches, with an initial driver tube pressure of 37 psia.

Since the 1-inch trips separated the flow, smaller trips were tried to see if tripping could be obtained without causing a separation. Figure 94 shows Mach number with and without 0.5-inch trips at z=84.5 inches and z=93.5 inches with an initial pressure of 8 psia. Further aft locations were used for the Pitot probe, since there was not any effect with the larger trips at z=75.3 inches. The figure shows that the trips cause a change in the separation at the forward location, making it appear more steady and uniform. At the aft location, there does not seem to be any change between using the trip ring and having the only the sting mount in the tunnel.

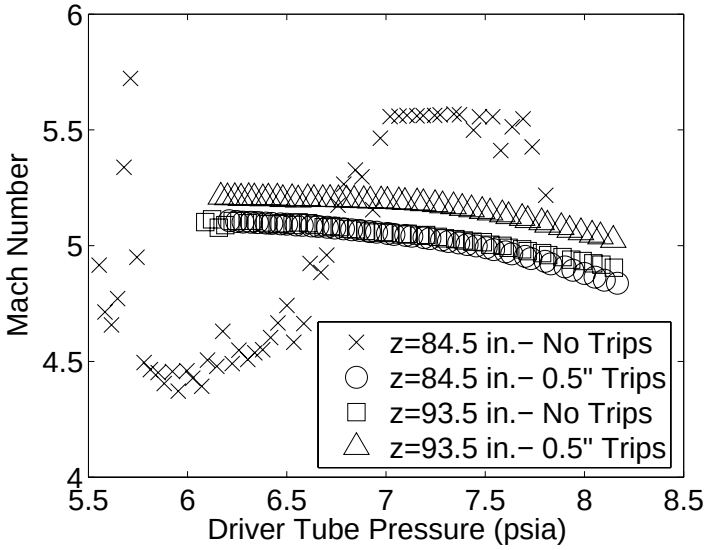

Figure 94: Mach number with trips placed at z=70.05 inches, with an initial driver tube pressure of 8 psia.

Figure 95 shows Mach numbers at a higher pressure of 20 psia, using the 0.5-inch trips, and without. At the highest pressure with the trips at the aft location, there is a brief period where the flow is near Mach 7. This is very strange since the area ratio required for Mach-7 flow is about twice that for Mach 6, which is what this tunnel was designed for. This means that there must be some strange flow nonuniformity to allow the pressure to drop low enough to show Mach 7 at any location. Other than the brief increase in Mach number to a higher value than should be possible, the trip ring does not help eliminate the separation.

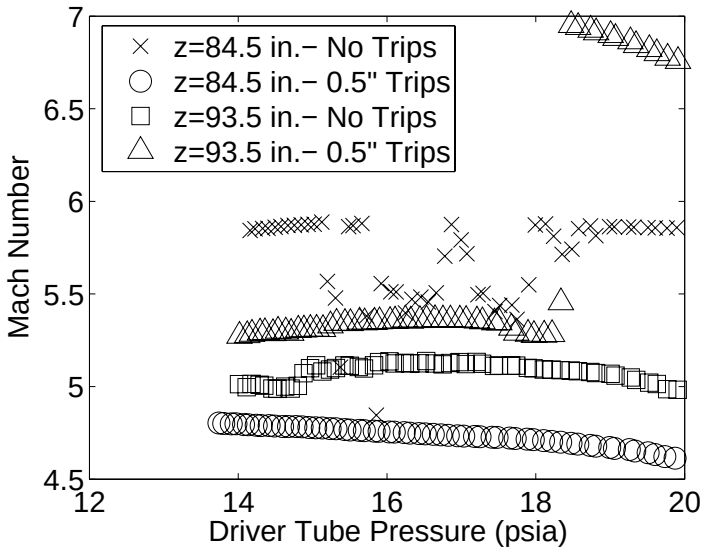

Figure 95: Mach number with trips placed at z=70.05 inches, with an initial driver tube pressure of 20 psia.

Figure 96 shows Mach numbers at an initial pressure of 37 psia, using the 0.5-inch trips, and without. At the aft location, using the trips, the flow shows Mach 7 for the entire run. It is very interesting that the Mach-7 flow is increased at higher pressures, but no explanation has been found that would be causing this Mach-7 flow. Without the trips, at the aft location, the flow is separated only in the middle of the run as was discussed previously. At the forward location, without the trips, there is no separation shown on the Pitot probe, but separation appears when the trips are used.

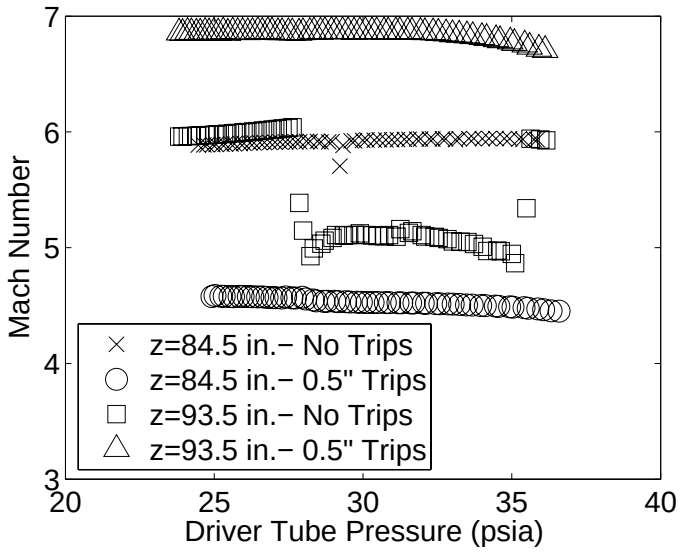

Figure 96: Mach number with trips placed at z=70.05 inches, with an initial driver tube pressure of 37 psia.

The trips placed right in front of the sting mount had no positive effect for any trip size, which is likely because there was not enough distance downstream of the trips for the boundary layer to transition. When the trips were placed further upstream, at z=70.05 inches, the trip ring had unusual and varied effects. At lower pressures, the trips caused a separation that appeared more steady than the one caused by the sting mount, but this could have been caused by the trip-ring separation extending farther forward, allowing the acoustic origin of the Pitot probe to be at a downstream, more stable part of the separation. With the smaller trips, with the probe placed at z=93.5 inches, and at pressures above 18 psia, the Pitot probe showed Mach-7 flow. It is possible the larger trips would have shown this as well, but measurements were not performed at that location. It is uncertain exactly what caused the Pitot pressures to drop low enough to show a Mach number that high.

4.4 Trip Effectiveness

After the measurements were conducted showing the ineffectiveness of the trips, a calculation was done of optimal trip size and the distance from trip location to transition, using an empirical correlation.[38] This correlation was for spherical trips, but should give an indication of what is necessary to trip the flow. The result was unreasonable, requiring spherical trips 4.5 inches in diameter that would cause transition 2 meters downstream of the trip location. As the diameter of the end of the nozzle is only about 9.5 inches, spherical trips of this size are not possible. Although the boundary layer present in the tunnel is well outside the range of boundary layers used to develop the correlation, it is possible that this boundary layer is really that difficult to trip.

4.5 Chapter Summary

The measurements with the compression rings all caused a larger separation than was present with the sting mount alone. Even the compression rings with very small maximum thickness or very small wedge angles showed an increase in the disturbance level. The measurements with the trip ring directly in front of the sting mount were unsuccessful, because they provided very little distance for transition to occur downstream of the trip location. When the trips were moved farther upstream, the results were unusual. The trips caused a separation, but in some cases seemed to reduce the separation from the sting mount. With the Pitot probe further back, the probe was

somehow able to measure flows near Mach 7. This should not be possible in this tunnel, and it is still uncertain why this occurred.

The difficulties in controlling the thick laminar boundary layers that have been examined here are very important to full-scale hypersonic vehicles flying in the upper atmosphere. A vehicle like that would likely have thick laminar boundary layers, similar to those in the Purdue quiet tunnel. The wedges used in the diffuser would have an effect similar to a deflected control surface. If this separates the boundary layer very far upstream, this could have unintended effects on the aerodynamics of the vehicle. Very thick laminar boundary layers are very difficult to trip, as shown in this chapter. For a flight vehicle, if tripping is to be employed to reduce shock/boundary layer interactions, the trips would likely need to be placed near the front of the vehicle, where the boundary layer is thinner. Tripping the boundary layer at the front of the vehicle would greatly increase the area of the vehicle with turbulent boundary layers, which would increase the heating, requiring increased vehicle weight and cost.

CHAPTER 5 - SUMMARY OF EXPERIMENTAL MEASUREMENTS

Large disturbances were found at the end of the nozzle of the Boeing/AFOSR Mach-6 Quiet Tunnel at Purdue University. These were found to originate from disturbances from the double-wedge sting mount in the diffuser. With a cone placed in the double-wedge sting mount a weaker shock was produced, which resulted in disturbances only when the tunnel boundary layer was laminar. The disturbances were caused by shock/boundary-layer interactions that separate the laminar boundary layer far upstream. The separation in the nozzle disappeared when the boundary layers were turbulent since turbulent boundary layers are much less susceptible to separation.

The source of the separation was verified by removing the sting mount. With the sting mount removed, the large disturbances and decreased Mach number in the nozzle disappeared except at very low pressures below 8 psia. These disturbances were found to originate from jets that reintegrate the air from the bleed system far downstream in the diffuser. These disturbances can be removed by directing the bleed air directly to the vacuum tank, but these disturbances are minor compared to those from the sting mount and any model placed in the tunnel.

A new streamlined sting mount was built to reduce the blockage and the shocks that would disturb the flow. The new sting mount has some improvements over the double-wedge sting mount but still causes separations in the nozzle. Axisymmetric

double wedges, or compression rings, were used to try to thin the boundary layer, since propagation distance is based on boundary layer thickness. Unfortunately, the adverse pressure gradient from the first wedge separated the flow more than the sting mount. Trip rings were also used to try to trip the boundary layer from laminar to turbulent, since turbulent boundary layers are much less susceptible to separation. The trip rings consisted of a thin ring holding set screws that were sticking into the flow. These also caused separation of the flow that was larger than the separation with the sting mount alone.

Measurements of the boundary layer were performed using Kulite pressure transducers and hot wires. These measurements gave an idea of the size of the separation. Measurements of the undisturbed boundary layer present with the sting mount removed showed good agreement with computations. Hot film measurements in front of the probes showed that the flow was being disturbed upstream of the probe location, though this did not greatly change the boundary layer profile.

Laminar boundary layers as thick as those in the Boeing/AFOSR Mach 6 Quiet Tunnel have not been studied in the past. Most wind tunnels operate with turbulent boundary layers, so shock/boundary-layer interactions are less critical. The NASA Langley quiet tunnels operated with open jet test sections, so there were no sidewalls for shocks from the model or sting mount to impinge on. Since there are few resources to consult on the subject, this has increased the difficulty of this research, and as yet, the problem remains unsolved.

The shock/boundary-layer interactions examined in this thesis are important to hypersonic vehicles, as well as to the operation of the Purdue Mach-6 Quiet Tunnel.

Thick laminar boundary layers are very likely on hypersonic vehicles in the upper atmosphere. Shock/boundary layer interactions will be present, especially near inlets and control surfaces. Large separations caused by shock/boundary layer interactions could greatly change the intended aerodynamics of a vehicle. Control of thick laminar boundary layers has been shown to be very difficult and more work is needed to gain a better understanding of these laminar boundary layers and how to control them.

CHAPTER 6 - A CONCEPT FOR REDUCING UPSTREAM EFFECTS

The separation at the back of the nozzle when the boundary layer is laminar must be prevented in order for this tunnel to meet its design goals. A few ideas have been examined in this thesis, but these generally increased the separation rather than decreasing it. However, knowledge gained from these attempts can be used to form ideas for the next attempts to correct this problem.

When the boundary layer is turbulent, any shocks impinging on the boundary layer do not cause the large separation that occurs when the boundary layer is laminar. This thesis has shown that it is very difficult to trip the boundary layer without disrupting the main flow. It might be possible to trip the boundary layer with roughness far enough upstream in the nozzle, with roughness elements that are small enough that the main flow is not disturbed. It is likely that this would be extremely sensitive to Reynolds number, though, and if the correct roughness could be found, it would likely only work for a very small pressure range. Placing jets far enough upstream to cause tripping that could be controlled might allow for adjustments for different Reynolds numbers, but this would probably be more likely to disrupt the main flow, and would require cutting holes in the polished nozzle. Because of these difficulties and the uncertainties about whether this could work, tripping the flow does not seem like the best solution to eliminate the separation.

Compression wedges were also used to try to reduce the separation. Separations are reduced by favorable pressure gradients, which are present on the backside of the compression ring. Unfortunately, in order to have this favorable pressure gradient with a compression ring, there must first be an unfavorable pressure gradient on the upstream side. It was found that the unfavorable pressure gradients of the compression rings tested caused a separation larger than was present without the compression ring. Because of the sensitivity of the laminar boundary layer in this tunnel to separations, it seems unlikely that a compression ring can be found that will be able to decrease the separation region.

The compression ring did not work because an unfavorable pressure gradient preceded the favorable pressure gradient that was supposed to stop the separation from propagating forward. A favorable pressure gradient would likely prevent the separation from propagating forward if it could be produced without first having an unfavorable pressure gradient. Creating a favorable pressure gradient at the end of the nozzle would involve having an increase in area, which could then be followed by a decrease in area downstream to match existing piping. Figure 97 shows a schematic of the tunnel with the first section of the diffuser replaced with a larger section. This chapter will discuss in detail some of the possibilities and variations of this idea. The initial idea was produced by the author, but modified and added to with the aid of discussions with Prof. Steven P. Schneider, from Purdue University, and Prof. Alexander Smits, from Princeton University.

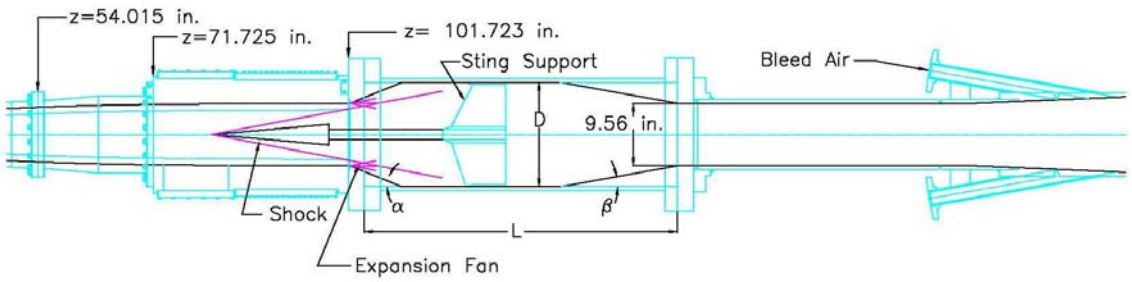

Figure 97: Schematic showing the first diffuser section replaced with one of larger area.

There are several dimensions that are not specified in this figure. Some of these are to be determined using results from computations currently underway by Randy Lillard at NASA JSC. The general idea is to have a new diffuser section of constant diameter that can be modified using inserts. Even though the computations should help decide what is most likely to work, the uncertainty will be so high that the only way to know for certain will be to try it in the tunnel.[39] Figure 98 shows a close-up of the new section shown in Figure 97. The length of the section is denoted by L, and the diameter is denoted by D. There are two inserts shown whose angles are denoted by α and β. The length and diameter cannot be changed after the section is built, without building a new section. However, the wedge angles can be changed, by just building a new insert.

Figure 97 and Figure 98 show a cone with a 5° half angle in the end of the nozzle. The shock from this cone is shown passing through the expansion fan where the rapid expansion begins. This will weaken the shock before it impinges on the wall. Shocks from the sting mount will also be weakened, since the flow will have passed through the shock from the cone. Any separation that is still present should not be able to propagate forward because of the strong favorable pressure gradient caused by the forward expansion.

At the end of the new section there is a ramp that recompresses the flow to the diameter of the existing second diffuser section. The second diffuser section has an initial diameter of 9.6 inches. It then expands out to a diameter of 12 inches, which is the diameter of the diaphragm section and the gate valve. If it turns out that recompressing the flow back to 9.6 inches causes larger separations than can be controlled by the expansion at the beginning of the new section, then the second diffuser section could also be replaced with a constant 12-inch diameter. This would reduce the amount of recompression required.

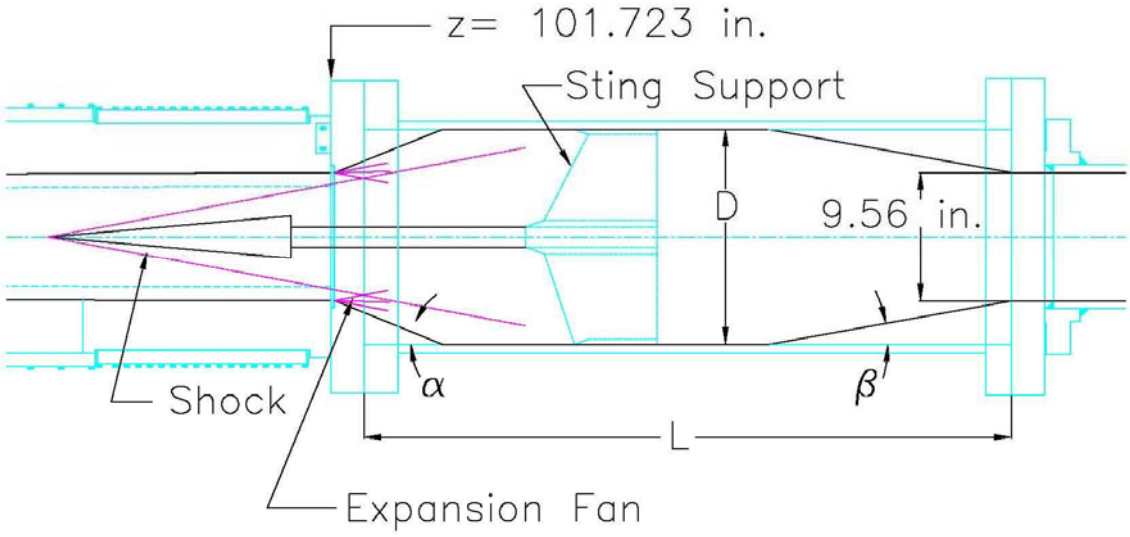

Figure 98: Schematic of new diffuser section with wedge at the front.

A critical area in the schematic in Figure 98 could be the recompression at the end of the first wedge, when the flow turns back parallel with the wall. Turning the flow back parallel to the sidewall will cause a shock that could cause a large separation. The shock strength at the end of the wedge could be reduced by decreasing the angle α, but that would also reduce the favorable pressure gradient at the beginning of the wedge. One possibility to have a large favorable pressure gradient at the end of the nozzle, but

have a weaker shock when turning the flow back, is to turn the flow using two compressions as shown in Figure 99. By breaking it up into two compressions, each compression is much weaker, and less likely to cause a large separation.

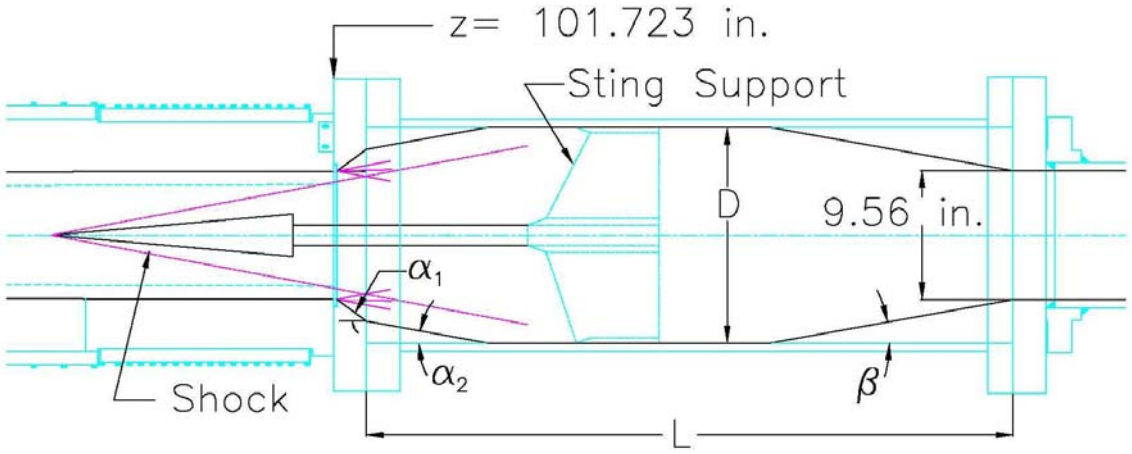

Figure 99: Schematic of new diffuser section with wedge with two compression angles.

Figure 100 shows the new section with a backward-facing step at the beginning of the section, instead of a wedge. A backward facing step might also be able to prevent a separation from traveling forward into the nozzle, which would have the effect of the favorable pressure gradient because of an expansion fan from the backward-facing step. The backward-facing step could also have an effect similar to the open-jet test section of the Langley Mach-6 Quiet Tunnel. The Langley tunnel did not have an issue with separation because there were no sidewalls for shocks to impinge on and separate the boundary layer. The backward-facing step would be somewhat similar in that there is no continuous sidewall for the separation to propagate forward on. The separation might not be able to hop over the step to affect the nozzle.

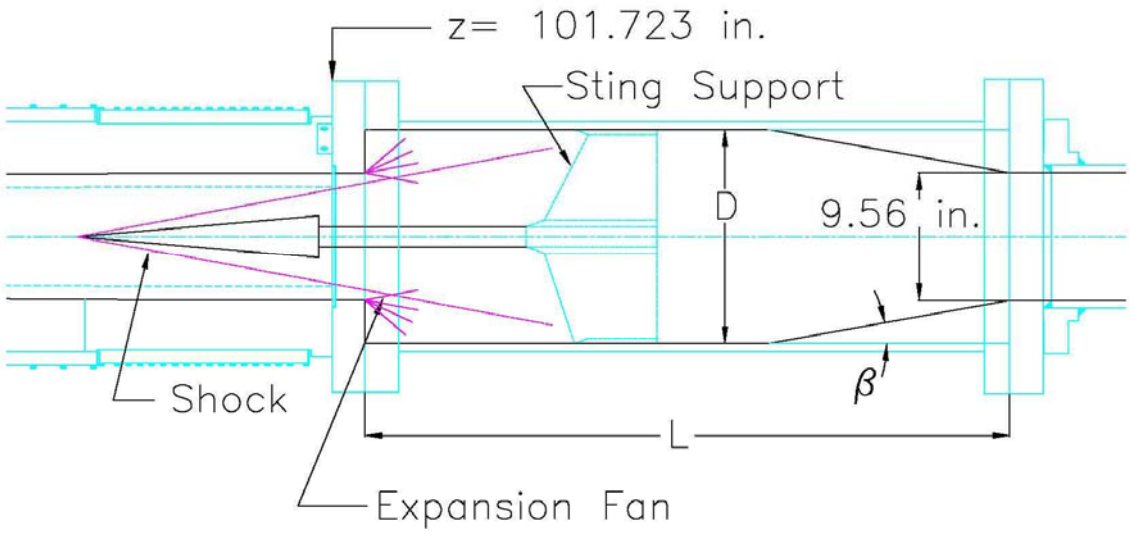

Figure 100: Schematic showing new section with a backward-facing step.

The previous schematics were shown with a cone model placed in the tunnel. Plans also call for testing models of reentry vehicles at high angles of attack. The shock of a model like this will be at a much larger angle than the cone, and require the model to be placed very close to the end of the nozzle so that the shock does not impinge the wall before the expansion. A 4-inch model placed at a 40° angle of attack with a 57° shock angle is shown in Figure 101. Because the model must be placed so far back, optical access will be limited. The rectangle at the end of the nozzle shows the location of the window. With the model placed as far forward as possible, it should be possible to get some optical access to the model, allowing the use of temperature sensitive paints.

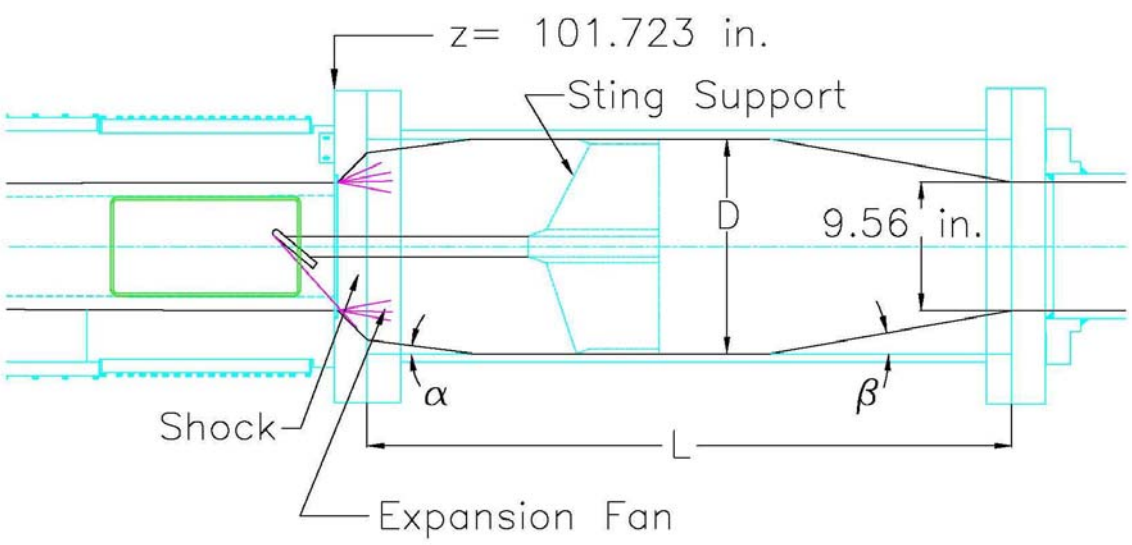

Figure 101: Schematic showing new section with a model at high angle of attack.

The new diffuser section, with its increase in area, cannot be bolted directly to the end of the nozzle because the inside diameter will likely be as large as, or larger than, the bolt placement at the end of the nozzle. An idea for a joining flange is shown in Figure 102. This figure shows a flange with counter-sunk holes for bolts to attach the flange to the nozzle. Studs can then be placed in the joining flange, at a larger radius to connect the new section to the joining flange. If the inner diameter of the new section is large enough that it opens up a leak path through the bolts to the nozzle, as shown in the figure, it will be necessary to use O-rings with the bolts into the nozzle. An angle can be cut in the flange to allow the expansion to begin as far upstream as possible.

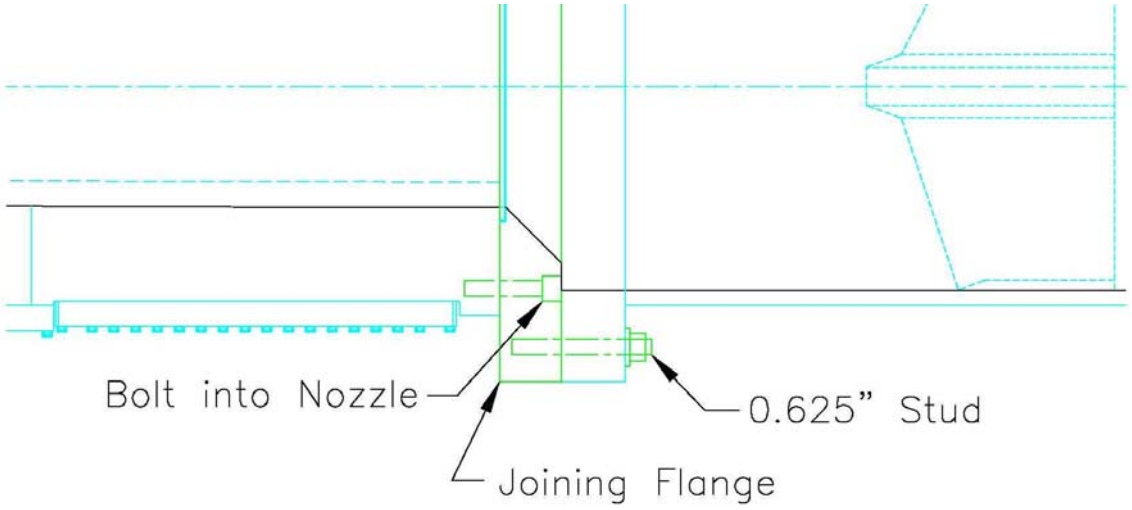

Figure 102: Detail showing how new section could be joined to the end of the nozzle.

This chapter has presented an idea for preventing separations from shock/boundary-layer interactions from disrupting the flow in the nozzle. This should allow models to be run with laminar boundary layers at a wide range of Reynolds numbers. Variations have been presented in a manner that allows several of the details to be modified depending on the results found. Computations will be performed that should help narrow down what is likely to work, but this problem is not well understood, and no solution can be assured until it is built and tested.

LIST OF REFERENCES

1. Joseph F. Shea. Report of the Defense Science Board task force on the National Aerospace Plane (NASP). Defense Technical Information Center Citation ADA201124, Sep 1988.

2. Paul V. Tartabini, Roger A. Lepsch, J. J. Korte, and Kathryn E. Wurster. A multidisciplinary performance analysis of a lifting-body single-stage-to-orbit vehicle. Paper 2000-1045, AIAA, January 2000.

3. Scott A. Berry, Aaron H. Auslender, Arthur D. Dilley, and John F. Calleja. Hypersonic boundary-layer trip development for Hyper-X. Journal of Spacecraft and Rockets. Vol. 38, No. 6. Nov-Dec 2001.

4. D. F. Fisher and N. S. Dougherty, Jr. Flight and wind-tunnel correlation of boundary-layer transition on the AEDC transition cone. Paper NASA-TM-84902, Nov. 1982.

5. S. R. Pate and C. J. Schueler. Radiated aerodynamic noise effects on boundary-layer transition in supersonic and hypersonic wind tunnels. *AIAA Journal*, 7(3): 450-457, March 1969.

6. P. C. Stainback. Hypersonic boundary-layer transition in the presence of wind-tunnel noise. *AIAA Journal*, 9(12): 2475-2476, December 1971.

7. F.-J. Chen, M.R. Malik, and I. E. Beckwith. Boundary-layer transition on a cone and flat plate at Mach 3.5. *AIAA Journal*, 27(6): 687-693, 1989.

8. Steven P. Schneider. Effects of high-speed tunnel noise on laminar-turbulent transition. *Journal of Spacecraft and Rockets*, Vol. 38 No. 3, May-June 2001.

9. John Laufer. Aerodynamic noise in supersonic wind tunnels. *Journal of Aerospace Sciences*, 28: 685-692, 1961.

10. I. E. Beckwith, T. R. Creel, F.-J. Chen, and J. M. Kendall. Free-stream noise and transition measurements on a cone in a Mach 3.5 pilot low-disturbance tunnel. TP 2180, NASA, 1983.

11. J. L. Stollery. Some Viscous Interactions Affecting the Design of Hypersonic Intakes and Nozzles. Advances in Hypersonics: Defining the Hypersonic Environment, Vol. 1. pp. 418-437, 1992.

12. Jean M. Delery. Shock Wave/Turbulent Boundary Layer Interaction and its Control. Progress in Aerospace Sciences. Vol. 22, pp. 209-279, 1985.

13. G. E. Gadd. Interactions Between Wholly Laminar or Wholly Turbulent Boundary Layers and Shock Waves Strong Enough to Cause Separation. Journal of the Aeronautical Sciences. Vol. 20, November, 1953, pp 729-739.

14. F. W. Barry, A. H. Shapiro, and E.P. Neumann. The Interaction of Shock Waves with Boundary Layers on a Flat Surface. Journal of the Aeronautical Sciences, April 1951, pp. 229-70.

15. J. Delery and J. G. Marvin. Shock-Wave Boundary Layer Interactions. AGARD-AG-280. February, 1986.

16. Steve Wilkinson, Private Communication, 2003.

17. Louis A. Cassel. Applying Jet Interaction Technology. Journal of Spacecraft and Rockets. Vol. 40, No. 4, July-August 2003, pp. 523-537.

18. R. H. Thomas, J. A. Schetz, and F. S. Billig. Gaseous Injection in High Speed Flow. Ninth International Symposium on Air Breathing Engines. Athens, Greece. September 1989.

19. David R. Stone and Aubrey M. Cary, Jr. Discrete Sonic Jets used as Boundary-Layer Trips at Mach Numbers of 6 and 8.5. NASA Technical Note TN D-6802, July 1972.

20. N. Qin and A. Redlich. Massively Separated Flows Due to Transverse Sonic Jet in Hypersonic Laminar Stream. Paper 96-1934, AIAA, June 1996.

21. Steven P. Schneider, Shin Matsumura, Shann Rufer, Craig Skoch, and Erick Swanson. Hypersonic Stability and Transition Experiments on Blunt Cones and a Generic Scramjet Forebody. Paper 2003-1130, AIAA, January 2003.

22. Steven P. Schneider, Craig Skoch, Shann Rufer, and Erick Swanson. Hypersonic Transition Research in the Boeing/AFOSR Mach-6 Quiet Tunnel. Paper 2003-3450, AIAA, June 2003.

23. H. Ludwieg. Tube wind tunnel: A special type of blowdown tunnel. AGARD Report 143, July 1957.

24. Steven P. Schneider. Design of a Mach-6 quiet-flow wind-tunnel nozzle using the e**N method for transition estimation. Paper 98-0547, AIAA, January 1998.

25. Steven P. Schneider. Design and fabrication of a 9-inch Mach-6 quiet-flow Ludwieg tube. Paper 98-2511, AIAA, June 1998.

26. Steven P. Schneider. Fabrication and testing of the Purdue Mach-6 quiet-flow Ludwieg tube. Paper 2000-0295, AIAA, January 2000.

27. Steven P. Schneider. Initial shakedown of the Purdue Mach-6 quiet-flow Ludwieg tube. Paper 2000-2592, AIAA, June 2000.

28. Steven P. Schneider, Shann Rufer, Laura Randall, and Craig Skoch. Shakedown of the Purdue Mach-6 quiet-flow Ludwieg tube. Paper 2001-0457, AIAA, January 2001.

29. Steven P. Schneider and Craig Skoch. Mean flow and noise measurements in the Purdue Mach-6 quiet-flow Ludwieg tube. Paper 2001-2778, AIAA, June 2001.

30. Steven P. Schneider, Craig Skoch, Shann Rufer, Erick Swanson, and Matthew Borg. Bypass Transition on the Nozzle Wall of the Boeing/AFOSR Mach-6 Quiet Tunnel. Paper 2004-0250, AIAA, January 2004.

31. S. P. Schneider and C. E. Haven. Quiet-flow Ludwieg tube for high-speed transition research. AIAA Journal, 33(4):688-693.

32. J. D. Schmisseur, J. O. Young, and S. P. Schneider. Measurement of Boundary-Layer Transition on the Flat Sidewall of a Rectangular Mach 4 Quiet-Flow Nozzle. Paper 96-0852, AIAA, January 1996.

33. Stephen R. Norris. Bruhn 6 Constant Temperature Anemometer Notes. Report, July 29, 1996, from Steven P. Schneider.

34. A. Nakayama, J. P. Stack, J. C. Lin, and W. O. Valarezo. Surface Hot-Film Technique for Measurements of Transition, Separation, and Reattachment Points. Paper 93-2918, AIAA, July 1993.

35. Steven P. Schneider, Craig Skoch, Shann Rufer, Shin Matsumura, and Erick Swanson. Transition Research in the Boeing/AFOSR Mach-6 Quiet Tunnel. Paper 2002-0302, AIAA, January 2002.

36. John D. Anderson, Jr. Fundamentals of Aerodynamics, 2nd ed. McGraw-Hill, Inc. New York, 1991.

37. Steven P. Schneider, Craig Skoch, Shann Rufer, Erick Swanson, and Matthew Borg. Bypass Transition on the Nozzle Wall of the Boeing/AFOSR Mach-6 Quiet Tunnel. Paper 2004-0250, AIAA, January 2004.

38. E. L. Morrisette, D. R. Stone, and A. H. Whitehead, Jr. Boundary-Layer Tripping with Emphasis on Hypersonic Flows. Viscous Drag Reduction, Plenum Press, New York, 1969, pp. 33-51

39. Alexander Smits, Princeton University, Private Communication, 2005.

APPENDIX

Table 1: Initial Driver Tube Pressures for Data in Figures

Figure Number	**Legend Description**	**Initial Driver Tube Pressures (psia)**
Figure 16	Original Nozzle	8.01, 10.01, 14.41
	Surrogate Nozzle	7.91, 11.66, 14.52, 18.00, 20.13, 21.51, 23.06, 25.04, 27.03, 28.97
	Surrogate Nozzle, Step Removed	20.00, 27.94, 35.00, 37.01, 39.97, 45.05
Figure 33 and Figure 34		7.98, 9.79, 9.98, 14.06, 14.21
Figure 36	No Sting Mount	8.03
	Double Wedge	7.98
Figure 37 and Figure 38	z=75.3 inches	8.03
	z=84.5 inches	8.03
	z=93.5 inches	8.03
Figure 40 and Figure 41	z=75.3 inches	20.02
	z=84.5 inches	19.96
	z=93.5 inches	20.00
Figure 54 and Figure 55	Passive Bleeds	8.03
	Active Bleeds	8.00
Figure 60 and Figure 61	No Sting Mount	8.03
	Sting Mount	8.02
Figure 62 and Figure 63	No Sting Mount	19.96
	Sting Mount	20.01, 20.01, 20.01
Figure 64 and Figure 65		20.04, 25.02, 29.93, 35.03, 37.03
Figure 67	z=75.3 inches	37.01
	z=84.5 inches	37.03
	z=93.5 inches	37.03
Figure 79 and Figure 80	z=75.3 in. - No Comp Ring	7.98
	z=75.3 in. - 1-inch Comp Ring	7.99
	z=84.5 in. - No Comp Ring	7.98
	z=84.5 in. - 1-inch Comp Ring	8.03
Figure 81 and Figure 82	No Compression Ring	14.49
	1” Comp Ring-10° angle	14.53
	0.75” Comp Ring	14.52
Figure 83 and Figure 84	No Trip Ring	14.49
	1” Trips	14.48
	1.5” Trips	14.54
	2.5” Trips	14.52
Figure 85 and Figure 86	No Trip Ring	14.51
	1” Trips	14.53
	2.5” Trips	14.54

Figure 88 and Figure 89	z=75.3 in. - No Trips	8.02
	z=75.3 in. - 1” Trips	8.01
	z=84.5 in. - No Trips	8.03
	z=84.5 in. - 1” Trips	8.01
Figure 90 and Figure 91	z=75.3 in. - No Trips	20.00
	z=75.3 in. - 1” Trips	20.01
	z=84.5 in. - No Trips	20.00
	z=84.5 in. - 1” Trips	20.02
Figure 92 and Figure 93	z=75.3 in. - No Trips	37.01
	z=75.3 in. - 1” Trips	37.01
	z=84.5 in. - No Trips	36.99
	z=84.5 in. - 1” Trips	37.00
Figure 94	z=84.5 in. - No Trips	8.03
	z=84.5 in. - 0.5” Trips	8.02
	z=93.5 in. - No Trips	8.02
	z=93.5 in. - 0.5” Trips	8.01
Figure 95	z=84.5 in. - No Trips	20.00
	z=84.5 in. - 0.5” Trips	19.98
	z=93.5 in. - No Trips	20.00
	z=93.5 in. - 0.5” Trips	20.02
Figure 96	z=84.5 in. - No Trips	36.99
	z=84.5 in. - 0.5” Trips	36.99
	z=93.5 in. - No Trips	37.04
	z=93.5 in. - 0.5” Trips	37.00

VITA

Craig Ryan Skoch was born in Manhattan, Kansas. He grew up in Parkville, Missouri; Liberty, Missouri; Moorpark, California; and St. Joseph, Missouri, where he graduated from Central High School. Craig received his B.S. in Aerospace Engineering from the University of Missouri - Rolla in 1999. While working on his B.S., he had internships with Boeing, working on the X-35 Joint Strike Fighter, and NASA Langley Research Summer Scholars, working on CFD for a proposed reentry vehicle. Craig received his M.S. in Aeronautics and Astronautics from Purdue University in 2001. In January 2006, Craig moved to Palmdale, California, where he is currently employed by Lockheed Martin Advanced Development Programs (Skunk Works).